Review

Shi Li[a], Cong Wang[a], Yu Yin, Elfed Lewis and Pengfei Wang*

Novel layered 2D materials for ultrafast photonics

https://doi.org/10.1515/nanoph-2020-0030
Received January 14, 2020; revised February 20, 2020; accepted February 20, 2020

Abstract: A range of new 2D materials have recently been reported, including topological insulators, transition-metal dichalcogenides, black phosphorus, MXenes, and metal-organic frameworks, which have demonstrated high optical nonlinearity and Pauli blocking for widespread use as saturable absorbers in pulsed lasers. 2D materials are emerging as a promising platform for ultrashort-pulse fiber laser technology. This review presents a catalog of the various pulsed laser applications based on the series of emerging 2D materials. In addition, novel optical devices using layered materials, such as optical modulators, optical switches, and all-optical devices, are also included. It is anticipated that the development of 2D materials will intensify in the future, providing potentially new and wide-ranging efficacy for 2D materials in ultrafast photonic technology.

Keywords: 2D materials; saturable absorber; nonlinear optics; laser.

[a]**Shi Li and Cong Wang:** These authors contributed equally to this work.
***Corresponding author: Pengfei Wang,** Key Laboratory of In-fiber Integrated Optics of the Ministry of Education, College of Physics and Optoelectronic Engineering, Harbin Engineering University, Harbin 150001, China; and Key Laboratory of Optoelectronic Devices and Systems of the Ministry of Education and Guangdong Province, College of Optoelectronic Engineering, Shenzhen University, Shenzhen 518060, China, e-mail: pengfei.wang@tudublin.ie
Shi Li and Yu Yin: Key Laboratory of In-fiber Integrated Optics of the Ministry of Education, College of Physics and Optoelectronic Engineering, Harbin Engineering University, Harbin 150001, China. https://orcid.org/0000-0001-8965-7241 (S. Li)
Cong Wang: Key Laboratory of Optoelectronic Devices and Systems of the Ministry of Education and Guangdong Province, College of Optoelectronic Engineering, Shenzhen University, Shenzhen 518060, China
Elfed Lewis: Optical Fiber Sensors Research Centre (OFSRC), Department of Electronic and Computer Engineering, University of Limerick, Limerick V94 T9PX, Ireland

1 Introduction

Over the last few decades, interdisciplinary research involving materials has become ubiquitous in this subject area, reflecting the trend evident throughout the scientific community. Researchers have come to realize that this model of research has grown in prominence and is currently driving advances in many disciplines [1]. For example, the discovery of a layered material, graphene (synthesized by Geim and Novoselov in 2004), aroused worldwide upsurge in graphene research in various fields because of its rich physical properties [2, 3]. Moreover, graphene is like a material "magic key", which has opened the doors to a class of novel layered materials with unique photonic and optoelectronic properties [4–7]. In the past decade, graphene has not only been involved in significant research breakthroughs in many fields [3, 8–14] but also led to the emergence of many graphene-like materials including topological insulators (TIs) [15–22], transition-metal dichalcogenides (TMDs) [23–28], black phosphorus (BP) [29–36], MXenes [37–41], and metal-organic frameworks (MOFs) [42, 43]. These novel 2D materials, as shown in Figure 1, have been discovered and developed with astonishing speed, thus greatly enriching the graphene-like material family.

Nonlinear photonics represents a field that has benefited immensely from the recent emergence of 2D layered materials because of their potentially excellent nonlinear optical properties [2, 10, 12, 17, 29, 44–66]. Additionally, there is a significant practical need for discovering suitable 2D materials for enhancing the performance of existing nonlinear photonics-based devices. For example, grapheme has been used as part of a pulse-shaping device because of its excellent saturable absorption characteristics [9, 11–14]. This important discovery was made independently by several different research groups, which widely indicated that grapheme could be used to demonstrate ultrafast fiber lasers. It laid the foundation for graphene's important role in ultrafast photonics research. On this basis, a large body of scientific research exists, and many new materials have been discovered and widely used in lasers, which have become a research hotspot in the field of ultrafast photonics [20, 33, 39, 67–69]. Since the discovery

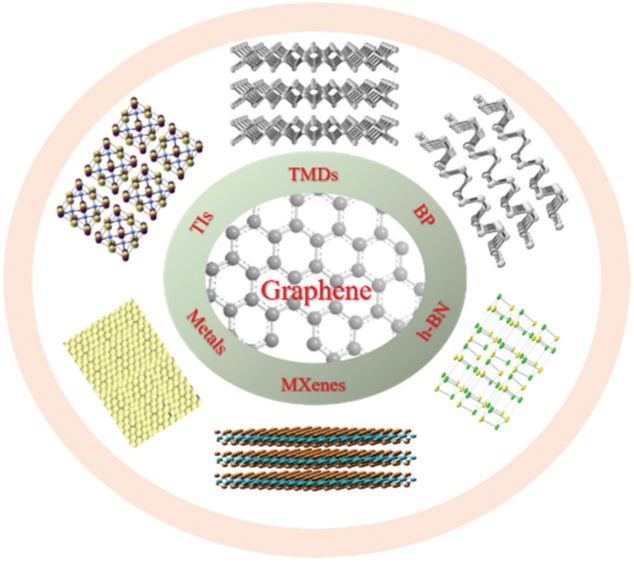

Figure 1: Schematic illustration of different kinds of typical ultrathin 2D materials, such as graphene, TMDs, BP, metals, MXenes.

of graphene, laser performance has greatly improved, and consequently laser research has rapidly advanced.

Novel optical devices based on layered materials, including optical modulators and optical switches, have also developed rapidly [70]. For example, an excellent optical modulator based on the evanescent field interaction between graphene and tapered microfibers has been demonstrated [71]. Recently, researchers not only achieved antimonene-based optical modulators but also demonstrated an actively Q-switched laser using the same antimonene-based all-optical modulator [72]. These wide applications of layered 2D materials have therefore become a true hotspot of activity in nonlinear photonics. A cascade of research results resulting from this significant work is also driving the rapid development of optical devices based on nonlinear phenomena, in general. However, a comprehensive summary of relevant studies is lacking in the literature. In this article, we therefore review the latest research on nonlinear photonics based on various layered materials, with particular emphasis on their fabrication methods, optical properties, and applications in ultrafast lasers and other nonlinear optical devices. The scientific achievements resulting from these studies are summarized in order to explore possible future developments of layered materials.

In this review, Section 1 provides a brief introduction to 2D materials. Section 2 deals with the fabrication methods, nonlinear optical properties, and integration strategies of saturable absorbers (SAs) based on layered 2D materials. Section 3 gives a brief review of laser applications based on the 2D materials, mainly including solid-state lasers (Section 3.1) and fiber lasers (Section 3.2). Lasers are not the only devices that benefit from the use of 2D materials; in Section 4, a series of other photonics devices are considered, including optical switches, optical modulators, and polarizers. Finally, a comprehensive conclusion and outlook are included.

2 Fabrication and nonlinear optical properties of the layered 2D materials

It is widely recognized that the preparation and physical properties of layered 2D materials have a huge influence on their optical properties. In this section, a brief introduction to the fabrication methods of layered 2D materials and their nonlinear optical properties is presented.

2.1 Fabrication methods

Layered 2D material fabrication methods can be broadly separated into two approaches: top-down exfoliation, and bottom-up growth, which are both shown in Figure 2A [73]. Specifically, top-down exfoliation mainly includes mechanical exfoliation, laser thinning, and solution-processing. Bottom-up growth mainly includes chemical vapor deposition (CVD), molecular beam epitaxy, hydrothermal method, pulsed magnetron sputtering, pulse laser deposition, and vapor phase sulfurization [74]. Detailed fabrication methods are summarized in Figure 2B [74].

Typical mechanical exfoliation methods involve the use of a Scotch tape™ for repeatedly cleaving layers from bulk layered crystal materials. Mechanical exfoliation has been used to fabricate high-quality single-crystal flakes for widespread use [75–80]. It was first used in the discovery of graphene from graphite flakes by Geim and Novoselov in 2004 [44]. This method is easy to carry out, and the resulting exfoliated mono- or few-layer materials have high completeness and few defects, making them suitable for fundamental scientific research [80]. However, the scalability and yield of layered 2D materials fabricated using this method are very hard to control [80].

Solution processing takes advantage of the interaction between specific solvents and bulk materials to exfoliate them into mono- or few-layer materials under a solution environment [81, 82]. To circumvent the defect of the Scotch

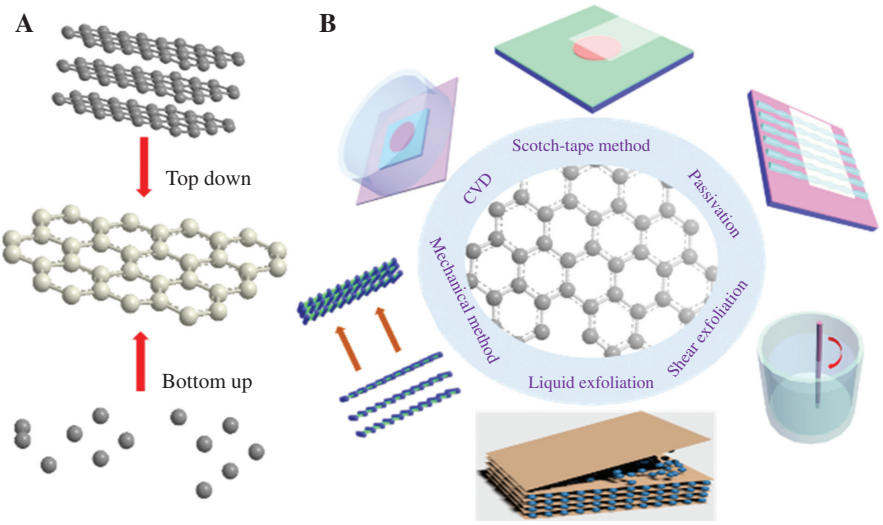

Figure 2: Schematic of the fabrication method of 2D materials.
(A) Two main approaches: top-down exfoliation and bottom up growth. (B) Detailed fabrication methods.

tape method, chemical exfoliation methods have been explored, albeit combined with a preceding step involving mechanical shearing such as grinding or ball milling, which can help overcome the so-called inter-sheet van der Waals interaction to form single- to few-layered sheets [83]. Lithium ion intercalation exfoliation is a typical chemical exfoliation method that uses lithium ions as an intercalating agent to widen the layer separation in bulk materials; then, mechanical force is applied by stirring or ultrasonication to dissociate the 2D materials [84]. This method can afford high yields of 2D nanosheets. However, the materials produced in this manner usually have deficiencies such as structure alteration, and postprocessing is sometimes required to improve the quality [80]. LPE (liquid-phase exfoliation) directly uses high-strength ultrasonication to generate micro bubbles, and the resulting forces within the materials cause a weakening of the van der Waals force between the layers; thus, LPE is a purely physical method. LPE provides a facile and low-cost method to produce large amounts of mono- and few-layer 2D materials, and no postprocessing is required as in chemical solution processing. For example, BP was first fabricated using LPE in 2015 [68], which resulted in an excellent nanosheet structure and a Z-scan curve. However, though monolayer nanosheets can be generated using LPE, their concentration compared to few-layer nanosheets is usually low [85].

In order to obtain defect-free, large-area sheets of 2D materials, CVD and wet chemical synthesis methods have been widely used. CVD has been used to produce high-quality, pristine, large-area, single-layer 2D nanosheets [86–90]. 2D materials fabricated using CVD has significant benefits of scale control and high purity. However, the film growth is limited by the low nucleation rate on bare substrates, and pretreatment of the substrate is often necessary to seed the 2D material's growth, resulting in inefficiency [80]. Pulsed-laser deposition (PLD) is a highly efficient method used to control the ratio of two different ions in the material film by controlling the evaporation rates of the two ions. Additionally, the film fabricated using PLD is of high purity due to the fact that the ion target is placed in a vacuum chamber, thereby avoiding contamination from the environment [85]. Pulsed magnetron sputtering is similar to PLD in that it focuses high-energy pulses onto a block target kept at a fixed position inside a vacuum chamber. Ionized Ar ions excited by the pulsed DC power supply bombard the material target, and the material gets deposited on the substrate. Materials fabricated using pulsed magnetron sputtering result in a uniform surface [91].

2.2 Nonlinear optical properties

In general, assuming an instantaneous dielectric response in an isotropic material, the relation between the induced polarization [$P(t)$, scalar] and the applied electric field [$E(t)$, scalar] is expressed by

$$P(t) = \varepsilon_0(\chi^{(1)}E(t) + \chi^{(2)}E^2(t) + \chi^{(3)}E^3(t) + \cdots), \quad (1)$$

where ε_0 is the permittivity of vacuum, $\chi^{(1)}$ is the linear susceptibility, and $\chi^{(2)}$ and $\chi^{(3)}$ are the second- and third-order nonlinear susceptibilities, respectively [92–94].

The third-order nonlinearity $\chi^{(3)}$ is responsible for third-harmonic generation, nonlinear refractive index change (nonlinear Kerr effect), and nonlinear absorption change (saturable absorption and multiphoton absorption). Generally, multiphoton absorption includes two-photon absorption (TPA), and $\chi^{(3)}$ is responsible for this. According to Eq. (1), the imaginary part corresponds to the decay of an exponential (Beer-Lambert law), where the exponential is a negative real number (absorption is positive). $\chi^{(3)}$ represents a third-order nonlinear phenomenon, which includes TPA. Furthermore, in TPA, the imaginary part of the susceptibility represents the absorption of two photons.

The nonlinearity represented by $\chi^{(3)}$ has been shown to be very large in graphene and other 2D materials [95, 96]. The changes of refractive index and optical absorption are dependent on the incident optical intensity, and the complex refractive index n can be expressed as [93–95]

$$n = n_0 + n_2 I - i\frac{\lambda}{4\pi}(\alpha_0 + \alpha_2 I), \tag{2}$$

Where I is the optical intensity, n_0 is the linear part, n_2 is the nonlinear refractive index (Kerr coefficient), and α_2 is the nonlinear absorption coefficient. Both n_2 and α_2 are interrelated with the real and complex part of Eq. (3) as

$$n_2 = \frac{1}{cn_0^2\varepsilon_0}\frac{3}{4}\mathrm{Re}(\chi^{(3)}),\ \alpha_2 = \frac{-\omega}{c^2 n_0^2 \varepsilon_0}\frac{3}{2}\mathrm{Im}(\chi^{(3)}). \tag{3}$$

It should be noted that the changes in optical absorption will have a strong effect on the refractive index for wavelengths near the absorption edge because of the Kramers-Kronig relation [94].

Saturable absorption is a phenomenon related to the imaginary part of $\chi^{(3)}$ as expressed in Eq. (3), where high-intensity light "bleaches" the material and reduces the optical absorption, which can be expressed as

$$\alpha = \frac{\alpha_0}{1 + I/I_S}, \tag{4}$$

where α_0 is the linear absorption coefficient, and I_S is the saturation intensity [94]. In the linear regime, where the incident optical intensity is relatively weak, the SA absorbs the incident light, resulting in the attenuation of light. When the incident optical intensity is high, the lower energy states are depleted, whereas the upper energy states are filled; thus, the saturation of absorption occurs, resulting in decreasing attenuation. Note that Eq. (4) can be approximated as $\alpha \approx \alpha_0 - \alpha_0 + I/I_S$ for small values of I. The normalized intensity is defined as I/I_S, and the normalized absorption is defined as $(1-\mathrm{e}^{-\alpha l})/(1-\mathrm{e}^{-\alpha_0 l})$ since the nonabsorbed light after transmission through a sample of thickness l is $\mathrm{e}^{-\alpha l} I$ and $\alpha_0 l = 0.1$. The saturation intensity I_S is given by the absorption cross-section σ and the recovery time τ as

$$I_S = \frac{\hbar\omega}{\sigma\tau} = \frac{E_S}{\tau}, \tag{5}$$

where ω is the optical angular frequency, and E_S is the saturation fluence [94, 97].

Saturable absorption is a universal phenomenon in any material that exhibits optical absorption due to the electronic transition between two energy levels. However, it is uncommon to find an SA with a fast recovery time suitable for generating ultrashort pulses at time scales of a few picoseconds to a few hundred femtoseconds. Graphene and some novel 2D materials such as TIs, TMDs, and MXene have inherently fast SA responses.

It should be noted that these materials may have the opposite effect on saturable absorption, namely reverse saturable absorption or optical limiting. The main cause of reverse saturable absorption is multiphoton absorption, such as TPA. Saturable absorption and reverse saturable absorption can coexist; in this case, Eq. (4) becomes

$$\alpha = \frac{\alpha_0}{1 + I/I_S} + \beta I, \tag{6}$$

where β is the TPA coefficient [98].

Under the guidance of the above theory, researchers began to explore experimentally the nonlinear optical properties of layered materials. Z-scan measurement is a common method for studying nonlinear optical processes, including saturable absorption, multiphoton absorption, reverse saturable absorption, and the Kerr effect [94]. Using this method, the nonlinear optical coefficients of many layered materials have been obtained, as illustrated in Table 1. It can be seen that 2D materials normally have great optical nonlinearity. Compared to graphene, TMDs, BP, and MXenes have larger nonlinearity, which has resulted in their becoming the most popular 2D materials following their discovery. For 2D materials, saturable absorption is usually believed to arise from Pauli blocking. Notably, the saturable absorption of 2D material-based absorbers beyond their direct bandgap, i.e. sub-bandgap absorption, can also occur, which is due to the defects, TPA, and the absorption of edge modes.

Geim and Novoselov were awarded the Nobel Prize in 2010 for their success in making graphene. The third-order nonlinearity of graphene was initially studied in 2009, which

Table 1: Summary of nonlinear optical properties of layered 2D materials.

Layered 2D material	Energy bandgap (eV)	Sample state	Laser parameter	T (%)	NLO response	I_s (MW/cm^2)	Im $\chi^{(3)}$ (esu)	References
Graphene	0	Dispersion	800 nm, 1 kHz, 100 fs	16.8	SA	$(583\times10^3)\pm(127\times10^3)$	$-(8.7\pm2.4)\times10^{-16}$	[99]
			1030 nm, 1 kHz, 340 fs	18.1		$(170\times10^3)\pm(51\times10^3)$	$-(6.9\pm2.3)\times10^{-15}$	
			515 nm, 1 Hz, 340 fs	13.61		$(473\times10^3)\pm(219\times10^3)$	$-(8.8\pm2.3)\times10^{-16}$	
Bi_2Te_3	~0.06	Dispersion	1550 nm, 35 fs				0.2×10^{-17} (n_2)	[100]
Bi_2Se_3	~0.3	Dispersion	800 nm, 1 kHz, 25 ns	46.7	SA	1.199×10^6	0.0097 (n_2)	[101]
			1562 nm, 20.8 MHz, 1.5 ps	30.55		1.26	0.86 (n_2)	
			1930 nm, 32.3 MHz, 2.8 ps	26.71		7.09	2.12 (n_2)	
MoS_2	~1.87	Nanosheets	800 nm, 1 kHz, 100 fs	32.6	SA	$(381\times10^3)\pm(346\times10^3)$	$-(1.38\pm0.45)\times10^{-14}$	[102]
WS_2	~1.98	Nanosheets	800 nm, 1 kHz, 40 fs	35.75	SA	156×10^3	$-(1.78\pm0.16)\times10^{-9}$	[25]
$MoSe_2$	~1.62	Dispersions	800 nm, 1 kHz, 100 fs	45.3	SA	$(590\times10^3)\pm(225\times10^3)$	$-(1.45\pm0.34)\times10^{-15}$	[99]
$MoTe_2$	/	Dispersions	800 nm, 1 kHz, 40 fs	86.3	SA	$(217\times10^3)\pm(11\times10^3)$	$-(2.13\pm0.66)\times10^{-15}$	[99]
WSe_2	/	Nanosheets	488 nm, CW	/	SA	/	/	[103]
NiS_2	~0.3	Nanosheets	800 nm, 2 kHz, 200 fs	/	SA	/	/	[104]
BP	0.3–2.0	Nanosheets	800 nm, 10 kHz	42.1	SA	8.7	-7.85×10^{-15}	[105]
			1330 nm, 50 kHz	45.9 ± 2.2		$(7.8\times10^3)\pm(0.5\times10^3)$	$-(1.83\pm0.29)\times10^{-14}$	
			1550 nm, 50 kHz	59.1 ± 0.1		$(5.3\times10^3)\pm(0.1\times10^3)$	$-(1.98\pm0.95)\times10^{-14}$	
			1972 nm, 50 kHz	55.3 ± 1.5		$(5.9\times10^3)\pm(0.3\times10^3)$	$-(1.41\pm0.4)\times10^{-13}$	
MXenes		Nanosheets	800 nm		SA	$(88.6\times10^3)\pm(5\times10^3)$	-4.74×10^{-14}	[106]
			1064 nm	38.3 ± 2.0		$(61.2\times10^3)\pm(5\times10^3)$	-3.53×10^{-14}	
			1550 nm			$(39.1\times10^3)\pm(5\times10^3)$	-4.96×10^{-14}	
			1800 nm			$(31.4\times10^3)\pm(5\times10^3)$	-10.1×10^{-14}	

indicated that scientific research is usually forward-looking and timely [107–109]. For example, researchers used Z-scan technology and pump-probe spectroscopy to study saturable absorption and carrier dynamics in graphene suspensions; the results of this work are shown in Figure 3A, B [11]. Meanwhile, another group of researchers studied the parametric process of few-layer graphene by four-wave mixing (FWM) [108]. They found that graphene has a very large third-order index and is basically nondispersive over some wavelength ranges. These studies were considered groundbreaking, and the results have greatly advanced nonlinear optics based on graphene and graphene-like materials.

On the basis of the success of the graphene study, researchers shortly discovered another important group of layered 2D nanomaterials called topological insulators (TIs). In 2012, different researchers found that the Bi_2Te_3 [15] and Bi_2Se_3 [16], two typical TIs, exhibited optical nonlinearity and saturable absorption, as shown in Figure 3C–F. An ultrafast pulsed fiber laser was also demonstrated based on the nonlinearity of TIs, which was in keeping with the expectations for the application of TI material properties. Since then, a large body of significant results on the optical properties and the applications of TI has emerged [100, 101, 110–113]. These studies show that TIs not only exhibit saturable absorption characteristics but also have a very large nonlinear refractive index, suggesting that they have great application potential in pulse-shaping and optical modulation.

With the development in graphene-like materials, layered TMDs, another group of layered 2D materials, have been widely studied. TMDs have a very typical sandwich-like atomic structure. Thus, the formula of TMDs can be expressed as MX_2 (M=Mo, W, Ti, Re, etc.; X=S, Se, Te, etc.). The TMD family has more than 40 members, as summarized in a previous report [114]. Because of the specific 2D confinement of electronic motion and the absence of interlayer coupling, layered TMDs possess a direct bandgap, making their nonlinear optical performance dramatically better than that of their bulk counterparts [114]. For example, researchers fabricated an MoS_2 nanoflake array film on glass substrates using an *in situ* growth method [102]. The nonlinear absorption (NLA) properties of the

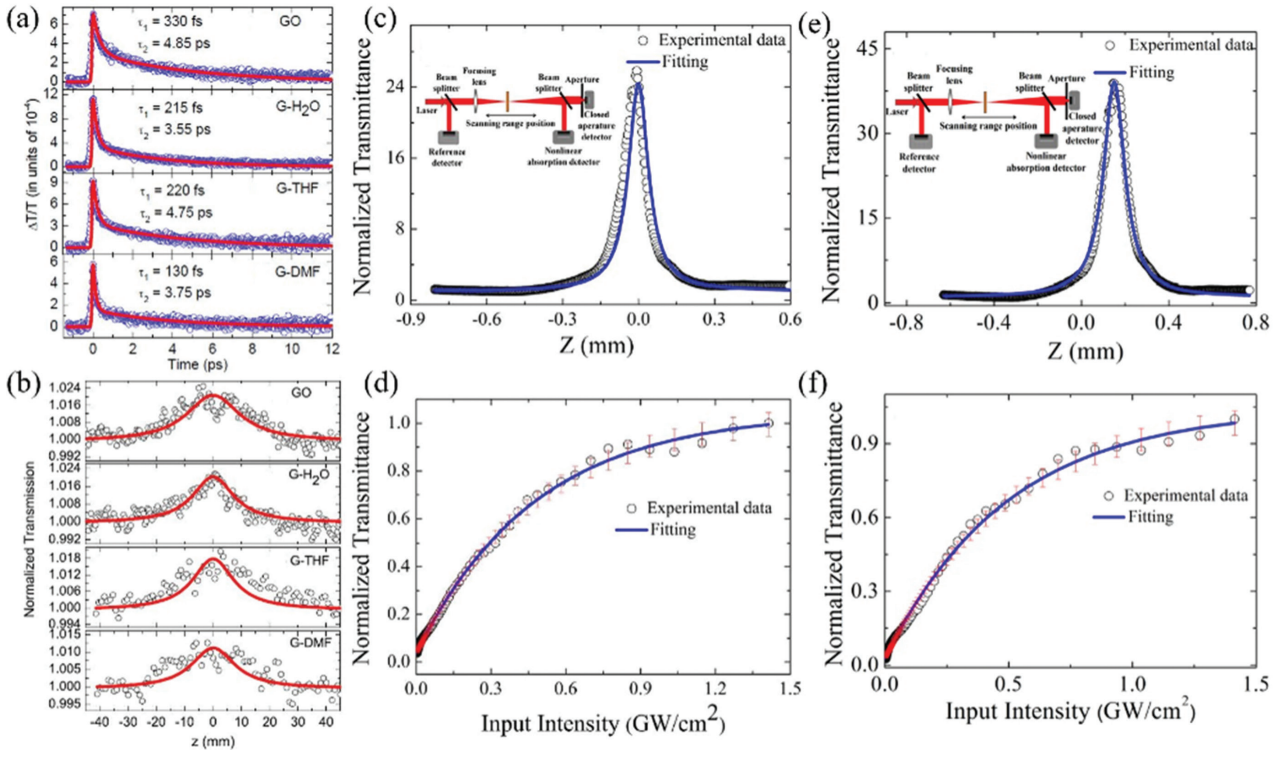

Figure 3: Nonlinear optical properties of graphene and TIs.
(A,B) Graphene. (A) Transient differential transmission spectra for graphene suspensions as a function of probe delay in the degenerate pump-probe experiment at 790 nm (1.57 eV). (B) Open aperture Z-scan data of the graphene suspensions. Reproduced with permission from Ref. [11]. Copyright 2009, American Institute of Physics. (C,D) Bi_2Te_3. (C) Typical Z-scan peak curve of Bi_2Te_3 at 1550 nm. Inset: Z-scan experimental setup. (D) The corresponding nonlinear saturable absorption curve. Reproduced with permission from Ref. [15]. Copyright 2012, American Institute of Physics. (E,F) Bi_2Se_3. (E) Typical Z-scan peak curve of Bi_2Se_3 at 1550 nm. Inset: Z-scan experimental setup. (F) The corresponding nonlinear saturable absorption curve. Reproduced with permission from Ref. [16]. Copyright 2012, American Institute of Physics.

MoS_2 nanoflake array films were investigated using an open-aperture Z-scan technique. The results are shown in Figure 4A–D, which indicate that MoS_2 exhibits excellent optical nonlinearity. Researchers predicted that the MoS_2 nanoflake can be used in optical devices such as ultrafast lasers and ultrafast optical switches owing to its good NLA properties and fast response. Furthermore, the MoS_2 nanoflake was shown to exhibit better saturable absorption than graphene measured under the same conditions by another group [25, 115–119]. Subsequently, WS_2 also proved to have saturable absorption properties, which is shown in Figure 4E–H [25]. In recent years, research of TMDs has become the focus of many fields including photonic devices, sensing, communications, etc. Many more TMDs including WSe_2 [103, 120], SnS_2 [121, 122], $SnSe_2$ [123], ReS_2 [124, 125], WTe_2 [91, 126, 127], and TiS_2 [128, 129] have also been extensively studied. These explorations have laid a solid foundation for their applications in nonlinear photonics.

BP is another material that has attracted much attention recently. It has been found that BP has a singular direct bandgap, which varies between 2 eV (single layer) and 0.3 eV (bulk) with the number of layers, and lies between the zero-bandgap graphene and relatively large bandgap TMDs, thus potentially overcoming the shortcomings of these 2D materials in the field of photonics [74, 130–132]. In 2015, researchers discovered the broadband nonlinear optical response of multilayer BP, as shown in Figure 5 [133]. Subsequently, this optical property was confirmed by other research groups [132, 134–138]. Overall, BP has very broad applications such as active and passive optical devices, especially in near-infrared and mid-infrared photonic systems. Additionally, BP quantum dots (BPQDs) were also investigated in 2016 [123]. BPQDs exhibit excellent nonlinear optical response with a modulation depth of about 36% and a saturable intensity of about 3.3 GW/cm^2. By using BPQDs as an optical SA, an ultrashort pulse with a pulse duration of about 1.08 ps centered at a wavelength of 1567.5 nm was generated in a mode-locked fiber laser.

Figure 5E shows the saturable absorption of 2D materials in detail, with a brief introduction included. When photons of the correct energy are incident on the material, electrons from the valence band (red) are excited to the conduction band (yellow). In the strong excitation state, the ground-state ions are depleted, and the excited state is fully occupied, and hence the absorption reaches saturation. Owing to this Pauli blocking process, it is impossible to have two identical electrons filling the same state, leading to the bleaching of light absorption. This is the common process of saturated absorption for 2D materials.

In 2017, another novel 2D nanomaterial, MXene, was studied, opening a new avenue of research. MXene has attracted considerable attention because of its graphene-like but highly tunable and tailorable electronic/optical properties [37, 106, 139, 140]. The general formula of MXene is $M_{n+1}X_nT_x$, where M is an early transition metal, X is C and/or N, T is the surface terminations (F, O, or OH), and $n = 1$, 2, or 3. Researchers found that a typical MXene has efficient SA with negligible lossy nonlinear absorption

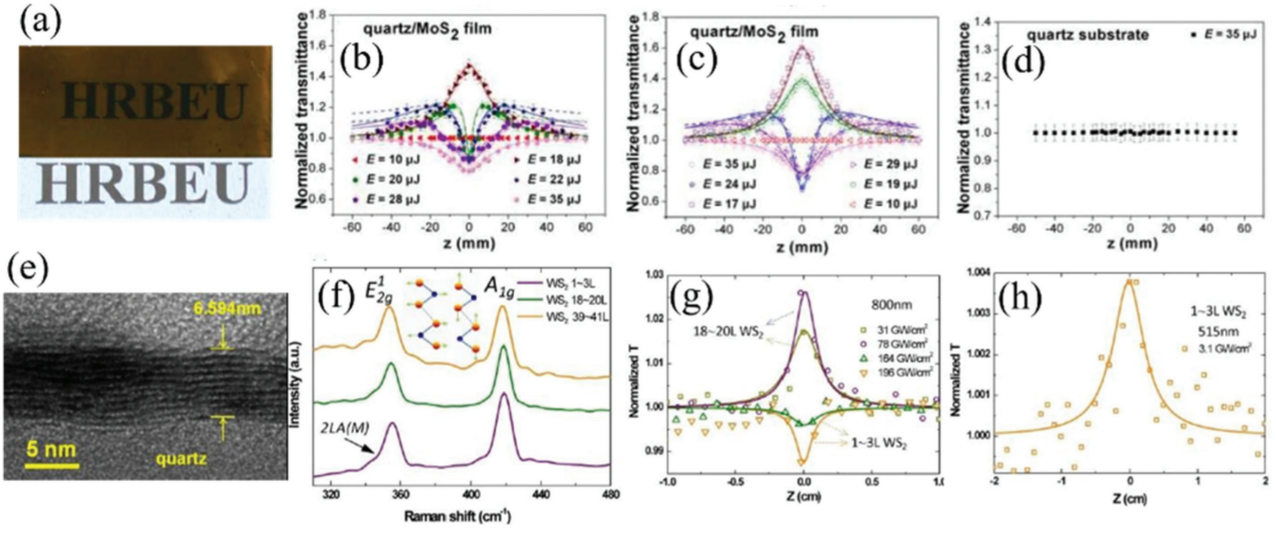

Figure 4: Nonlinear optical properties of MoS_2 and WS_2.
(A–D) MoS_2. (A) Photographs of the quartz/MoS_2 film and quartz glass substrate. (B) and (C) The OA Z-scan curves of the quartz/MoS_2 film. (D) The OA Z-scan curves of the quartz film. Reproduced with permission from Ref. [102]. Copyright 2014, The Royal Society of Chemistry. (E–H) WS_2. (E) Photographs of 8–10 L WS_2 film. (F) Raman spectra of the WS_2. (G) Z-scan results at 800 nm (40 fs). (H) Z-scan results at 515 nm (340 fs). Reproduced with permission from Ref. [25]. Copyright 2015, The American Chemical Society.

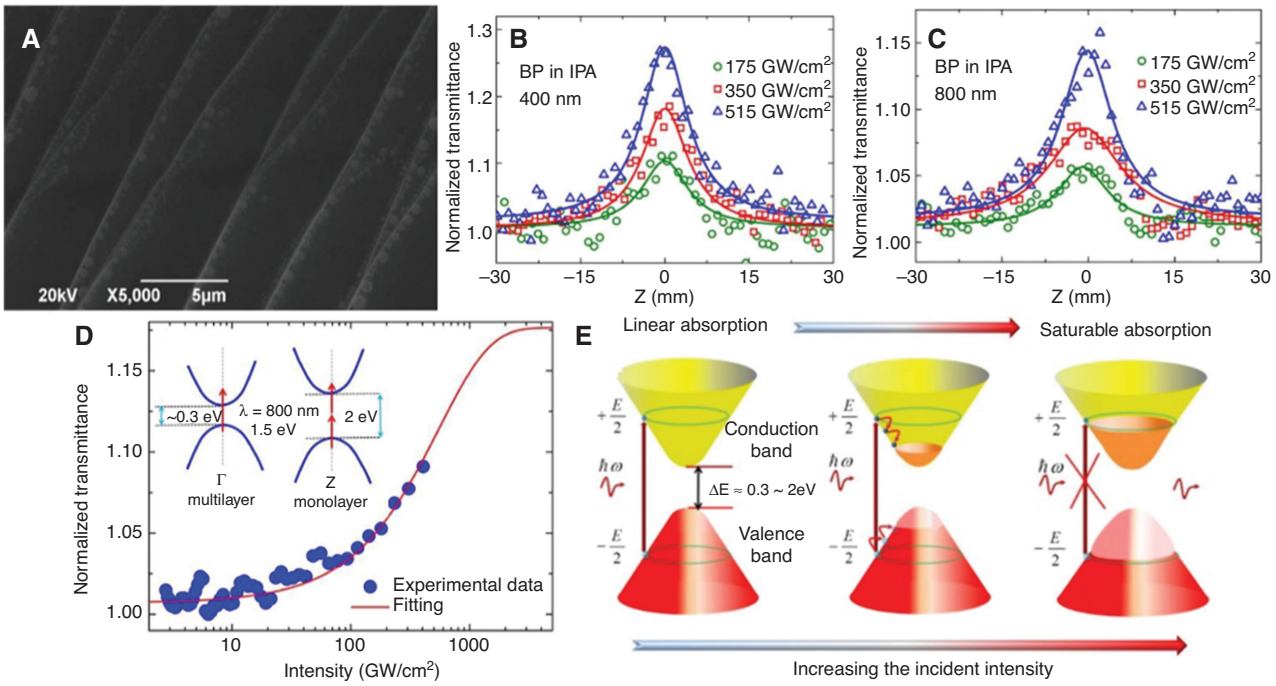

Figure 5: Nonlinear optical properties of few-layer BP.
(A) SEM image of BP. (B) and (C) Open aperture Z-scan measurements of BP NPs dispersions under different intensities at 400 and 800 nm. (D) Relation between normalized transmittance and input intensity for BP nanoparticle dispersions at 800 nm. (E) Schematic diagram of the saturable absorption in multilayer BP NPs. Reproduced with permission from Ref. [133]. Copyright 2015, Optical Society of America.

components in the spectral range 800–1800 nm, which is indicated in a typical MXene, $Ti_3C_2T_x$, which was deliberately chosen as the investigation object to highlight broadband nonlinear optical response in the near-infrared region [106]. The corresponding results are shown in Figure 6. Researchers not only predicted that MXene could be used in an ultrafast fiber laser system as an SA but also successfully demonstrated the MXene-based pulsed fiber laser. The optical properties and applications of MXenes were subsequently confirmed by other research groups [37, 38]. Thus, MXenes also have huge application potential in broadband lasers and passive optical devices, especially in near-infrared and mid-infrared photonic systems.

In the above studies, an important issue is the formation mechanism of saturable absorption of layered materials. It is found that most layered materials, such as graphene, TIs, and BP, have an energy-band structure of the symmetric Dirac-cone type. Physically, any electron can be excited into the conduction band when the intensity of incident light is larger than the bandgap of the layered material. Then, the distribution rapidly thermalizes and cools down to form a hot Fermi-Dirac distribution. Through a dynamic process, electrons and holes recombine until the equilibrium distribution is restored. This describes the linear optical transition under low excitation intensity. However, as the light intensity increases to higher levels, the number of photocarriers increases instantaneously and fills the energy states near the edge of the conduction and valence bands, and the absorption is blocked owing to the Pauli blocking principle. Eventually, photons at specific wavelengths can transmit through the layered materials without absorption. This mechanism plays a key role in pulse-shaping and has been widely used in pulsed lasers.

The fact that a material exhibits saturable absorption at specific wavelengths is a precondition for its application in pulse-shaping devices. In the latter part of the next section, we describe how SAs in passively mode-locked/Q-switched lasers have taken advantage of this mechanism. Different optical materials have different bandgaps, the bandgap being a key parameter in determining their suitability for operation in nonlinear optical devices. Sub-bandgap absorption, as opposed to conventional saturable absorption, is also a common phenomenon in device applications, which may be attributed to material defects, TPA, or edge-mode absorption. In addition, unlike graphene, TMDs and BP have bandgaps that vary with the number of layers, and their absorption mechanism is more complex. These results indicate that the current understanding of the saturable absorption of layered materials is at an early stage and may need further investigations. Other optical properties, including

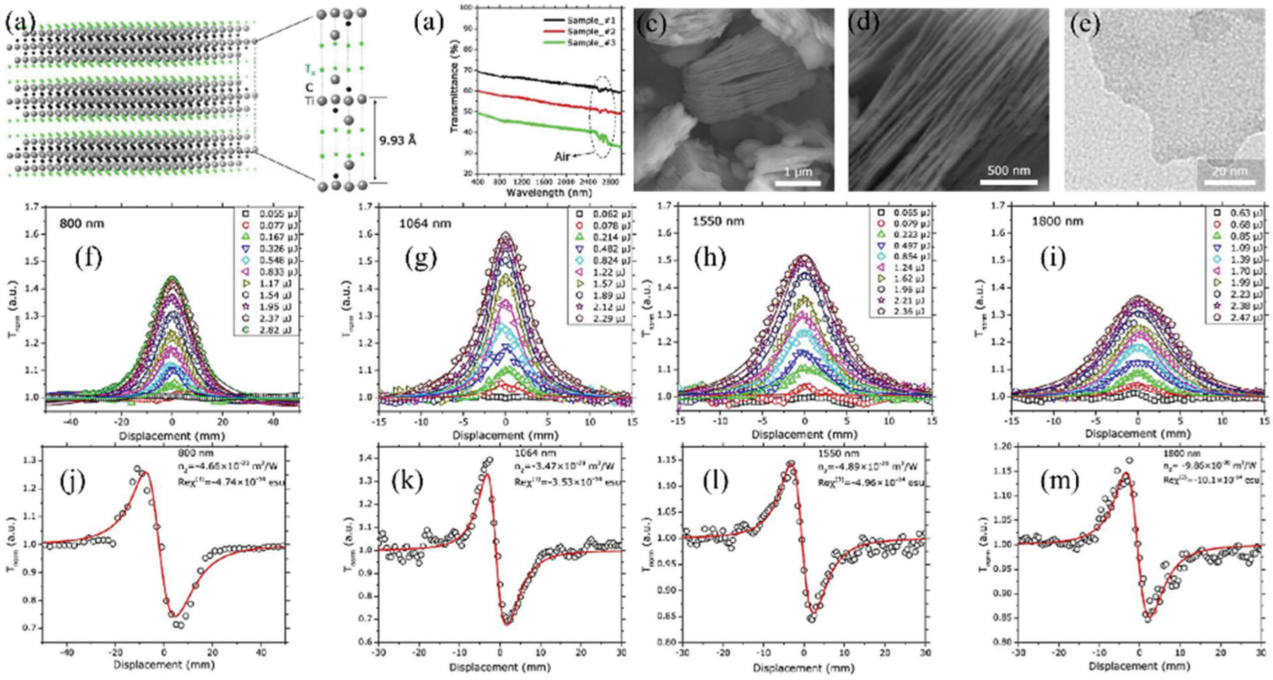

Figure 6: Nonlinear optical properties of few-layer MXene ($Ti_3C_2T_x$, (T=F, O, or OH)).
(A) Three atomic layers of MXene $Ti_3C_2T_x$. (B) Linear transmittance. (C) and (D) SEM images. (E) High-resolution TEM image. (E,F) Open aperture Z-scan characterization of MXene $Ti_3C_2T_x$ at wavelengths 800, 1064, 1550, and 1800 nm. (J–M) Closed-aperture Z-scan characterization of MXene $Ti_3C_2T_x$ at wavelengths 800, 1064, 1550, and 1800 nm. Reproduced with permission from Ref. [106]. Copyright 2017, John Wiley and Sons.

third-harmonic generation [141], parametric processes [142], and stimulated Brillouin scattering [143], have also been explored, all of which promote the development of nonlinear optics based on layered materials.

2.3 Integration strategies of layered 2D materials-based SA

To satisfy the requirement for use in a laser cavity, it is necessary that the fabricated 2D materials be further processed prior to being incorporated into the devices. There are many integration strategies that have been developed to "fit" the 2D materials into the laser cavity. These strategies are normally different for different lasers and are used mainly in solid-state lasers and fiber lasers. For solid-state lasers, the interaction between the 2D material and the laser beam normally occurs in free space (at the surface of the material), which results in a relatively straightforward coupling [144–146]. In the case of fiber lasers, owing to their unique structure, the interaction between the 2D material and the laser beam reflects the fiber geometry, and therefore several special integration strategies have been developed. Figure 7 summarizes the integration scenarios that have been widely used [147].

The 2D materials are normally transferred onto a plain substrate (a gold mirror, CaF_2 lens, or sapphire lens), which is normally used in solid-state lasers in any case, and shown in Figure 7A. The most common method for achieving this is CVD. The transfer process comprises a few steps including coating the polymer on the material, removing the original substrate by chemical etching, transferring the 2D material-polymer thin film onto the target substrate, and removing the polymer by acetone. The fabricated SA device can operate on the basis of transmission coupling or reflective coupling, depending on the laser cavity design and the substrate material [148–150].

As stated above, many integration strategies exist in the case of fiber lasers. The simple method involves embedding 2D materials in a polymer thin film, which may be poly(vinyl acrylate; PVA) [68, 151–154], poly(methyl methacrylate; PMMA) [155], or any other polymer. Generally, the SA film can be many tens of micrometers thick [68, 104, 151–154, 156–158]. It is worth noting that the fabricated material film can be cut into many tens of individual SA elements, and the SA element could be designed as a 1×1 cm^2 square (normally about 0.01 mm thick), which matches well with the small fiber core (~9 μm fiber core of a standard single-mode fiber). As shown in Figure 7B, the SA film can be sandwiched

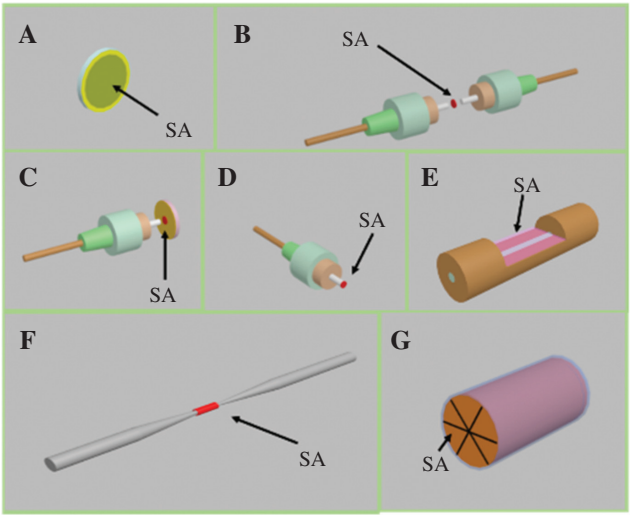

Figure 7: Incorporation schemes for 2D material saturable absorbers.
(A) Transferring SA onto the substrate for free-space coupling, and sandwiching the thin-film SA between (B) two fiber connectors and (C) a fiber connector and a mirror. Transferring or depositing SA on (D) fiber end, (E) side-polished fiber, and (F) tapered fiber. (G) Filling SA into a photonic crystal fiber.

between two fiber connectors in the case of transmission coupling. Reflective coupling is normally achieved with the SA film sandwiched between a fiber connector and a mirror (Figure 7C). The integration strategies shown in Figure 7B and C are simple, stable, and robust against physical damage. However, the low thermal stability of the polymer thin film can introduce mechanical distortion in the coupling and hence represents a potential source of interference. In the case of devices with high average output power or high peak power, this may result in the degradation of laser performance, possibly resulting in irreparable damage of the SA film [153, 155]. In order to avoid the adverse influence of the polymer layer, researchers have successfully transferred 2D materials directly onto the fiber end (Figure 7D), side-polished fiber (Figure 7E), or a tapered fiber (Figure 7F) using the CVD method. Optically driven deposition represents an alternative approach for SA deposition. In this case, the fiber is located in the dispersed optical field of the 2D material (e.g. prepared by LPE method) and external light is injected. The leaked light from the fiber attracts the 2D nanosheets and attaches them. This method can be used to deposit 2D materials on a fiber tip, a side-polished fiber, or a tapered fiber. By monitoring the instantaneous light intensity in the fiber, the deposition process can be accurately controlled to deposit the required amount of 2D material on the fiber. For 2D material transferred/deposited on a side-polished or tapered fiber, only the evanescent field of the light beam in the fiber interacts with the material, which reduces the light intensity in the material and prevents it from suffering thermal damage. Additionally, side-polished fibers and tapered fibers provide a very long interaction length and therefore are preferred platforms in many experiments investigating optical nonlinearity [91]. The photonic crystal fiber (PCF) has also proved to be a novel platform for SA material integration [91]. By filling a 2D material into the hollow channels of a PCF, an SA can be formed, as shown in Figure 7G. This method provides a long interaction length between the 2D material and the light beam. Moreover, the PCF method also allows a greater contact area between the 2D material and light. This PCF fabrication method also normally has a very high damage threshold, which is useful for achieving high power output. This method solves the vulnerability problem of 2D materials in a unique way. However, a clear defect still exists. The greatest problem is the relatively large coupling loss between the PCF and the standard optical fiber, which normally results in a significant loss in the laser cavity. Also, a PCF is generally more expensive than standard optical fiber, which means that devices based on this type of SAs potentially have a higher cost.

3 Pulsed lasers based on various layered 2D materials

3.1 Solid-state lasers

The world's first laser was a solid-state laser [159]. Thus, solid-state lasers occupy a special position in the field of laser research. Generally, the active medium of a solid-state laser consists of a glass or crystalline "host" material, to which is added a "dopant" such as neodymium, chromium, erbium, thulium, or ytterbium. In order to achieve pulsed operation in a solid-state laser, a suitable SA is usually needed, which is the basis for the use of 2D materials in solid-state lasers. In this section, a brief review of the applications of layered materials in mode-locked and Q-switched solid-state lasers is provided.

3.1.1 Mode-locking operation

Mode locking is used to generate ultrashort pulses from lasers. An output coupler partially transmits a small fraction of the laser pulse out of the laser resonator equally

spaced by the resonator round-trip time. Typically, an intracavity loss modulator is used to collect the laser light in short pulses around the minimum of the loss modulation with a period given by the cavity round-trip time. Generally, much shorter pulses with passive mode locking can be obtained using an SA because the recovery of the absorber can be very fast, resulting in fast loss modulation.

As described in Section 2.3, the interaction between 2D materials and the laser beam is usually implemented in free space in the case of solid-state lasers. The SA is generally transferred directly onto the optical mirrors by deposition or spin-coating, forming a saturable absorption mirror (SAM), which is subsequently placed within the solid-state laser device to achieve mode-locking. A great deal of recent research effort has been directed toward the application of 2D materials in lasers, since 2D-material-based solid-state laser initially came into being and this activity has since grown rapidly. Graphene and graphene-like materials have been widely studied in solid-state lasers as SAs. To date, numerous mode-locked solid-state lasers using layered 2D materials such as graphene, TIs, TMDs, BP, and MXenes have been reported, as summarized in Table 2.

It can be seen that these lasers have excellent performance with respect to pulse width, repetition rate, and pulse energy. For example, researchers achieved femtosecond pulses from a mode-locked Cr^{2+}:ZnS laser based on graphene [175], and their results are shown in Figure 8A–C. A Yb:YAG laser based on WS_2 [150], a Nd:YVO_4 laser based on BP [181], and a Yb:KYW laser based on MXene [182] have also been investigated, as shown in Figure 8D–L.

In order to extend the lasing wavelength of a pulsed solid-state laser, various gain media have been used, including Nd:YAG [164, 166], Yb:KGW [163], Nd:$GdVO_4$ [165], Cr:forsterite [170], Tm:$YALO_3$ [173], Tm:CLNGG [172], Ti:sapphire [162], Tm:Lu_2O_3 [174], Cr:ZnS [175–177], Yb:GAGG [183], Cr:YAG [171], Nd:YVO_4 [178, 181], Yb:YAG [150], Yb:CYA [167], Tm:MgW [184], and Yb,Lu:CALGO [180]. Mode-locked solid-state lasers have been demonstrated beyond the 3-μm band. The various gain media and SA materials therefore provide a brand new approach for ultrafast solid-state laser research.

3.1.2 Q-switching operation

An SA may also produce Q-switching, where the laser emits bunches of mode-locked pulses, which may or may not have a stable Q-switching envelope. Q-switching

Table 2: Summary of mode-locked solid-state lasers based on layered 2D materials.

Layered 2D material	Method	Gain medium	Central wavelength (nm)	Rep. rate (MHz)	Pulse width (ps)	Pulse energy (nJ)	Output power (mW)	References
Graphene	SAM	Nd:YVO_4	531.7	71.4	0.374	1.6	117	[160]
		Alexandrite	740	5.56	0.065	1.4	/	[161]
		Ti:sapphire	800	99.4	0.063	480	/	[162]
		Yb:KGW	1031	86	0.428	5.9	504	[163]
		Nd:YAG	1064	88	4	/	100	[164]
		Nd:$GdVO_4$	1065	43	16	8.4	360	[165]
		Nd:YAG	1064	112	15.6	18	2	[166]
		Yb:$CYAlO_4$	1068	113/5	0.032	/	26.2	[167]
		Yb:YAG	1048	105.7	0.367	18.3	1930	[168]
		VECSEL	1030	1760	0.353	2.8	10.2	[169]
		Cr:forsterite	1240	74.65	0.094	/	230	[170]
		Cr:YAG	1516	85	0.091	/	107	[171]
		Tm:CLNGG	2018	99	0.729	/	60.2	[172]
		Tm:$YAlO_3$	2023	71.8	10	3.7	268	[173]
		Tm:Lu_2O_3	2067	110	0.41	2.45	270	[174]
		Cr:ZnS	1220–2408	112.22	2.4	7.8	880	[175]
		Cr:ZnS	2370	46	0.87	15.5	700	[176]
		Cr:ZnS	2370	108	0.041	2.3	250	[177]
WS_2	SAM	Yb:YAG	1057.5	86.7	0.736	/	270	[150]
MoS_2	SAM	Nd:YVO_4	1064.3	79.5	800	/	295	[178]
		Tm:LLF	1918	83.3	/	0.0415	583	[179]
BP	SAM	Yb,Lu:CALGO	1053.4	63.3	0.272	6.48	820	[180]
		Nd:YVO_4	1064.1	140	6.1	3.29	/	[181]
MXene	SAM	Yb:KYW	1053.2	64.06	0.316	12	770	[182]

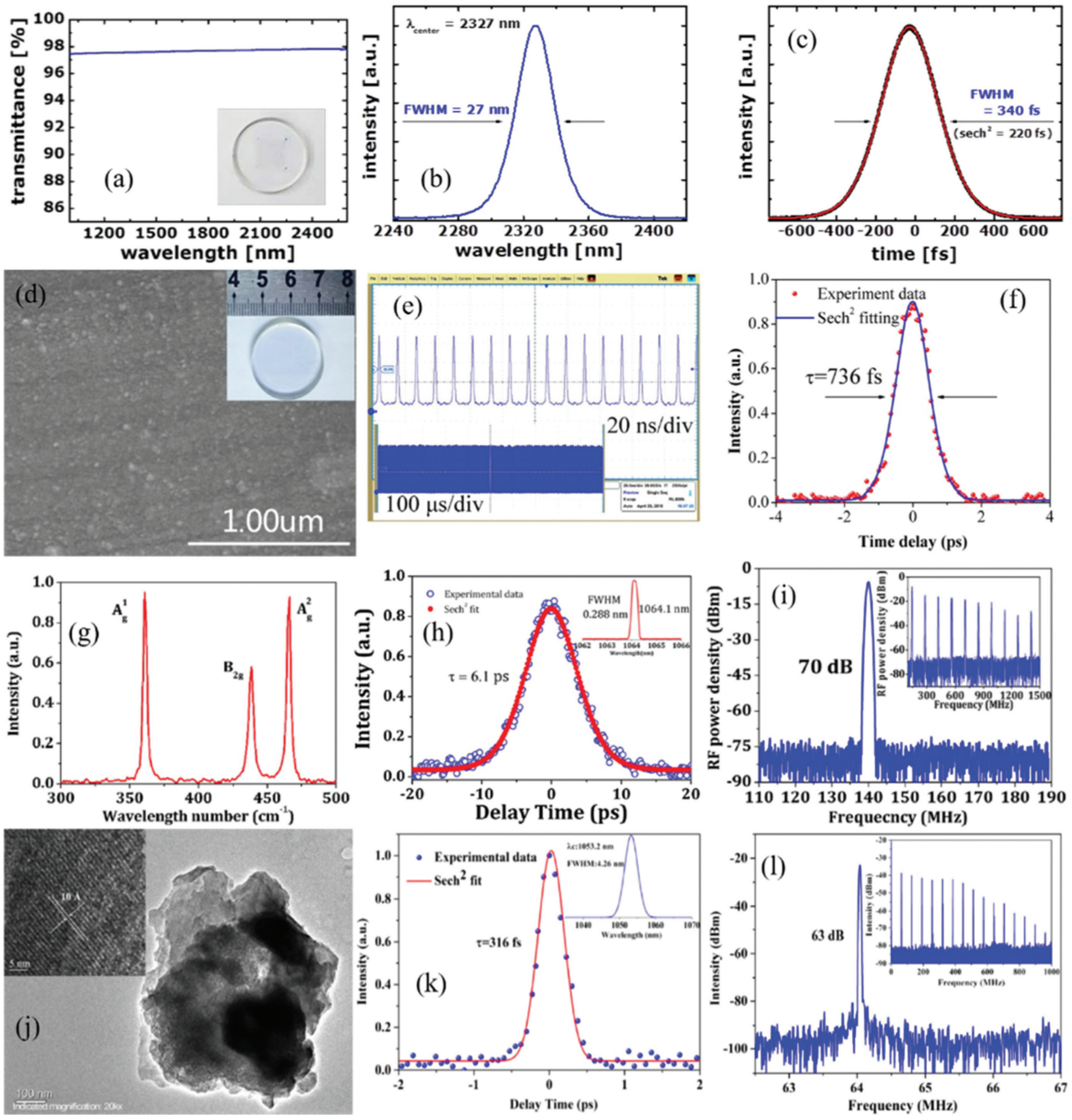

Figure 8: Mode-locked solid-state lasers with layered material-based SAs.
(A–C) Graphene. (A) Linear transmission and photo image of graphene SA (inset). (B) Optical spectrum. (C) Autocorrelation trace. Reproduced with permission from Ref. [175]. Copyright 2016, Optical Society of America. (D–F) WS_2. (D) SEM image of WS_2 film and image of the SiO_2 substrate (inset). (E) Pulse train. (F) Autocorrelation trace. Reproduced with permission from Ref. [150]. Copyright 2015, Optical Society of America. (G–I) BP. (G) Raman spectrum of BP. (H) Autocorrelation trace and optical spectrum (inset). (I) RF spectrum and wide-range RF spectrum (inset). Reproduced with permission from Ref. [181]. Copyright 2015, Optical Society of America. (J–L) MXene, $Ti_3C_2T_x$ (T=O, OH, or F). (J) TEM of MXene. (H) Autocorrelation trace and optical spectrum (inset). (I) RF spectrum and wide-range RF spectrum (inset). Reproduced with permission from Ref. [182]. Copyright 2018, Optical Society of America.

instabilities occur when the pulse energy temporarily increases because of noise fluctuations in the laser, which then further increases because of the stronger saturation of the SA. This is balanced by a stronger saturation of the gain. If the gain is not sufficiently saturated, then the pulse energy will increase further and self-Q-switching occurs.

In addition to their use in mode-locked lasers referred to above, layered materials have also been introduced into

Q-switched solid-state lasers to obtain pulses of high peak power. It is well established that layered materials have SA properties and can be used to make Q-switchers. On the basis of this, researchers have successfully fabricated a graphene Q-switcher and applied it to solid-state lasers to achieve Q-switched pulses [185], as shown in Figure 9A–C. Subsequently, Q-switched solid-state lasers were also realized using MoS_2 [186] and a TI [18]. These earlier efforts have greatly promoted the subsequent development of layered materials in Q-switched solid-state lasers.

Compared to mode-locked solid-state lasers, Q-switched solid-state lasers have high pulse energy ranging from microjoules to millijoules. Moreover, these Q-switched lasers have several distinct characteristics. First, they cover a very wide wavelength range from the visible to near-infrared and mid-infrared, that is, 0.6–3 μm. Second, multi-wavelength output has been realized as well as single-wavelength operation. As can be seen from Table 3, multi-wavelength Q-switched lasers at 1, 2, and 3 μm have appeared in recent years. Third, in order to compensate for the shortcomings of a single approach, researchers have also developed a hybrid Q-switching scheme that combines the layered-material-based Q-switcher with an active Q-switcher. A summary of Q-switched solid-state lasers based on layered 2D materials, including graphene, TIs, TMDs, BP, and MXenes, is included in Table 3.

Compared to Q-switched solid-state lasers, mode-locked solid-state lasers based on 2D materials are relatively few. For this, there are some reasons. One reason is the photothermal effect caused by the coupling between

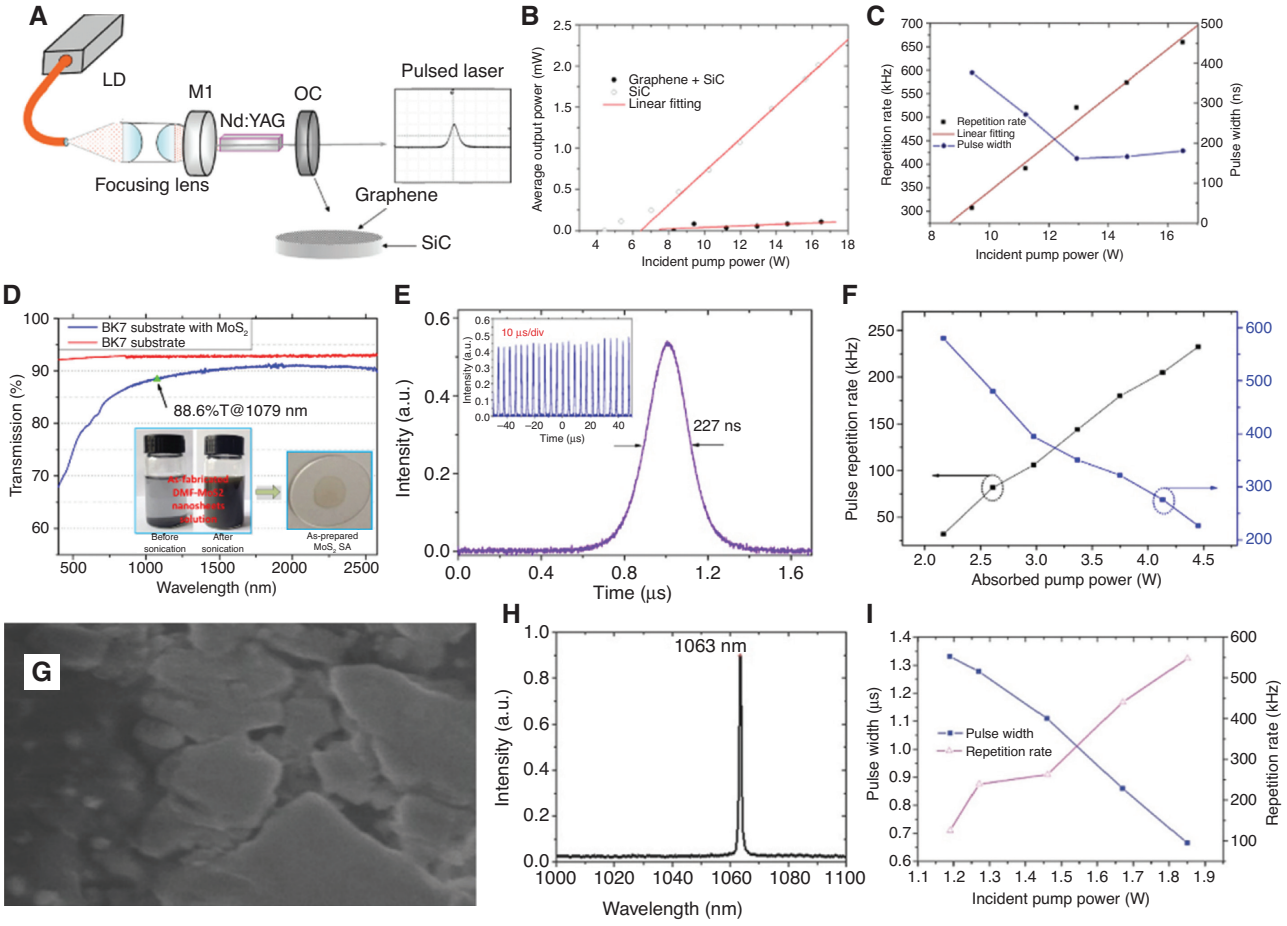

Figure 9: Q-switching solid-state lasers with layered material-based SAs.
(A–C) Graphene. (A) Experimental setup of Nd:YAG pulsed lasers based on graphene. (B) Output power versus incident pump power. (C) Repetition rate and pulse width versus incident pump power. Reproduced with permission from Ref. [185]. Copyright 2010, American Chemical Society. (D–F) MoS_2. (D) Transmission spectra of the blank BK7 and MoS_2-transferred BK7 glass substrates. (E) Single pulse profile of the Q-switched Nd:YAP laser and the pulse train (inset). (F) Evolution of the pulse repetition rate and the pulse width with the absorbed pump power. Reproduced with permission from Ref. [186]. Copyright 2014, Optical Society of America. (G–I) Bi_2Se_3. (G) TEM of Bi_2Se_3. (H) Optical spectrum. (I) Evolution of the pulse repetition rate and the pulse width with the absorbed pump power. Reproduced with permission from Ref. [18]. Copyright 2013. John Wiley and Sons.

Table 3: Summary of Q-switched solid-state lasers based on layered 2D materials.

Layered 2D material	Method	Gain medium	Central wavelength (nm)	Rep. rate (kHz)	Pulse width (ns)	Pulse energy (μJ)	Output power (mW)	References
Graphene	SAM	Nd:YAG	1064	660	161	0.1592	105	[185]
		Yb:YAG	1032	285	522	0.65	185	[187]
		Nd, Mg:$LiTaO_3$	1082/1092	133	176	2.75	365	[188]
		Nd:YAG	1123	46.8	1513.1	/	332	[189]
		Nd:$GdVO_4$	1340	43	450	2.5	260	[190]
		Er:YAG	1645	35.6	2340	7.05	251	[191]
		Ho:YAG	1907	64	2600	9.3	264	[192]
		Tm:$KLu(WO_4)_2$	1948	190	285	1.6	310	[193]
		Tm:YAG	2011	27.9	2080	1.74	38	[194]
		Cr:ZnSe	2400	154	157	1.66	256	[195]
Graphene oxide	SAM	Nd:$GdVO_4$	1063	704	105	3.2	2300	[196]
		Nd:YAG	1064	167	192	16.2	2700	[197]
		Nd:YAG	1064	92.9	523	/	/	[198]
Bi_2Se_3	SAM	Nd:$GdVO_4$	1063	547	666	58.5 nJ	32	[18]
		Nd:YVO_4	1066.6	135	0.25	0.56 nJ	/	[199]
		Nd:$LiYF_4$	1313	161.3	0.433	1.23 nJ	/	[200]
		Tm:LuAG	2027	118	0.62	18.4 nJ	/	[201]
Bi_2Te_3	SAM	Yb:$LuPO_4$	1014.5	1670	34	3 nJ	5020	[202]
		Tm:LuAG	2021.7	145.5	233	/	1740	[203]
MoS_2	SAM	Yb:$LuPO_4$	1020.8	429	83	4.8 nJ	/	[204]
		Nd:$GdVO_4$	1902	48.09	2	2.08 nJ	/	[205]
		Tm:CLNGG	1979	110	6	0.72 nJ	/	[206]
		Er:Lu_2O_3	2840	121	0.335	8.5 nJ	/	[207]
WS_2	SAM	Nd:YVO_4	1064	135	2.3	0.145 nJ	/	[208]
		Nd:YVO_4	1064	135	2300	0.145	19.6	[209]
		Nd:YVO_4	1064	10	0.81	/	233	[210]
		Er:Y_2O_3	2710–2740	29.4	720	7.92	/	[211]
BP	SAM	Yb:CYA	1046	113.6	0.62	0.3257 nJ	/	[212]
		Er:YAG	1645	40	3.2	2.15	/	[213]
		Er:YAG	1645	40	2.9	2.4	/	[213]
		Nd:YVO_4	1064.4	/	2.86	0.166	/	[214]
		Tm:YAP	1988	19.25	1.78	7.84 nJ	/	[215]
		Ho^{3+}, Pr^{3+}:$LiLuF_4$	2950	158.7	0.1943	2.4 nJ	/	[216]
WSe_2	SAM	Tm, Ho:LLF	2950	89.3	571	1.65	147	[217]
ReS_2	SAM	Pr:YLF	640	520	160	/	52	[218]
		Nd:YAG	1064	644	139	/	120	
		Tm:YAP	1991	677	415	/	245	
SnSe2	SAM	Nd:YAG	1300	/	323	0.61	/	[219]
		Tm:YLF	1900	/	716	2.07	/	
$MoTe_2$	SAM	Tm:$CaYAlO_4$	1941	70.9	690	10.58	750	[220]
$PtSe_2$	SAM	Tm:YAP	1987	58	244	24.3	/	[221]
$ReSe_2$	SAM	Er:YAP	2730/2800	244.6	202.8	2.2	/	[222]

light and materials. As shown in Figure 3, 2D materials are normally transferred on a plain substrate when used in solid-state lasers, which makes it difficult to overcome the shortcomings due to the photothermal effect. When the photothermal effect accumulates, the SA gets irreparably damaged. This limits not only the ability to mode-lock but also the overall device performance. Another reason is that in the solid-state laser cavity it is difficult to adjust the dispersion in the absence of a prism pair and a chirped mirror. Normally, in order to ensure mode-locked pulsed operation by the SA device, unnecessary components should not be used in the cavity. On the contrary, Q-switched pulsed laser operation is relatively easily achieved, which is confirmed by the results provided in Table 3.

3.2 Fiber lasers

A fiber laser is a laser fabricated using a glass fiber doped with a rare-earth element as the gain medium. In the

context of photonic devices for telecommunications and sensing, the fiber laser has seen significant development due to its excellent beam quality, high efficiency, capability to rapidly radiate heat (due to miniature dimensions), compact structure, and high reliability. Fiber laser also has great development potential in industrial production and currently has a large market share [223]. In order to obtain the output pulses, two pulse-shaping mechanisms, namely mode-locking and Q-switching, are mostly used, which provides great opportunity for SA materials to be adopted in a pulse-shaping device. Over the past decade, SAs made of layered materials have been widely used in passively mode-locked/Q-switched lasers, and significant results have been achieved [106, 128, 147, 224–227]. In this section we give a brief review of the research history and recent achievements with respect to fiber lasers based on layered 2D materials.

3.2.1 Mode-locking operation

Graphene was initially studied as an SA to achieve an ultrafast fiber laser in 2009 by different groups from the Nanyang Technological University and Cambridge University [9, 13, 14, 228]. For example, large-energy pulse generation was observed in an erbium-doped fiber laser passively mode-locked with atomic layer graphene [14]. Stable mode-locked pulses with single pulse energy of up to 7.3 nJ and pulse width of 415 fs have been directly generated from the laser, as shown in Figure 10. Their findings suggest that graphene has SA properties, which can also be used for ultrafast optical applications. This indicated that grapheme forms the basis of an excellent pulse-shaping device with a wide operation range and fast response due to its zero bandgap and ultrafast carrier dynamics [14]. In addition, compared to traditional SAs (SESAMs and CNTs), graphene does not require bandgap optimization and diameter or chiral adjustment, thus greatly simplifying the preparation process. With these advantages, graphene and its derivatives, such as graphene oxide, reduced graphene oxide, and graphene composite materials, have been widely developed for uses in mode-locked fiber lasers [9, 77, 85, 229–263]. A brief summary of mode-locked fiber lasers based on layered 2D materials is included in Table 4. In terms of the performance of these mode-locked lasers based on graphene, some exciting results have been obtained, including the minimum pulse width and maximum output power of 29 fs [296] and 174 mW [310], respectively. For TIs, the corresponding figures were 128 fs [329] and 45.3 mW [324], for TMDs they

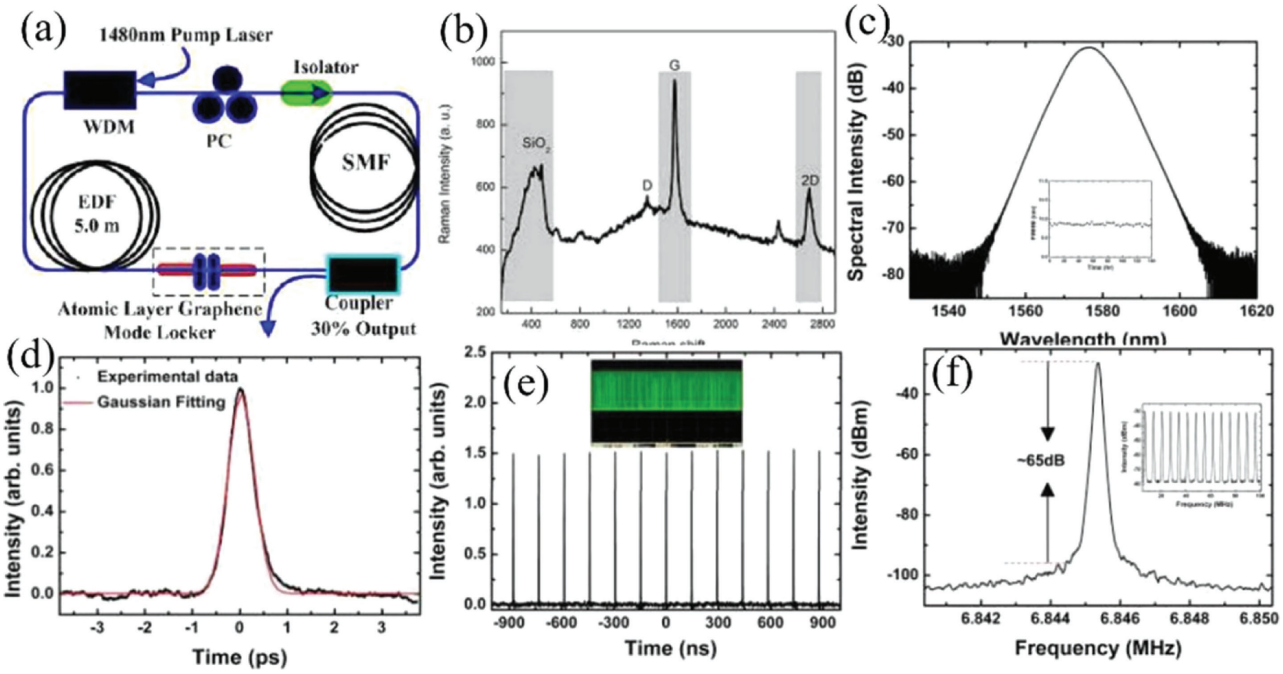

Figure 10: Mode-locked fiber lasers with graphene SA at the 1.55-μm region.
(A) Schematic of the fiber laser. (B). Raman spectra of the graphene film. (C) Optical spectrum. (D) Autocorrelation traces of the pulses. (E) Oscilloscope trace of the single pulse emission. Inset: pulse train of CW mode-locking in millisecond time scale. (F) Fundamental radio frequency (RF) spectrum of the laser output. Inset: wideband RF spectrum up to 100 MHz. Reproduced with permission from Ref. [14]. Copyright 2009, American Chemical Society.

Table 4: Summary of mode-locked fiber lasers based on layered 2D materials.

Gain medium	Layered 2D material	Method	Central wavelength (nm)	Rep. rate (MHz)	Pulse width (ps)	Pulse energy (nJ)	Output power (mW)	References
YDF	Graphene	Sandwiched	1180	0.4	200 ns	/	/	[264]
			1035	16.29	6500	0.81	/	[265]
			1069.8	0.9	580	0.41	0.37	[266]
		Tapered fiber	1031.43/1034.94/1038.43	0.5515	74.6	6.4	3.53	[267]
			1061.8/1068.8	1.78	4.23	1.713	3.05	[268]
		Super-capacitor	1255	4.54	0.084	/	/	[255]
	Graphene oxide	Sandwiched	1029.5	/	190	/	/	[269]
			1064.9	2.99	520	159.4	147.8	[270]
			1029	/	191	/	539	[271]
			1056.5/1062.3/1069.5	14.2	/	/	/	[272]
	Bi_2Se_3	Sandwiched	1040	16	380	1.06	17.1	[273]
		Sandwiched	1031.7	44.6	47	0.756	/	[20]
	Bi_2Te_3	HC-PCF	1065.4	28.73	575.8	/	/	[274]
	Sb_2Te_3	D-shaped fiber	1036.7	19.28	5.3	/	4	[275]
			1065.3	19.28	5.9	0.81	/	[275]
	MoS_2	Sandwiched	1054.3	6.58	800	/	9.3	[276]
			1029.78	22.44	13.8	1.54	34.6	[277]
		Microfiber	1042.6	6.74	656	/	2.37	[278]
	SnS_2	Sandwiched	1062.66	39.33	656	/	2.23	[28]
		D-shaped fiber	1031	3.759554	282	/	/	[279]
	InS	Sandwiched	1033.3/1038.4	1.02	486.7	/	1.91	[280]
	PtS2	Sandwiched	1072	11.2	/	/	/	[281]
	WS_2	D-shaped fiber	1052.45	23.26	0.713	1.29	/	[282]
			1063.6	630	5.57	13.6	/	[283]
	BP	Sandwiched	1085.5	13.5	7.54	/	80	[284]
		Microfiber	1064.4	16.77	51	1.13	18.9	[285]
	MoC_2	Sandwiched	1061.8	3.23	418	/	/	[286]
	MXene	D-shaped fiber	1065.89	18.96	480	0.47	9	[106]
EDF	Graphene	Sandwiched	1565	42.8	0.19	0.09	0.4	[235]
			1560.5	2.22 GHz	0.9	/	9.6	[238]
			1557	114.1	0.57	/	/	[240]
			1532	5.27	0.85	/	/	[233]
			1566	6.22	0.88	/	/	[77]
			1559	19.9	0.463	/	/	[228]
			1555	27.4	0.174	0.044	1.2	[230]
			1570–1600	6.95	1.08	/	/	[287]
			1589.68	6.95	0.694	3	13.1 dBm	[13]
			1576.3	6.84	0.415	7.3	/	[14]
			1565	1.79	0.756	/	2	[9]
			1576	10.9	3.2	/	4.8 dBm	[231]
			1572.6	91.5	/	/	/	[234]
			1525–1559	8	1	0.125	1	[288]
			1570–1600	/	70	/	/	[289]
			1570–1600	1.5	49	2.3	/	[45]
			1564	19.3	0.87	0.0104	/	[265]
			1560	54.9	0.81	/	1	[290]
			1560	490	0.97	/	/	[291]
			1564	57.96	0.315	0.033	1.9	[292]
			1561	5.5	1.23	20	3	[237]
			1550	332.5	600	/	/	[293]
			1556–1560	46.126	0.57	0.0228	/	[294]
			1562	/	/	/	/	[295]
			1561.4	9.9	1	1	10.5	[256]
			1550	18.67	0.029	2.8	52	[296]

Table 4 (continued)

Gain medium	Layered 2D material	Method	Central wavelength (nm)	Rep. rate (MHz)	Pulse width (ps)	Pulse energy (nJ)	Output power (mW)	References
			1560	28.5	1.027	0.24	2.9	[262]
			1557	48.14	0.216	/	1.3	[297]
			1545	21.15	0.088	0.071	1.5	[297]
			1560	25.8	0.364	2	15	[253]
			1574	/	0.33	/	/	[251]
			1560	8.22	1.12	/	/	[298]
			1533.4	8.4	0.9	1.38	11.63	[299]
			1556.1	9.1	0.94	1.57	14.27	
		Microfiber	1565	33	0.494	/	/	[257]
			1545.5–1550	27	14	/	/	[241]
			1557.56	3.33	15.7	1.26	4.2	[264]
			1559	312.5	0.679	/	/	[300]
			1555	/	0.765	/	/	[301]
			1550	111.7	2.32	1.34	3	[302]
			1559.74/1560.54	100 GHz	1.63	/	/	[303]
			1550	/	3.5	/	/	[304]
			1531.3	1.89	1.21	/	0.45	[305]
			1530/1531.5/ 1533/1534.5	8.034	8.8	4.06	32.6	[306]
		D-shaped fiber	1561.6	6.99	1.3	7.25	/	[229]
			1560	14.64	0.78	/	/	[307]
			1558.2	4.77	1.07	3.08	/	[263]
			1607.7	37.7	0.377	/	/	[308]
			1557	12.29	0.256	/	/	[309]
			1565	16.99	13.8	10.2	174	[310]
			1563	11.53	0.713	/	/	[249]
		F-P cavity	1562	9.67 GHz	0.865	/	/	[239]
		PCF	1567.6	25	0.65	/	/	[311]
	Graphene oxide	Sandwiched	1560	/	0.7505	/	/	[269]
			1565.9	37.2	0.613	0.0223	0.83	[312]
			1561.8	62.2	0.735	/	0.82	[313]
			1559	40.15	0.9538	/	0.299	[314]
			1559.6	22.7	1.5	/	1	[250]
		Silica film	1558	58	0.39	0.0337	92	[244]
		PCF	1561.2	7.68	4850	0.56	4.3	[236]
		SAM	1531	19.5	11	1.2	23.3	[315]
			1555.92	48.2	0.502	/	2.7	[259]
	Reduced graphene oxide	Microfiber	1564.6/1567.4	7.9	/	/	8	[316]
	Bi_2Se_3	Sandwiched	1557.5	12.5	0.66	/	1.8	[317]
			1547.6–1548.4/ 1549.2–1550/ 1551.4–1552.2	8.95	30	1.12	/	[318]
			1567.2/1568/ 1568.8/1569.2	8.83	22	1.1	/	[319]
			1561.6/1562.1	3.54	13.6 ns	2.824	/	[320]
		SAM	1557–1565	1.21	1.57	/	/	[16]
		Microfiber	1560.88	3.125 GHz	1.754	4.5 pJ	6.4	[321]
	Bi_2Te_3	D-shape fiber	1547	15.11	0.543	/	/	[322]
			1555.9	773.85	0.63	/	1.4	[323]
		SAM	1554–1564	1.21	1.21	/	/	[15]
		Microfiber	1558.5	2.04 GHz	2.49	/	5.02	[17]
			1564.1	2.95 GHz	0.92	/	45.3	[324]
			559.4/1557.7	239/388	1.3	/	/	[22]
		Sandwiched	1557	8.635	1.08	/	0.25	[325]

Table 4 (continued)

Gain medium	Layered 2D material	Method	Central wavelength (nm)	Rep. rate (MHz)	Pulse width (ps)	Pulse energy (nJ)	Output power (mW)	References
			1548–1570	10.71	4.5	2.8	/	[155]
	Sb_2Te_3	Sandwiched	1558.6	4.75	1.8	/	0.5	[326]
			1558.2	304	2.2	/	4.5	[327]
		D-shape fiber	1568.8	33.07	0.195	/	9	[328]
			1565	22.32	0.128	0.0448	/	[329]
			1558	25.38	0.167	0.21	.	[67]
		Microfiber	1561	34.5	0.27	/	1	[330]
	MoS_2	Sandwiched	1568.9	8.288	1.28	/	5.1	[331]
			1569.5	12.09	0.71	/	1.78	[332]
			1557	15.67	581	0.613	9.6	[333]
		D-shaped fiber	1560	14.53	0.2	/	3	[334]
			1568	26.02	4.98	0.08	/	[335]
		Microfiber	1558	2.5 GHz	3	/	5.39	[336]
			1596	3.63	171	/	1.8	[337]
			1594	1.6077	1.65	/	0.35	
			1595	1.3152	2.5	/	/	
	WS_2	Microfiber	1561	24.93	0.369	/	1.93	[338]
			1558.5	19.58	0.675	/	0.625	[339]
			1540	135	0.067	/	/	[340]
			1557	8.86	1.32	/	110	[24]
			1557	460.7	0.66	6.23	/	[151]
			1558.5/1566	8.83	0.585	1.14	/	[341]
			1568.55/1569	2.14	11	6.64	/	[342]
		Sandwiched	1568.3	0.487	1.49	/	62.5	[343]
	$MoSe_2$	Sandwiched	1558.25	8.028	1.45	/	0.4	[344]
		D-shaped fiber	1557.3	3.27 GHz	0.688	/	22.8	[345]
	$MoTe_2$	Sandwiched	1561	5.26	1.2	/	/	[346]
		Microfiber	1559.57	26.6	0.229	2.14	57	[347]
	WSe_2	Microfiber	1556.42	14.02	0.477	/	/	[348]
	WTe_2	D-shaped fiber	1556.2	13.98	0.77	/	0.04	[126]
	SnS_2	Sandwiched	1560	29.6	152	0.48	14.2	[349]
			1536.7/1562.6	2.1	5.3	11.5	24.4	[157]
		D-shaped fiber	1561	4.397604	1.63	/	/	[279]
	ReS_2	Sandwiched	1558	5.48	1.6	/	0.4	[124]
		Microfiber	1563.3	1.78	3.8	/	/	[350]
	In_2Se_3	Sandwiched	1532.5	0.5863	389.2 ns	20.4	11.96	[351]
		Microfiber	1565	40.9	0.276	2.03	83.2	[352]
	TiS_2	Sandwiched	1569.5	5.34	1.04	5.05	/	[128]
		Microfiber	1563.3	22.7	0.812	25.3 pJ	/	[129]
	PtS_2	Sandwiched	1572	15.04	2.1	/	1.1	[281]
	$PtSe_2$	D-shaped fiber	1567.07	8.24	0.861	/	/	[353]
		Microfiber	1563	23.3	1.02	0.53	/	[354]
	BP	Sandwiched	1571.45	5.96	0.946	/	/	[354]
			1558.7	0.786	14.7	/	/	[32]
			1560.5	28.2	0.242	/	0.5	[355]
			1562	12.5	0.635	/	/	[356]
			1555	23.9	0.102	0.071	1.7	[357]
			1562	5.426	1.236	/	/	[358]
			1545–1579	60.5	0.28	/	/	[359]
			1557.2/1557.7/1558.2	1.65	9.41	/	/	[360]
			1533/1558	20.8	/	/	/	[361]
		Microfiber	1575.1	34.27	0.437	0.055	1.9	[285]
			1532–1570	4.69	0.94	/	5.6	[33]
			1569.24	60.5	280	/	/	[359]

Table 4 (continued)

Gain medium	Layered 2D material	Method	Central wavelength (nm)	Rep. rate (MHz)	Pulse width (ps)	Pulse energy (nJ)	Output power (mW)	References
	MXene	D-shaped fiber	1557	15.4	0.66	/	0.05	[37]
			1555.01	7.28	159	0.041	3	[106]
TDF	Graphene	Sandwiched	1940	6.46	3.6	0.4	2	[362]
			1953.3	16.937	2.1	0.08	130	[363]
			1884	20.5	1.2	/	1.35	[364]
			1930.3	0.964	122	35.3	/	[365]
			1945	58.87	0.2	0.22	13	[366]
			2060	20.98	0.19	2.55	54	[367]
		D-shaped fiber	1910	19.31	0.773	6	115	[368]
		Microfiber	1880–1940	19.7	1.9	/	1.96	[369]
	Graphene Oxide	Sandwiched	1961.6	27.37	1.36	/	/	[312]
	Bi_2Te_3	D-shaped fiber	1935	27.9	0.795	0.72	/	[370]
		Microfiber	1909.5	21.5	1.26	/	/	[21]
	MoS_2	SAM	1905	9.67	843	15.5	/	[148]
	WS_2	D-shaped fiber	1941	34.8	1.3	0.0172	/	[342]
	SnS_2	D-shaped fiber	1910	1.987646	/	/	/	[279]
	WSe_2	Microfiber	1886.22	11.36	1.18			[348]
	$MoTe_2$	Microfiber	1934.85	15.37	1.3	13.8	212	[347]
			1930.22	14.353	0.952	2.56	36.7	
	In_2Se_3	Microfiber	1932	15.8	1.02	7.1	112.4	[352]
	WTe_2	Microfiber	1915.5	18.72	1.25	2.13	/	[91]
	WSe_2	Microfiber	1863.96	11.36	1.16	/	32.5	[371]
	BP	Sandwiched	1910	36.8	0.739	0.0407	1.5	[35]
			2094	29.1	1.9	0.379	11	[372]
HDF	Graphene	Sandwiched	2066.8	38	1.97	1.2941	44	[373]
Er^{3+}-ZBLAN	Graphene	Sandwiched	2784.5	25.4	42	0.7	100	[374]
	BP	SAM	2783	24	42	25.5	/	[375]
			3489	28.91	/	/	40	[376]
		Sandwiched	2771.1	27.4	/	/	/	[377]
Ho^{3+}/Pr^{3+}-ZBLAN	BP	SAM	2866.7	13.987	8.6	6.2	/	[377]

were 67 fs [340] and 212 mW [347], and for BP they were 102 fs [357] and 80 mW [284], respectively.

In addition to its basic sandwiched structure, graphene is well suited for integration with microstructured optical fibers (tapered fibers, side-polished fibers, or photonic crystal fibers) and all constitute effective methods to fabricate graphene mode-lockers. These developments have served to deepen the understanding of graphene and to encourage the development of mode-locked lasers. Nevertheless, graphene also shows some weaknesses in laser applications. For example, it is known that graphene has no bandgap and its optical modulation depth is very weak (≈2.3%/layer), which limits its application in tunable operation and in situations requiring strong laser-material interaction [3, 70, 114, 378]. In order to find new layered 2D materials better than graphene, researchers have devoted a great deal of energy in exploring more new materials. As new layered graphene-like materials, TIs have been discovered with an energy band structure of symmetry Dirac cone due to their strong spin-or bit interaction, which implies that they can be developed into a new kind of SAs [18, 100]. TIs were also confirmed as possessing excellent nonlinear optical properties and were used as SAs for demonstrating the ultrafast fiber laser in 2012 [15], as shown in Figure 11A–D.

TIs have a nonzero bandgap and a large modulation depth (up to 95%), which are beneficial for improving the performance of mode-locked fiber lasers. Various mode-locked fiber lasers based on Tis, including Bi_2Se_3 [16, 20], Bi_2Te_3 [21, 110, 322], and Sb_2Te_3 [67, 147], have been developed, as shown in Table 4. These results indicate that, in addition to their established attractive electrical and thermal properties, TIs also have attractive application prospects for nonlinear photonics.

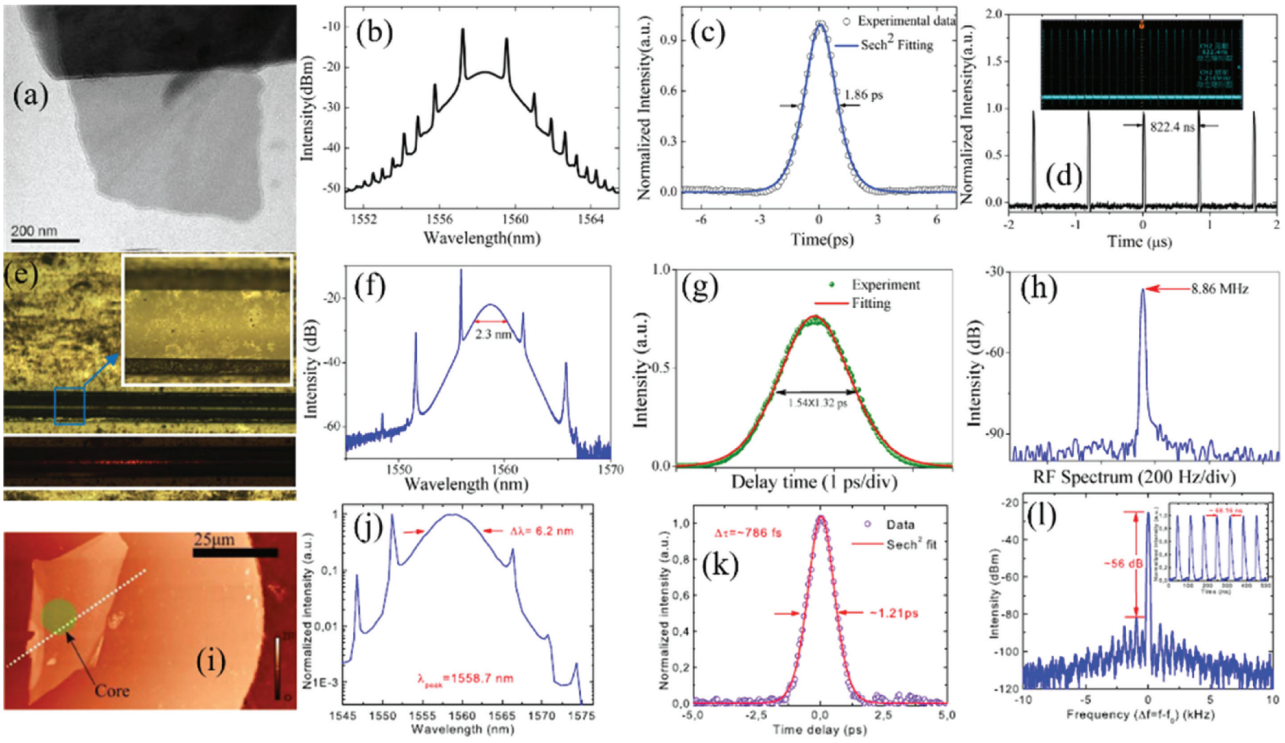

Figure 11: Mode-locked fiber lasers with various SAs at the 1.55-μm region.
(A–D) Bi_2Te_3. (A) TEM images of the Bi_2Te_3. (B) Optical spectrum. (C) Autocorrelation traces. (D) Pulse train. Reproduced with permission from Ref. [15]. Copyright 2012, American Institute of Physics. (E–H) WS_2. (E) Photograph of the D-shaped fiber coated with WS_2. (F) Optical spectrum. (G) Autocorrelation traces. (H) RF spectrum. Reproduced with permission from Ref. [24]. Copyright 2015, Springer. (I–L) BP. (I) AFM image of transferred BP film on the fiber end. (J) Optical spectrum. (K) Autocorrelation traces. (L) RF spectrum and wide-range RF spectrum (inset). Reproduced with permission from Ref. [32]. Copyright 2015, Springer.

TMDs represent a broad range of emerging nonlinear optical materials that cover a broad range of the transition-metal elements. Layered TMDs possess a direct bandgap, making their nonlinear optical performance dramatically better than those of their bulk counterparts. The different direct bandgap values of various TMDs mean that it is possible choose different TMDs to meet the specific demand of lasing wavelengths [114]. Among these materials, layered MoS_2 was first studied. In 2013, the SA behavior of few-layer MoS_2 was initially observed [102]. In 2014, another group of researchers identified its broadband SA properties and applied it to fiber lasers, realizing soliton mode-locking [276]. These findings have greatly promoted the development of few-layer MoS_2 in mode-locked lasers, leading to significant progress in this area.

Layered WS_2 also has a direct bandgap and exhibits excellent nonlinear optical properties. For example, researchers have demonstrated soliton mode-locked fiber lasers by transferring layered WS_2 onto a D-shaped fiber, which uses the interaction between the evanescent field and WS_2 to promote the nonlinear SA of WS_2 [282], as shown in Figure 10E–H. Following the success of MoS_2 and WS_2, a wide range of layered TMD materials have emerged and have been investigated, including $MoSe_2$ [68, 344, 379, 380], WSe_2 [76, 120, 153, 371], $MoTe_2$ [220], WTe_2 [91, 126, 127], SnS_2 [28, 121, 123, 349], $SnSe_2$ [123], ReS_2 [124], TiS_2 [128], In_2Se_3 [381, 382], etc. They are also summarized in Table 4. It is worth noting that the number of layers (including oxidative and defective surfaces) of the layered TMDs does not degrade their SA performance. For example, researchers have achieved a femtosecond mode-locked laser using SnS_2, which has a bandgap of 2.4 eV [279]. These studies indicate that, as with graphene and TIs, TMDs represent significant and promising layered 2D materials for mode-locked lasers.

It is abnormal that some 2D materials have been successfully incorporated into mode-locked fiber lasers whose central wavelengths are beyond the bandgap of these materials. Among the numerous 2D materials, SnS_2 is selected to illustrate this abnormal optical phenomenon as a typical case because of its relatively large direct bandgap of 2.24 eV. SnS_2 has been used to prove that mode-locked pulsed operation can be achieved from 1.0 to 2.0 μm [28, 105, 330, 357]. For a 1.55-μm pulsed laser [105], the photon energy of the laser is about 0.8 eV, which is smaller than the bandgap of SnS_2. The SA of SnS_2 is, therefore, due not to the direct bandgap but to sub-bandgap absorption. It is

widely known that no sub-bandgap absorption exists in perfect crystals. However, sub-bandgap absorption at low photon energy can be widely obtained, which is mostly due to the energy level within the bandgap arising from the edge states in a finite system. Sub-bandgap SA phenomena have appeared in many reports on ultrafast fiber lasers based on WS_2 [24, 322] and MoS_2 [131] SAs. The SA of SnS_2 and the experimental results obtained in this work have confirmed the existence of sub-bandgap absorption, which originates from atomic defects in SnS_2.

Since 2014, BP, a new layered 2D material, has attracted worldwide attention primarily due to its narrow bandgap, which can bridge the void between zero-bandgap graphene and wide-bandgap TMDs. This development has important applications in the near- and mid-infrared range [29, 30, 383, 384] photonic devices. The bandgap of BP can be adjusted by the number of its layers, which offers great flexibility for many practical applications. The number of layers can be controlled according to the demand of the bandgap. Its lattice is composed of two atomic layers, each of which consists of a twisted chain of phosphorus atoms. This unique feature makes it easy for BP to combine with many atmospheric molecules and biomolecules, and hence it

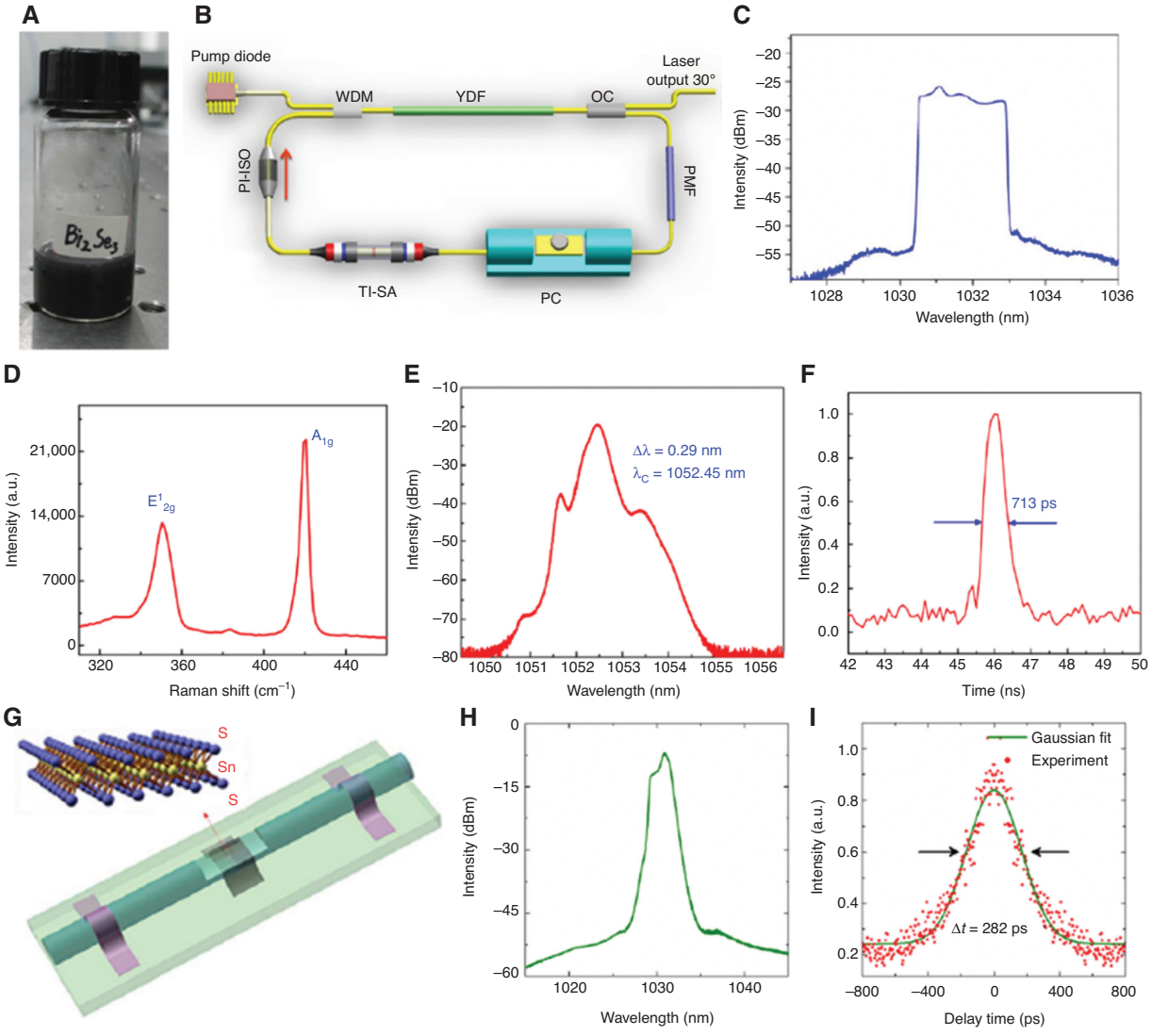

Figure 12: Mode-locked fiber lasers with various SAs at the 1.0-μm region.
(A–C) Bi_2Te_3. (A) Solution of Bi_2Te_3. (B) Schematic of the fiber laser. (C) Optical spectrum. Reproduced with permission from Ref. [20]. Copyright 2014, Optical Society of America. (D–F) WS_2. (D) Raman spectrum of WS_2. (E) Optical spectrum. (F) Pulse profile. Reproduced with permission from Ref. [282]. Copyright 2015, Optical Society of America. (G–I) SnS_2. (G) Schematic diagram of SDF; inset: crystal structure of monolayer SnS_2. (H) Optical spectrum. (I) Autocorrelation traces. Reproduced with permission from Ref. [279]. Copyright 2017, American Institute of Physics.

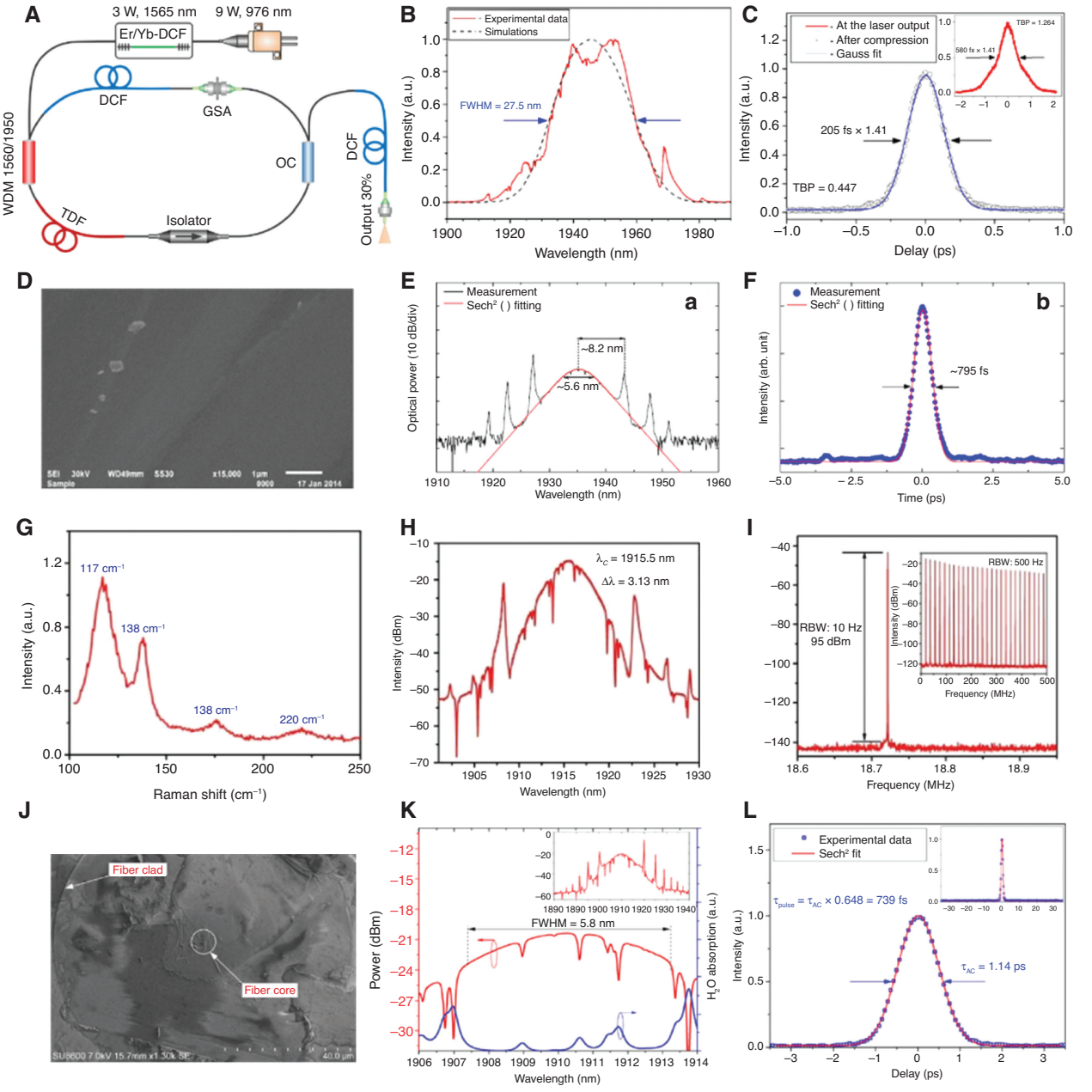

Figure 13: Mode-locked fiber lasers with various SAs at the 2.0-μm region.
(A–C) Graphene. (A) Schematic of fiber laser. (B) Optical spectrum. (C) Autocorrelation traces. Reproduced with permission from Ref. [366]. Copyright 2017, Optical Society of America. (D–F) Bi_2Te_3. (D) TEM of Bi_2Te_3. (E) Optical spectrum. (F) Autocorrelation traces. Reproduced with permission from Ref. [21]. Copyright 2014, Optical Society of America. (G–I) WTe_2. (G) Raman spectrum of WTe_2. (H) Optical spectrum. (I) Autocorrelation traces and pulse train (inset). Reproduced with permission from Ref. [91]. Copyright 2017, Optical Society of America. (J–L) BP. (J) SEM image of the fiber connector end facet with marked fiber cladding and core. (K) Optical spectrum. (L) Autocorrelation traces. Reproduced with permission from Ref. [35]. Copyright 2015, Optical Society of America.

has a great potential for many application fields within physics, chemistry, biology, and energy [132, 385–387]. BP was initially identified as a viable ultrafast photonic material in 2015. Also, researchers found the SA characteristics of BP in the wavelength range of 1.55 μm, and quickly applied it to pulsed fiber lasers [32], as shown in Figure 11I–L. This work has attracted great attention from many research groups and has resulted in many significant findings [355–357], as shown in Table 4. These findings have not only enriched the understanding of the nonlinear optical properties of BP but also identified several suitable applications for it, which in turn have greatly promoted the simultaneous development of advanced materials and laser photonics.

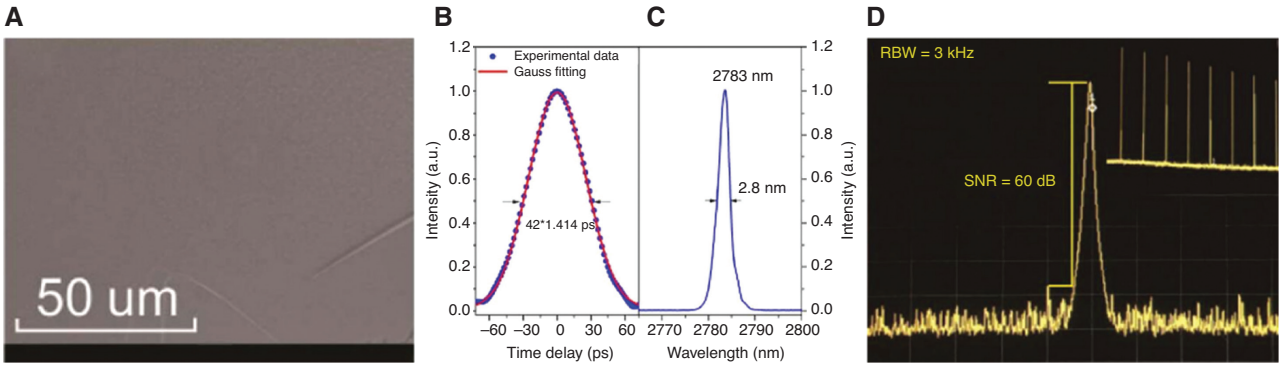

Figure 14: Mode-locked fiber lasers with various SAs at the 2.8-μm region based on BP.
(A) SEM of BP. (B) Autocorrelation traces. (C) Optical spectrum. (D) RF spectrum and wide-range RF spectrum (inset). Reproduced with permission from Ref. [375]. Copyright 2016, Optical Society of America.

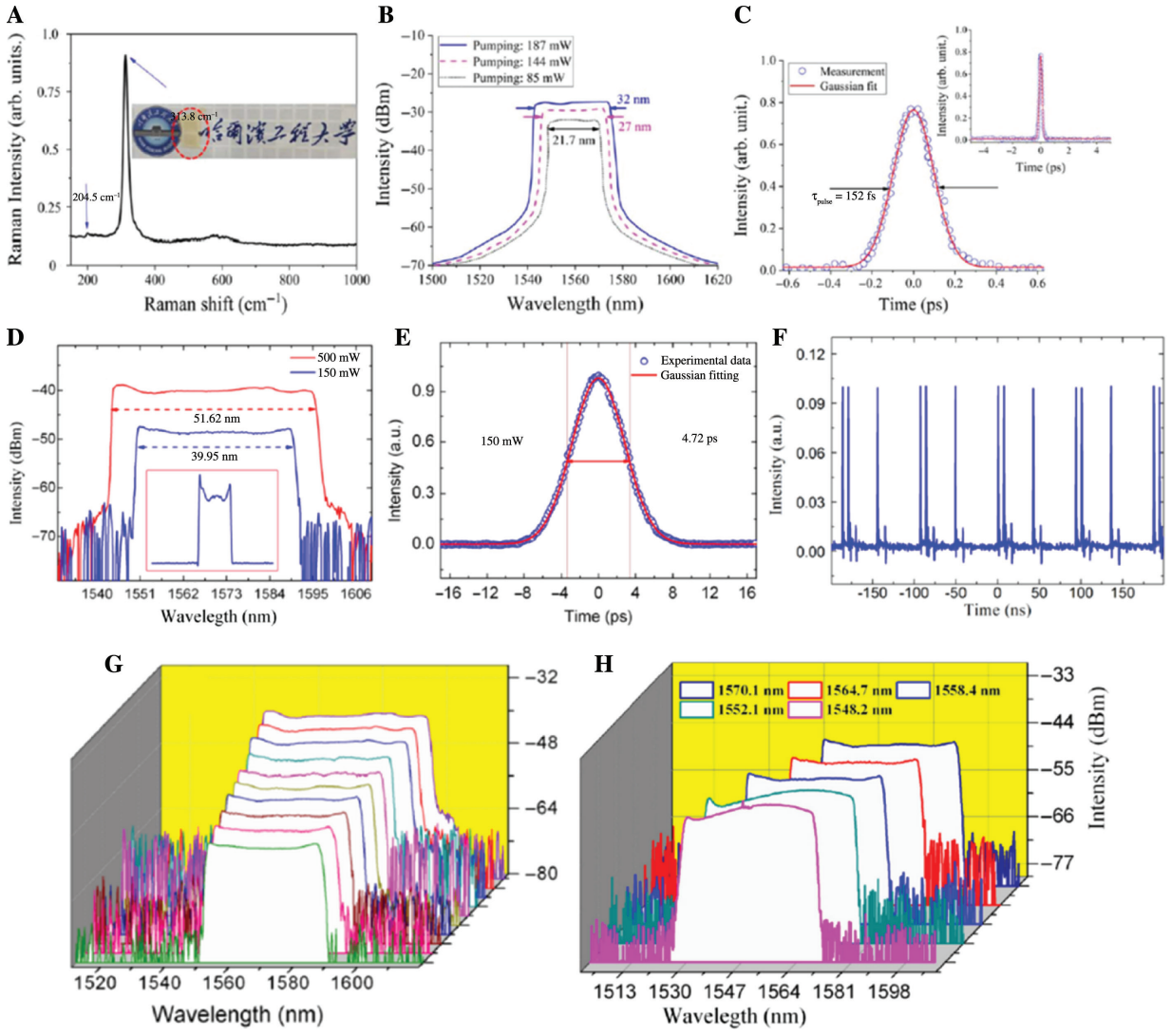

Figure 15: High-performance mode-locked fiber lasers with various SA.
(A–C) SnS_2. (A) Raman spectrum of SnS_2 and image of the SnS_2-PVA film (inset). (B) Optical spectrum. (C) Autocorrelation traces. Reproduced with permission from Ref. [349]. Copyright 2019, The Japan Society of Applied Physics. (D–H) TI. (D) Optical spectra. (E) Pulse profile. (F) Multi-pulse state with three pulses. (G) The evolution of dissipative solitons pulse spectra with different pump powers. (H) Wavelength-tunable optical spectra. Reproduced with permission from Ref. [155]. Copyright 2015, Optical Society of America.

The Er-doped silica fiber laser is the most widely recognized and studied fiber laser. In addition to this, 1-, 2-, and 3-μm pulsed lasers using layered materials, such as graphene, TIs, TMDs, and BP, have also been successfully developed. For these mode-locked lasers, some exciting results have already been achieved. Some of these fiber lasers are shown in Figures 12–14, and these have strongly promoted the development of pulsed lasers operating at various wavelength regions and extended ultrafast photonics applications of layered 2D materials.

In addition to the achievements mentioned above, mode-locked fiber lasers based on layered materials have greatly improved in terms of pulse energy, repetition rate, and operation in the mid-infrared waveband. The sum of these individual improvements provides for a better understanding of potential future applications of layered materials in fiber lasers. For a long time, the realization of mode-locked lasers of high pulse energy has been a hot topic in the field of ultrafast photonics due to their potential applications in optical frequency measurement, optical sensing, and information storage. To this end, researchers have proposed and developed several kinds of high-energy pulses, such as dissipative solitons, self-similar pulses, rectangular pulses, and noise-like pulses. Among them, dissipative solitons have attracted special attention because their pulse energy may be several orders of magnitude higher than that of conventional solitons. Thereafter, dissipative soliton fiber lasers using layered materials, including graphene [266, 270, 289, 310, 316, 388], graphene oxide [20, 271, 315], TIs [67, 155, 275, 329], MoS_2 [335], WS_2 [282, 283], and BP [389, 390] have been developed rapidly, and great progress has been made in pulse energy and pulse width. For example, stable dissipative soliton pulse train operation was successfully obtained using SnS_2 as the SA as shown in Figure 15A–C [349]. Pulses of 152 fs were produced using 0.48 nJ of pulse energy in an all-fiber laser cavity following compression in a single-mode fiber. In 2015, researchers used few-layer Bi_2Te_3 flakes as an SA and generated stable dissipative soliton mode-locking with a 3-dB spectral bandwidth up to 51.62 nm and a tunable wavelength range of 22 nm as shown in Figure 15D–H [155]. These excellent achievements have promoted the development of layered materials in high-performance laser pulses. Generally, different soliton states can be generated by manipulating the cavity parameters, especially the cavity dispersion [337, 391]: conventional solitons are usually observed in the anomalous dispersion regime with typical Kelly sidebands; dispersion-managed solitons appear with a smooth Gaussian-shaped spectral profile when the positive and negative dispersion components form a near-zero-dispersion laser cavity together; dissipative soliton operation is usually observed in fiber lasers with strong positive dispersion, which can be realized as the result of the balance between normal cavity dispersion, fiber nonlinearity, gain, loss, and spectral filtering.

3.2.2 Q-switched operation

Compared to mode-locked fiber laser operation, Q-switched operation in fiber lasers has significant advantages if striving to obtain high peak power pulsed output. The excellent nonlinear optical properties of the novel layered 2D materials such as graphene, TIs, TMDs, BP, and MXenes make them excellent candidates for use as Q-switchers [95, 392]. Examples of successful implementations of Q-switched fiber lasers based on layered materials including graphene [393, 394], TIs [19, 147], TMDs [68, 124, 379, 395–397], BP [31, 69, 387, 398] and MXenes [37, 399] have been obtained, as illustrated in Table 5. In terms of the performance of these mode-locked lasers based on graphene, some exciting results have been obtained, including minimum pulse width and maximum output power of 760 ns [436] and 1125 mW [440], respectively. For TMDs, the corresponding figures are 155 ns [429] and 30.2 mW [104]. For BP, the minimum pulse width is 383 ns [444].

It can be seen that these lasers exhibit excellent performance in terms of output power, pulse width, repetition rate, and peak power, which are not inferior to those of traditional lasers based on semiconductor SA mirrors and carbon nanotubes. For example, soon after BP had been used in the mode-locked fiber laser in 2015, researchers used it to obtain Q-switched pulses [31], as shown in Figure 16A–D. Subsequently, a novel implementation using TMDs of NiS_2 was confirmed for use as a Q-switcher over a broad range with pulse widths of 237 and 505 ns. Outputs were obtained at the wavelengths 1561 and 1915 nm [104], as shown in Figure 16E–H. MXene is also a typical novel layered 2D material. It was also confirmed that it could be used in fiber lasers to achieve a Q-switched pulse output [37], as shown in Figure 16I–K.

More importantly, Q-switched lasers based on layered 2D materials cover a wide wavelength range from the visible to near-infrared and mid-infrared. The gain medium comprises a wide range of active materials including Pr, Yb, Er, and Tm as dopants. Q-switched fiber lasers have therefore been widely studied and, consequently, single-wavelength and multi-wavelength lasing have been achieved, as well as wavelength tuning. These efforts have injected vitality into the research of Q-switched fiber lasers and provided new opportunities for their commercialization.

Table 5: Summary of Q-switched fiber lasers based on layered 2D materials.

Gain medium	Layered 2D material	Method	Central wavelength (nm)	Rep. rate (kHz)	Pulse width (μs)	Pulse energy (nJ)	Average power (mW)	References
YDF	Graphene	Sandwiched	1029–1037.4	3–3.9	39.8–56.1	10.3	10.3	[400]
			1066.83	5.93–20.03	3.1–15	5300	106.2	[401]
		SAM	1064.2	140–257	70	46	12	[394]
		Microfiber	1060	30.32–101.29	2.61–5.21	/	0.99	[402]
	Bi_2Se_3	Sandwiched	1060	8.3–29.1	1.95	17.9	/	[403]
	MoS_2	Sandwiched	1066.5	6.4–28.9	5.8–17	32.6	/	[395]
			1030–1070	65.3–89	2.68–4.4	1.1	/	[404]
	WS_2	Sandwiched	1030	24.9–36.7	3.2–6.4	13.6	/	[405]
	$MoSe_2$	Sandwiched	1060	60–74.9	2.8–4.6	116	/	[379]
	BP	Microfiber	1064.7	26–76	2–5.5	/	1.4	[406]
EDF	Graphene	Sandwiched	1566.17/1566.35	3.3–65.9	3.7	16.7	1.1	[393]
			1522–1555	36–103	2	40	2.4	[407]
			1554–1560.23	2.8–63	2.5–51	72.5	4.57	[400]
			1519.3–1569.9	8.5–29.05	4.6	82.61	0.2225–2.4	[408]
			1564/1566	104–116	1.85–3.85	125	14.6	[409]
			1531.12/1556.79	12.6–26.5	8.2–26.5	70	/	[410]
	Graphene oxide	Sandwiched	15550–150	22–61	6.6–13.7	63.9	9.3	[411]
	Bi_2Se_3	Sandwiched	1545–1565	4.5–12.88	13.4–36	13.3	/	[412]
			1530	6.2–40.1	4.9	39.8	/	[413]
			1565	459–940	1.9–7.76	23.8	/	[414]
			1550.5	63.2–68.9	1.49–2.54	0.797	/	[415]
	Bi_2Te_3	Sandwiched	1510–1589	2.15–12.8	13–49	1525	/	[19]
			1550	31.54–49.4	3.7–5.2	125	5.5	[416]
		D-shaped fiber	1559.5	8.74–21.24	4.88–8.46	3.8	/	[417]
			1562.9	7.5–42.8	2.81–9.36	12.7	/	[418]
	MoS_2	Sandwiched	1560	6.5–27	5.4–23.3	63.2	/	[395]
			1520–1568	10.6–34.5	5–9	160	/	[419]
			1550–1575	22	6–35	150	/	[420]
			1549.91	10.6–173.1	1.66–6.11	27.2	/	[421]
			1560.5	28.6–114.8	1.92–3.7	8.2	/	[422]
			1560	36.8–91.7	3.2–5.1	0.029	/	[423]
			1552	26.6–40.9	3.9–5.4	/	3.5	[424]
			1560	7.758–41.45	9.92–13.534	184.7	/	[68]
		SAM	1549.83	116–131	0.66–0.76	152	/	[425]
	WS_2	Sandwiched	1527–1565	65.3–106.2	1.57–2.11	28.8	/	[426]
			1558	79–97	1.1–3.4	179.6	/	[405]
			1547.5	80–120	1–3.1	0.05	/	[427]
			1560	47–77.925	3.966–6.707	1179.4	/	[68]
			1559	16.15–60.88	2.39–7.6	195	9.5	[428]
		SAM	1560	29.5–367.8	0.155–1.27	68.5	/	[429]
		D-shaped fiber	1567.8	82–134	0.92–2.82	19	/	[430]
	$MoSe_2$	Sandwiched	1566	26.5–35.4	4.8–7.9	825	/	[379]
			1560	60.72–66.85	4.04–6.506	365.9	/	[68]
			1558	64–122	1.53	140.7	17.16	[431]
			1557.6	47.5–105.7	1.09	224	23.2	[432]
	WSe_2	Sandwiched	1560	46.28–85.36	4.063–9.182	484.8	/	[68]
			1562	77–242	1.2	110	26.7	[431]
			1560	4.5–49.6	3.1–7.9	33.2	1.23	[433]
	SnS_2	Sandwiched	1532.7	172.3–233	510–1010	/	9.33	[122]
	NiS_2	Sandwiched	1561.86	195.3–243.9	0.237	1.23	30.2	[104]
	$ReSe_2$	Sandwiched	1566	16.64	4.98	36	/	[434]
	PtS_2	Sandwiched	1568.8	24.6	4.2	45.6	1.1	[435]
TDF	Graphene	SAM	1957	103–252	0.76–1.4	0.38	96	[436]
	Graphene Oxide	Sandwiched	1950.27	33.5–83.2	1.1–1.5	0.877 mJ	/	[437]
		Microfiber	2032	20–45	3.8–9	6.71	302	[438]

Table 5 (continued)

3.2.3 Nonlinear optical phenomenon in soliton shaping

Gain medium	Layered 2D material	Method	Central wavelength (nm)	Rep. rate (kHz)	Pulse width (μs)	Pulse energy (nJ)	Average power (mW)	References
	MoS_2	Sandwiched	2030	33.6–48.1	1.76–2.5	1000	/	[395]
	$MoSe_2$	Sandwiched	1924	14–21.8	5.5–16	42	/	[379]
	NiS_2	Sandwiched	1915.5	182.6–214.7	0.505–1.14	1.32	28.4	[104]
Er-ZBLAN	Graphene	SAM	2783	7–37	2.9–7	1670	62	[439]
	BP	SAM	2779	39–63	1.18–2.1	7.7	/	[69]
Ho-ZBLAN	Graphene	D-shape fiber	1192.6	24–111	800–5730	440	1125	[440]
	Bi_2Se_3	SAM	2979.9	46–81.96	1.37–4.83	3.99	/	[441]
Pr-ZBLAN	MoS_2	Sandwiched	602	50.8–118.4	0.602–1.955	5.5	/	[442]
			635.5	240.4–438.6	0.227	0.03	/	[443]
	WS_2	Sandwiched	625.1	232.7–512.8	0.207	0.04	/	[443]
			604	67.3–127.9	0.435–1.101	6.4	/	[442]
	$MoSe_2$	Sandwiched	635.4	357.1–555.1	0.24	0.02	/	[443]
	BP	Sandwiched	635.4	108.8–409.8	0.383–1.56	27.6	/	[444]
Dy-ZBLAN	BP	SAM	2970–3230	47–86	0.74–1.8	/	/	[445]

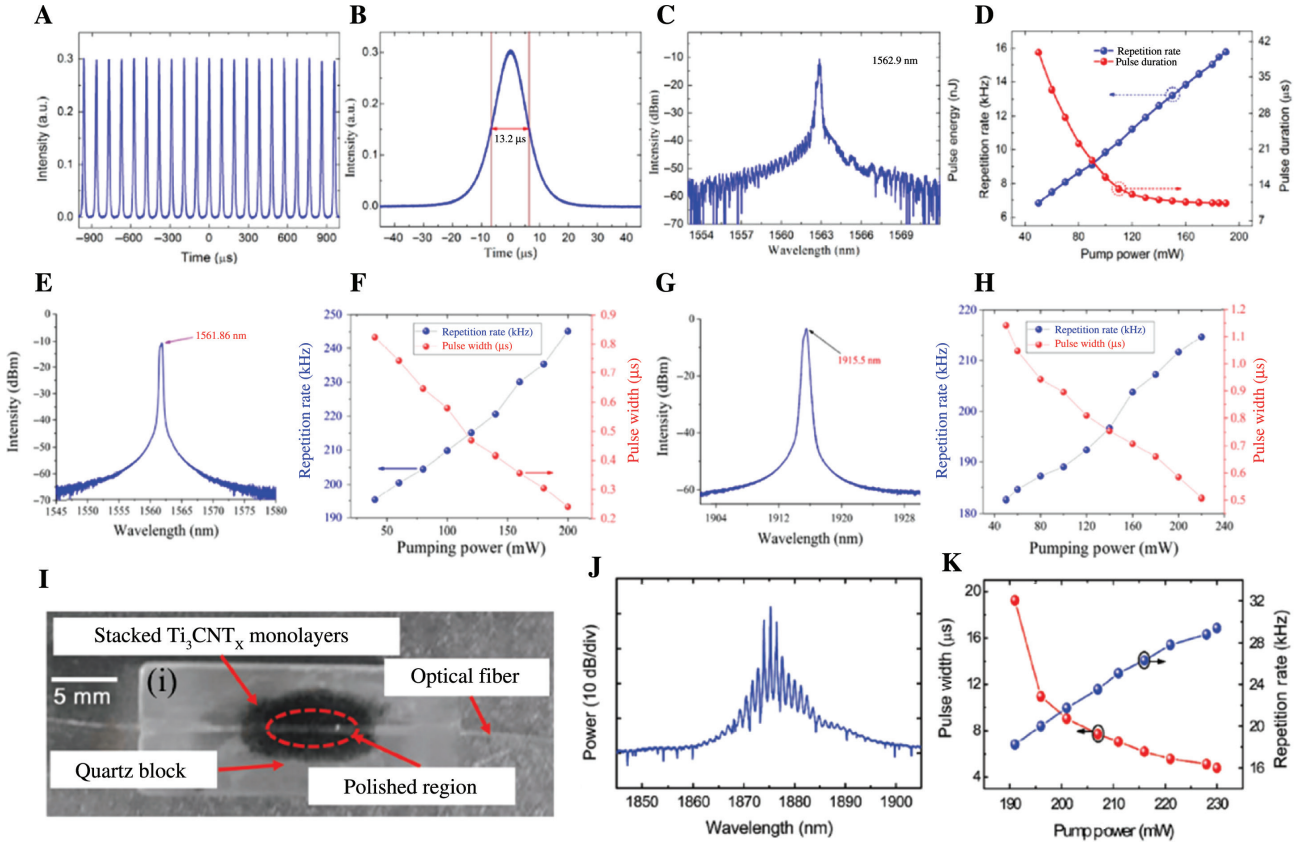

Figure 16: Q-switching fiber lasers with various SAs.
(A–D) BP. (A) Pulse train. (B) Schematic of the fiber laser. (C) Optical spectrum. (D) Evolutions of the pulse repetition rate and the pulse width with absorbed pump power. Reproduced with permission from Ref. [31]. Copyright 2015, Optical Society of America. (E–H) NiS_2. (E) Optical spectrum at 1.55 μm. (F) Evolutions of the pulse repetition rate and the pulse width with the absorbed pump power at 1.55 μm. (G) Optical spectrum at 2.0 μm. (H) Evolutions of the pulse repetition rate and the pulse width with the absorbed pump power at 2.0 μm. Reproduced with permission from Ref. [104]. Copyright 2019, Optical Society of America. (I–K) MXene. (I) Photo of the prepared side-polished fiber deposited with MXene. (J) Optical spectrum. (K) Evolutions of the pulse repetition rate and the pulse width with the absorbed pump power. Reproduced with permission from Ref. [37]. Copyright 2017, John Wiley and Sons.

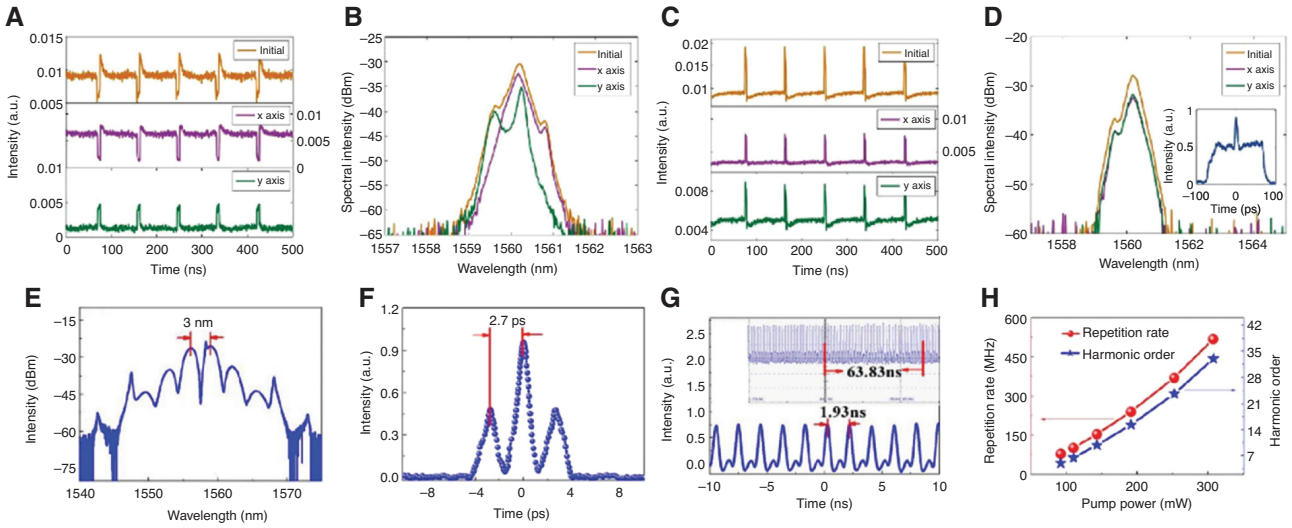

Figure 17: Versatile soliton pulse generated with layered 2D materials.
(A–E) Bi_2Te_3. (A) Bright-dark pulse traces before (initial) and after (x-axis and y-axis) passing through PBS. (B) Bright-dark pulse optical spectra before (initial) and after (x-axis and y-axis) passing through PBS. (C) Pulse traces of fundamental noise-like pulses before (initial) and after (x-axis and y-axis) passing through the PBS. (D) Corresponding optical spectra (inset: autocorrelation trace of the total pulse). Reproduced with permission from Ref. [446]. Copyright 2016, Springer Nature. (E–H) MoS_2 based bound-state soliton mode-locked fiber laser. (E) Optical spectrum. (F) Autocorrelation trace. (G) Bound-state pulse oscilloscope trace with a pump power of 307 mW. (H) Repetition rate and harmonic number under a different pump power. Reproduced with permission from Ref. [333]. Copyright 2018, Optical Society of America.

In the previous two sections, we reviewed the applications of layered materials in mode-locked/Q-switched fiber lasers. For these lasers, the SA property of layered materials plays a key role. The Kerr nonlinearity is also very important in mode-locked fiber lasers, which has attracted great attention in the field of nonlinear optics. As described in Section 2.2, most layered materials show strong Kerr nonlinearity. Thus, if nonlinear optical devices based on layered materials are introduced into fiber lasers, it could also become a good platform for the study of nonlinear optical phenomenon.

Since 2010, versatile soliton pulses, including conventional solitons, dark solitons, and even rogue waves, have been observed in mode-locked fiber lasers based on layered materials such as graphene, TIs, TMDs, and BP. For example, researchers obtained bright-dark pulse pairs and noise-like pulses in the same fiber laser using Bi_2Te_3 as SA as shown in Figure 17A–D [446]. In 2018, bound-state soliton operation using MoS_2 as SA was also demonstrated as shown in Figure 17E–H [333].

As mentioned previously, although nonlinear optical phenomena caused by layered 2D materials are many, researchers have not yet utilized their full potential. In order to obtain stronger nonlinear optical phenomena using layered 2D materials, a new method was proposed, combining such materials with microfiber structures, primarily using the microfiber resonator, an approach that has yielded promising results. In 2018, researchers used a microfiber knot structure incorporating graphene as SA and successfully obtained a multi-wavelength spectrum in both Yb- and Er-doped fiber laser systems [447], as shown in Figure 18A–H. After that, a larger wavelength spectrum using a microfiber knot resonator incorporating WS_2 as SA was obtained [448], as shown in Figure 18I–L. Also a microfiber coil resonator incorporating BP has been successfully inserted into a Tm-doped fiber laser, thereby achieving an output spectrum containing 12 wavelengths [449], as shown in Figure 18M–P. The above developments have provided a new platform to maximize the optical nonlinearity of layered 2D materials and inject vitality into the research of high-nonlinearity phenomena and resulted in new opportunities for their commercialization. Multi-wavelength fiber lasers represent an important development in the context of laser applications. However, there remains a problem of how to maximize the nonlinearity of the material, which is the key to producing a larger number of wavelengths. In the above experiments, a new method was proposed, giving exciting results using 2D materials incorporating a microfiber resonator. The results confirmed that the novel SA device enhanced the nonlinearity of the 2D materials, which resulted in improved laser performance. Figure 18 shows the flat optical spectra, good pulse train, as well as an especially high consistency between the free spectral response of the microfiber resonator and the channel spacing of the spectra. The compact size and easy fabrication of the novel SA device provided a new solution to

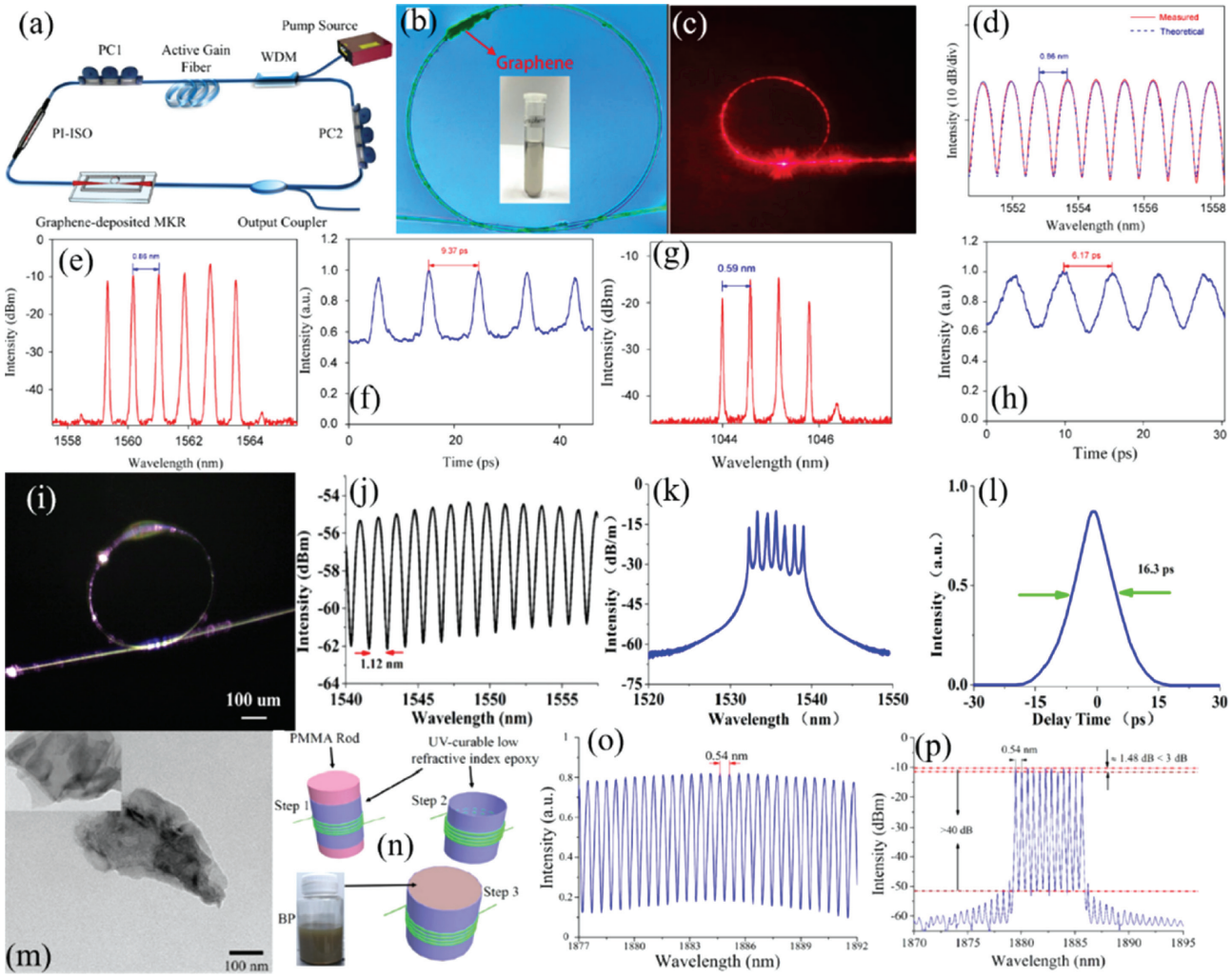

Figure 18: Versatile multiwavelength fiber laser based on microfiber structure incorporating layered 2D materials. (A–H) Graphene. (A) Schematic of the fiber laser. (B) Microscopy image of the graphene-deposited microfiber knot resonator. (C) Scattering evanescent field along the graphene-deposited microfiber knot resonator. (D) Spectral response. (E) Optical spectrum. (F) Autocorrelation trace. (G) Optical spectrum. (H) Autocorrelation trace. Reproduced with permission from Ref. [447]. Copyright 2018, Optical Society of America. (I–L) WS_2. (I) Photograph of the WS_2 device based on the microfiber knot. (J) Spectral response. (K) Optical spectrum. (L) Autocorrelation trace. Reproduced with permission from Ref. [448]. Copyright 2018, IEEE. (M–P) BP. (M) TMD of BP. (N) Schematic illustrations for the construction of the microfiber coil resonator incorporating BP (MCR-BP). (O) Spectral response. (P) Optical spectrum. Reproduced with permission from Ref. [449]. Copyright 2019, Elsevier.

making a novel fiber laser device that has low loss, is more compact, and has excellent output capability.

Numerous laser applications have been developed using 2D materials. For graphene, its zero bandgap can be an advantage, which has resulted in its use for a wide waveband. On the other hand, zero bandgap can also be a disadvantage because it results in low modulation depth. Compared to graphene, TIs normally have a large modulation depth, which is highly beneficial for achieving pulsed laser operation. Apart from TIs, other widely studied 2D materials include layered TMDs. Their large family and direct bandgap make TMDs good potential candidate materials for use in optics and optoelectronic devices. Soon afterward, it was discovered that BP has a singular direct bandgap, which varies between 2 eV (single layer) and 0.3 eV (bulk) with the number of layers varying between the zero-bandgap graphene and the relatively large-bandgap TMDs, thus making up for the shortcomings of these 2D materials in the field of photonics. As a whole, different 2D materials have different characteristics, which allow them to attain excellent performance in different optical fields.

2D materials have some advantages over other technologies when used in laser applications. The first is their high nonlinearity, which means that 2D materials have great potential for use in many laser applications although

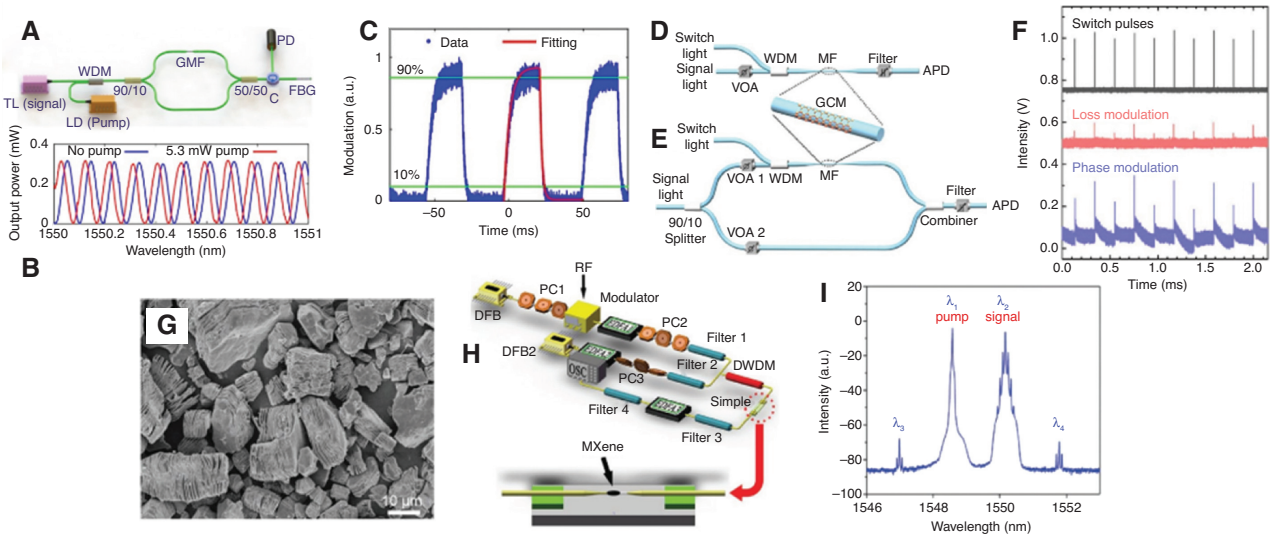

Figure 19: Optical modulation based on various layered 2D materials.
(A–C) Graphene. (A) Schematic diagram of the modulators. (B) Transmission. (C) Optical modulation. Reproduced with permission from Ref. [450]. Copyright 2015, Optical Society of America. (D–F) Graphene. (D, E) Schematic diagram of the modulators. (F) Switching pulse of all-optical modulation. Reproduced with permission from Ref. [451]. Copyright 2016, Optical Society of America. (G–J) MXene. (G) SEM image of the MXene flake. (H) Experimental setup of a four-wave mixing (FWM) all-optical wavelength converter. (I) Wavelength conversion. (J) Output FWM spectral evolution. Reproduced with permission from Ref. [40]. Copyright 2019, John Wiley and Sons.

other materials also have nonlinearity [3, 18, 66, 114]. The second is the ease of fabrication. Numerous methods can be used to fabricate 2D materials, which are normally simple and cheap, which means 2D materials have a strong basis for future industrial production [73, 78]. The third is their compact size. Normally, SA devices require only a small piece of 2D material (related to Section 2.3), which makes them ideal for use in compact laser devices. 2D materials still have some disadvantages, namely low damage threshold and difficulty in controlling their optical properties. The damage thresholds of graphene and graphene-like 2D materials are not high, which limits their use in high-power laser applications [3, 114]. If the power is too high, there is a risk of irreparable damage to the material. For the fabrication of 2D materials, a major challenge is that optical properties differ even if the same preparation method is used, i.e. lack of repeatability [75]. On the whole, 2D materials possess attractive qualities as well as some flaws. The goal is therefore to overcome these deficits through focused investigation of 2D materials.

4 Other photonics applications based on layered 2D materials

In recent years, optical modulators have attracted a great interest due to their wide applications in optical interconnection, environmental monitoring, medicine, and security. High nonlinearity plays an important role in modulator design. However, the widely used nonlinear optical materials, including chalcogenide glass and highly nonlinear optical fibers, have many limitations such as large absorption and scattering losses, small phase shift, and vulnerability to laser damage in optical modulators [70]. However, thanks to the large third-order nonlinearity and other excellent physical properties, including strong light-material interaction, broadband optical response, fast relaxation, controllable optical properties, and high compatibility with other photonic structures, layered materials may pave the way for the development of optical modulators [70].

2D materials were initially used in 2004, initiated by the discovery of atomic-layer graphene, thus launching investigations of 2D materials and their promising applications [70]. Graphene, owing to its highly attractive optical properties, including broadband nonlinear absorption, high mobility of carriers, and so on, can be considered an excellent candidate as an optical modulation medium. Graphene was reported as being feasible for use in many aspects of optical signal processing and optical computing, including phase shifting [450, 451], optical switching [452, 453], wavelength conversion [454, 455], and signal regeneration [456]. For example, in 2015, a graphene-based all-fiber phase shifter was designed and demonstrated, which could be optically controlled using

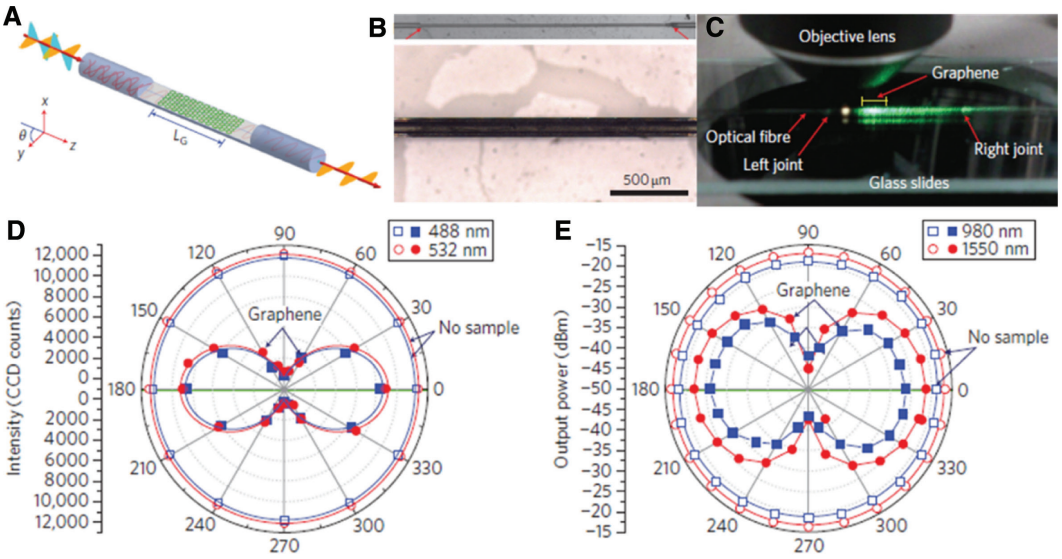

Figure 20: Broadband graphene polarizer.
(A) Schematic model of fiber-to-graphene coupler based on a side-polished optical fiber. L_G, propagation distance. (B) Optical image of the microfiber and microfiber incorporating graphene. (C) Polarized diagram of the laser beam along s and p polarization. (D) Polar diagram at 488 and 532 nm, respectively. (E) Polar diagram at 980 and 1550 nm, respectively. Reproduced with permission from Ref. [457]. Copyright 2011, Springer Nature.

a low pump power [450], as shown in Figure 19A–C. Soon afterward, another group designed an all-optical, all-fiber, fast Mach-Zehnder interferometer modulator based on graphene, which had a relatively high modulation depth and overall transmittance [451]. It operated through optically induced phase modulation in the graphene incorporating a microfiber contained in one arm and relied on wave interference at the output of the Mach-Zehnder interferometer, as shown in Figure 19D–F. Nevertheless, graphene as an all-optical device is limited by its weak modulation depth and zero bandgap. Enlightened by the discovery of graphene, several types of graphene-like 2D materials have been reported: TIs, TMDs, BP, MXenes, and so on. For example, the MXene $Ti_3C_2T_x$, prepared using a liquid acid etching method, was developed as a novel all-optical device by depositing it on a microfiber, which showed excellent nonlinear optical properties in the telecommunication band. The fabricated device was employed as a wavelength converter based on nonlinear FWM with a conversion efficiency of –59 dB while carrying a 10-GHz signal, as shown in Figure 19G–J.

In addition to optical modulators, other optical devices including optical polarizers [457–460], optical filters [461], optical isolators [462, 463], optical switches [450, 464–466], optical parametric devices [467], light-control-light devices [468], and even all-optical signal processors [469, 470] have been widely studied. For example, a broadband polarizer based on graphene was developed to support transverse mode surface wave transmission in the visible and near-infrared bands [457], as shown in Figure 20. It should be pointed out that the development of these all-optical devices is relatively new, and much work remains to be done in this area.

To date, research in 2D material-based optical modulation has made great progress in almost all aspects, ranging from theoretical design to material preparation, integration techniques, and modulator configurations. Initial results have unambiguously indicated the great opportunities for using 2D materials for optical modulation. However, past and current research has mostly focused on material properties and conceptualizing devices. For achieving practical applications, great challenges remain, which may in turn bring great opportunities and become the new driving force in this field. Against this background, an actively Q-switched laser with an antimonene-based all-optical modulator has been devised based on the high photothermal efficiency (48%) and broadband response in antimonene [72]. It was demonstrated that this actively modulated laser is a device with all optically tunable output parameters (e.g. output repetition rate), environmental stability, and easy synchronization, as shown in Figure 21. It is anticipated that this active antimonene-based all-optical modulator with its advantages of large modulation depth, low energy consumption, and high conversion efficiency has great potential in all-optical information processing and pulsed

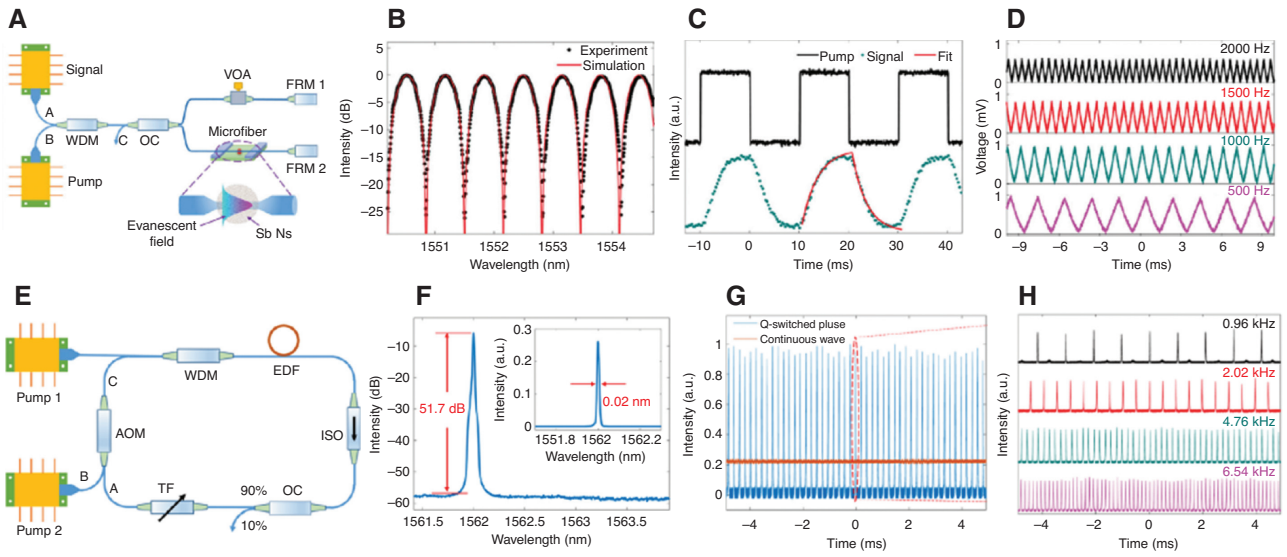

Figure 21: An all-optical, actively Q-switched fiber laser by an antimonene-based optical modulator.
(A) Schematic diagram of an acousto-optic modulator (AOM). (B) Measured interferometric spectrum. (C) Intensity modulation. (D) Waveforms at different modulation frequencies. (E) Schematic diagram of actively Q-switched fiber laser by the antimonene nanosheets-based AOM. (F) Measured spectrum at the repetition rate of 4.76 kHz; inset: linear coordinate. (G) Typical pulse trains and continuous wave. (H) Pulse trains at different repetition rates. Reproduced with permission from Ref. [72]. Copyright 2019, John Wiley and Sons.

laser engineering. This achievement may lead to further applications of the excellent nonlinear optical properties of layered 2D materials, making it possible to combine multiple nonlinear optical devices.

5 Conclusions and outlook

Since the advent of graphene, the development of layered 2D materials has accelerated rapidly. To date, 2D material-based optical modulation has made great progress in almost all aspects, ranging from theoretical design to material preparation, integration techniques, and pulsed laser and modulator configurations. Research related to layered 2D materials has correspondingly grown rapidly in the field of nonlinear photonics. This is due to the continuous innovation in material preparation technology, which has also improved the general properties of the layered 2D materials, especially their optical nonlinearity. It is widely acknowledged that the development of layered 2D materials alone cannot provide all the solutions to the development of pulsed laser and nonlinear photonics devices, but their development and implementation have made a major contribution in moving them forward toward commercial devices. The important position and application of layered 2D materials in the optical field have been identified and thoroughly reviewed. The research and development is also in keeping with the current trend of interdisciplinary scientific research. However, for full implementation in practical applications, great challenges remain, which may, however, create great opportunities and become the new driving force in this field.

To date, novel 2D materials have made significant contributions to the area of nonlinear photonics applications due mainly to the unremitting efforts of scientific researchers [169, 172, 201, 254, 322, 324, 332, 358, 359, 373, 381]. However, the greatest remaining challenge is industrialization or commercialization of the technology. The nonlinear optical characteristics of 2D materials have a major influence in the performance of lasers and optical modulators. If SAs or other modulator devices based on 2D materials exhibit uniform characteristics as in the case of SESAM, industrialization and commercialization could become a reality, which will have an incalculable impact on the research and application of 2D materials. Other challenges remain, including overcoming the photothermal effect caused by the interaction between light and the materials. Some methods have been investigated to overcome the photothermal effect [33, 303, 339, 447, 448, 458, 471], but SAs or other modulator devices based on 2D materials continue to be exposed to the risk of destruction. It is therefore important to discover new ways to overcome this shortcoming.

As an outlook and a brief summary of this article, some of the important future directions in this field are as follows:

- The performance of pulsed lasers based on the layered 2D materials continues to improve. Numerous experimental results have proved that high pulse energy and high peak power can be achieved in both solid-state lasers and fiber lasers based on 2D materials. One goal for the future is to reduce the pulse width for high peak power generation. Specific methods may include optimizing the 2D material fabrication methods and adopting an integrated approach, improvement in the design of the laser cavity, and loss reduction. Another goal is a deep investigation into the mode-locked/Q-switched lasers in the ultraviolet and 2.7–4-μm wavebands, which are very important for the national defense and industrial production. In the above wavebands, there is a lack of studies on 2D material-based lasers. It is predictable that the research of mode-locked/Q-switched lasers in the ultraviolet and 2.7–4 μm wavebands will become an important topic in the future.
- More nonlinear optical phenomena, including multi-soliton molecules and rogue waves, may be discovered and well explained in the case of fiber lasers based on 2D materials. Optical nonlinearity of 2D materials is the basis of all nonlinear phenomena in fiber lasers. It is therefore important to further investigate the optical nonlinearity of 2D materials. Multi-soliton molecules and rogue waves are typical nonlinear phenomena in fiber lasers. However, the related investigation and explanation are currently lacking. The study of nonlinear optical phenomena in fiber lasers will therefore be of great benefit for the understanding of optical nonlinearity of 2D materials.
- The exploration of new mechanisms and configurations should continue for 2D material-based optical modulation, such as mechanically or magnetically induced effects. To date, numerous optical modulation devices have been studied. In the future, the exploration of new high-efficiency devices based on 2D materials will become significant. Mechanical devices have access to a wide range of application fields including magnetically induced devices, which is a rapidly developing application area. It is predicted that mechanical and magnetic devices based on 2D materials have significant potential for future investigations.
- It is envisaged that novel 2D materials will continue to be synthesized, and exploring their nonlinear optical properties and related device applications will be major topics for future investigations. The discovered 2D materials offer many new opportunities in interdisciplinary research between materials science and photonics. Many aspects and properties of emerging 2D materials therefore require further study.

Acknowledgments: This work was supported by the National Key R&D Program of China under Grant 2016YFE0126500. It was also supported in part by the National Key program of the National Natural Science Foundation of China (NSFC) under Grant 61935006, the Fundamental Research Funds for Central Universities under Grant HEUCFG201841, 3072019CF2513, and the 111 project (B13015) awarded to the Harbin Engineering University.

References

[1] Keller U. Recent developments in compact ultrafast lasers. Nature 2003;424:831.
[2] Novoselov KS, Jiang D, Schedin F, et al. Two-dimensional atomic crystals. Proc Natl Acad Sci 2005;102:10451–3.
[3] Geim AK, Novoselov KS. "The rise of graphene," in nanoscience and technology: a collection of reviews from nature journals. World Sci 2010:11–9.
[4] Zheng G, Chen Y, Huang H, et al. Improved transfer quality of CVD-grown graphene by ultrasonic processing of target substrates: applications for ultra-fast laser photonics. ACS Appl Mater Interfaces 2013;5:10288–93.
[5] Li H-J, Wang L-L, Zhang H, et al. Graphene-based mid-infrared, tunable, electrically controlled plasmonic filter. Appl Phys Express 2014;7:024301.
[6] Song YF, Zhang H, Tang DY, Shen DY. Polarization rotation vector solitons in a graphene mode-locked fiber laser. Opt Express 2012;20:27283–9.
[7] Song YF, Zhang H, Zhao LM, Shen DY, Tang DY. Coexistence and interaction of vector and bound vector solitons in a dispersion-managed fiber laser mode locked by graphene. Opt Express 2016;24:1814–22.
[8] Geim A, Ak NKS. The rise of graphene. Nature Mater 2007;6:183.
[9] Bao Q, Zhang H, Wang Y, et al. Atomic-layer graphene as a saturable absorber for ultrafast pulsed lasers. Adv Funct Mater 2009;19:3077–83.
[10] Geim AK. Graphene: status and prospects. Science 2009;324:1530–4.
[11] Kumar S, Anija M, Kamaraju N, et al. Femtosecond carrier dynamics and saturable absorption in graphene suspensions. Appl Phys Lett 2009;95:191911.
[12] Xia F, Mueller T, Lin Y-M, Valdes-Garcia A, Avouris P. Ultrafast graphene photodetector. Nat Nanotechnol 2009;4:839.
[13] Zhang H, Bao Q, Tang D, Zhao L, Loh K. Large energy soliton erbium-doped fiber laser with a graphene-polymer composite mode locker. Appl Phys Lett 2009;95:141103.
[14] Zhang H, Tang D, Zhao L, Bao Q, Loh K. Large energy mode locking of an erbium-doped fiber laser with atomic layer graphene. Opt Express 2009;17:17630–5.
[15] Zhao C, Zhang H, Qi X, et al. Ultra-short pulse generation by a topological insulator based saturable absorber. Appl Phys Lett 2012;101:211106.
[16] Zhao C, Zou Y, Chen Y, et al. Wavelength-tunable picosecond soliton fiber laser with topological insulator: Bi_2Se_3 as a mode locker. Opt Express 2012;20:27888–95.

[17] Luo Z-C, Liu M, Liu H, et al. 2 GHz passively harmonic mode-locked fiber laser by a microfiber-based topological insulator saturable absorber. Opt Lett 2013;38:5212–5.
[18] Yu H, Zhang H, Wang Y, et al. Topological insulator as an optical modulator for pulsed solid-state lasers. Laser Photon Rev 2013;7:L77–83.
[19] Chen Y, Zhao C, Chen S, et al. Large energy, wavelength widely tunable, topological insulator Q-switched erbium-doped fiber laser. IEEE J Sel Top Quantum Electron 2014;20:315–22.
[20] Dou Z, Song Y, Tian J, Liu J, Yu Z, Fang X. Mode-locked ytterbium-doped fiber laser based on topological insulator: Bi_2Se_3. Opt Express 2014;22:24055–61.
[21] Jung M, Lee J, Koo J, et al. A femtosecond pulse fiber laser at 1935 nm using a bulk-structured Bi_2Te_3 topological insulator. Opt Express 2014;22:7865–74.
[22] Liu M, Zhao N, Liu H, et al. Dual-wavelength harmonically mode-locked fiber laser with topological insulator saturable absorber. IEEE Photon Technol Lett 2014;26:983–6.
[23] Ramakrishna Matte H, Gomathi A, Manna AK, et al. MoS_2 and WS_2 analogues of graphene. Angew Chem Int Ed 2010;49:4059–62.
[24] Mao D, Wang Y, Ma C, et al. WS_2 mode-locked ultrafast fiber laser. Sci Rep 2015;5:7965.
[25] Zhang S, Dong N, Mcevoy N, et al. Direct observation of degenerate two-photon absorption and its saturation in WS_2 and MoS_2 monolayer and few-layer films. ACS Nano 2015;9:7142–50.
[26] Lee J, Park J, Koo J, Jhon YM, Lee JH. Harmonically mode-locked femtosecond fiber laser using non-uniform, WS_2-particle deposited side-polished fiber. J Opt 2016;18:035502.
[27] Torres-Torres C, Perea-López N, Elías AL, et al. Third order nonlinear optical response exhibited by mono-and few-layers of WS_2. 2D Mater 2016;3:021005.
[28] Li J, Zhao Y, Chen Q, Niu K, Sun R, Zhang H. Passively mode-locked ytterbium-doped fiber laser based on SnS_2 as saturable absorber. IEEE Photon J 2017;9:1–7.
[29] Buscema M, Groenendijk DJ, Blanter SI, Steele GA, Van Der Zant HS, Castellanos-Gomez A. Fast and broadband photoresponse of few-layer black phosphorus field-effect transistors. Nano Lett 2014;14:3347–52.
[30] Castellanos-Gomez A, Vicarelli L, Prada E, et al. Isolation and characterization of few-layer black phosphorus. 2D Mater 2014;1:025001.
[31] Chen Y, Jiang G, Chen S, et al. Mechanically exfoliated black phosphorus as a new saturable absorber for both Q-switching and mode-locking laser operation. Opt Express 2015;23:12823–33.
[32] Li D, Jussila H, Karvonen L, Ye G, Lipsanen H, Chen X, Sun Z. Polarization and thickness dependent absorption properties of black phosphorus: new saturable absorber for ultrafast pulse generation. Sci Rep 2015;5:15899.
[33] Luo Z-C, Liu M, Guo Z-N, et al. Microfiber-based few-layer black phosphorus saturable absorber for ultra-fast fiber laser. Opt Express 2015;23:20030–9.
[34] Mu H, Lin S, Wang Z, et al. Black phosphorus–polymer composites for pulsed lasers. Adv Opt Mater 2015;3:1447–53.
[35] Sotor J, Sobon G, Kowalczyk M, Macherzynski W, Paletko P, Abramski KM. Ultrafast thulium-doped fiber laser mode locked with black phosphorus. Opt Lett 2015;40:3885–8.
[36] Du J, Zhang M, Guo Z, et al. Phosphorene quantum dot saturable absorbers for ultrafast fiber lasers. Sci Rep 2017;7:42357.
[37] Jhon YI, Koo J, Anasori B, et al. Metallic MXene saturable absorber for femtosecond mode-locked lasers. Adv Mater 2017;29:1702496.
[38] Feng X-Y, Ding B-Y, Liang W-Y, et al. MXene $Ti_3C_2T_x$ absorber for a 1.06 μm passively Q-switched ceramic laser. Laser Phys Lett 2018;15:085805.
[39] Jiang X, Liu S, Liang W, et al. Broadband nonlinear photonics in few-layer MXene $Ti_3C_2T_x$ (T=F, O, or OH). Laser Photon Rev 2018;12:1870013.
[40] Song Y, Chen Y, Jiang X, et al. Nonlinear few-layer MXene-assisted all-optical wavelength conversion at telecommunication band. Adv Opt Mater 2019;7:1801777.
[41] Wang C, Wang Y, Jiang X, et al. MXene $Ti_3C_2T_x$: a promising photothermal conversion material and application in all-optical modulation and all-optical information loading. Adv Opt Mater 2019;7:1900060.
[42] Bhimanapati GR, Lin Z, Meunier V, et al. Recent advances in two-dimensional materials beyond graphene. ACS Nano 2015;9:11509–39.
[43] Kong X, Liu Q, Zhang C, Peng Z, Chen Q. Elemental two-dimensional nanosheets beyond graphene. Chem Soc Rev 2017;46:2127–57.
[44] Novoselov KS, Geim AK, Morozov SV, et al. Electric field effect in atomically thin carbon films. Science 2004;306:666–9.
[45] Zhang H, Tang D, Knize R, Zhao L, Bao Q, Loh KP. Graphene mode locked, wavelength-tunable, dissipative soliton fiber laser. Appl Phys Lett 2010;96:111112.
[46] Huang Y, Sutter E, Sadowski JT, et al. Tin disulfide – an emerging layered metal dichalcogenide semiconductor: materials properties and device characteristics. ACS Nano 2014;8:10743–55.
[47] Ponraj JS, Xu Z-Q, Dhanabalan SC, et al. Photonics and optoelectronics of two-dimensional materials beyond graphene. Nanotechnology 2016;27:462001.
[48] Xia F, Wang H, Xiao D, Dubey M, Ramasubramaniam A. Two-dimensional material nanophotonics. Nat Photon 2014;8:899.
[49] Gong C, Hu K, Wang X, et al. 2D nanomaterial arrays for electronics and optoelectronics. Adv Funct Mater 2018;28:1706559.
[50] Xie Z, Xing C, Huang W, et al. Ultrathin 2D nonlayered tellurium nanosheets: facile liquid-phase exfoliation, characterization, and photoresponse with high performance and enhanced stability. Adv Funct Mater 2018;28:1705833.
[51] Xie Z, Zhang F, Liang Z, et al. Revealing of the ultrafast third-order nonlinear optical response and enabled photonic application in two-dimensional tin sulfide. Photon Res 2019;7:494–502.
[52] Wu L, Xie Z, Lu L, et al. Few-layer tin sulfide: a promising black-phosphorus-analogue 2D material with exceptionally large nonlinear optical response, high stability, and applications in all-optical switching and wavelength conversion. Adv Opt Mater 2018;6:1700985.
[53] Xing C, Xie Z, Liang Z, et al. 2D nonlayered selenium nanosheets: facile synthesis, photoluminescence, and ultrafast photonics. Adv Opt Mater 2017;5:1700884.
[54] Huang W, Xie Z, Fan T, et al. Black-phosphorus-analogue tin monosulfide: an emerging optoelectronic two-dimensional material for high-performance photodetection with improved stability under ambient/harsh conditions. J Mater Chem C 2018;6:9582–93.

[55] Xie Z, Wang D, Fan T, et al. Black phosphorus analogue tin sulfide nanosheets: synthesis and application as near-infrared photothermal agents and drug delivery platforms for cancer therapy. J Mater Chem B 2018;6:4747–55.
[56] Fan T, Xie Z, Huang W, Li Z, Zhang H. Two-dimensional non-layered selenium nanoflakes: facile fabrications and applications for self-powered photo-detector. Nanotechnology 2019;30. Available at: https://iopscience.iop.org/article/10.1088/1361-6528/aafc0f/pdf.
[57] Xing C, Huang W, Xie Z, et al. Ultrasmall bismuth quantum dots: facile liquid-phase exfoliation, characterization, and application in high-performance UV–Vis photodetector. ACS Photon 2018;5:621–9.
[58] Xie Z, Chen S, Duo Y, et al. Biocompatible two-dimensional titanium nanosheets for multimodal imaging-guided cancer theranostics. ACS Appl Mater Interfaces 2019;11:22129–40.
[59] Xie Z, Peng Y-P, Yu L, et al. Solar-inspired water purification based on emerging 2D mater: status and challenges. Solar RRL 2020;4:1900400.
[60] Liang X, Ye X, Wang C, et al. Photothermal cancer immunotherapy by erythrocyte membrane-coated black phosphorus formulation. J Control Release 2019;296:150–61.
[61] Zhang Y, Lim C-K, Dai Z, et al. Photonics and optoelectronics using nano-structured hybrid perovskite media and their optical cavities. Phys Rep 2019;795:1–51.
[62] Liu J, Xue Y, Wang Z, et al. Two-dimensional $CH_3NH_3PbI_3$ perovskite: synthesis and optoelectronic application. ACS Nano 2016;10:3536–42.
[63] Zhang Y, Liu J, Wang Z, et al. Synthesis, properties, and optical applications of low-dimensional perovskites. Chem Commun 2016;52:13637–55.
[64] Guo S, Zhang Y, Ge Y, Zhang S, Zeng H, Zhang H. 2D V-V binary materials: status and challenges. Adv Mater 2019;31:1902352.
[65] Li P, Chen Y, Yang T, et al. Two-dimensional $CH_3NH_3PbI_3$ perovskite nanosheets for ultrafast pulsed fiber lasers. ACS Appl Mater Interfaces 2017;9:12759–65.
[66] Song Y, Shi X, Wu C, Tang D, Zhang H. Recent progress of study on optical solitons in fiber lasers. Appl Phys Rev 2019;6:021313.
[67] Boguslawski J, Sobon G, Zybala R, Sotor J. Dissipative soliton generation in Er-doped fiber laser mode-locked by Sb_2Te_3 topological insulator. Opt Lett 2015;40:2786–9.
[68] Chen B, Zhang X, Wu K, Wang H, Wang J, Chen J. Q-switched fiber laser based on transition metal dichalcogenides MoS_2, $MoSe_2$, WS_2, and WSe_2. Opt Express 2015;23:26723–37.
[69] Qin Z, Xie G, Zhang H, et al. Black phosphorus as saturable absorber for the Q-switched Er: ZBLAN fiber laser at 2.8 μm. Opt Express 2015;23:24713–8.
[70] Sun Z, Martinez A, Wang F. Optical modulators with 2D layered materials. Nat Photon 2016;10:227.
[71] Liao Y, Feng G, Zhou H, Mo J, Sun H, Zhou S. Ultra-broadband all-optical graphene modulator. IEEE Photon Technol Lett 2018;30:661–4.
[72] Wang Y, Huang W, Wang C, et al. An all-optical, actively Q-switched fiber laser by an antimonene-based optical modulator. Laser Photon Rev 2019;13:1800313.
[73] Shams SS, Zhang R, Zhu J. Graphene synthesis: a review. Mater Sci Pol 2015;33:566–78.
[74] Dhanabalan SC, Ponraj JS, Guo Z, Li S, Bao Q, Zhang H. Emerging trends in phosphorene fabrication towards next generation devices. Adv Sci 2017;4:1600305.
[75] Yi M, Shen Z. A review on mechanical exfoliation for the scalable production of graphene. J Mater Chem A 2015;3:11700–15.
[76] Li H, Lu G, Wang Y, et al. Mechanical exfoliation and characterization of single-and few-layer nanosheets of WSe_2, TaS_2, and $TaSe_2$. Small 2013;9:1974–81.
[77] Martinez A, Fuse K, Yamashita S. Mechanical exfoliation of graphene for the passive mode-locking of fiber lasers. Appl Phys Lett 2011;99:121107.
[78] Mannix AJ, Kiraly B, Hersam MC, Guisinger NP. Synthesis and chemistry of elemental 2D materials. Nat Rev Chem 2017;1:0014.
[79] Tang Q, Zhou Z. Graphene-analogous low-dimensional materials. Prog Mater Sci 2013;58:1244–315.
[80] Agarwal V, Chatterjee K. Recent advances in the field of transition metal dichalcogenides for biomedical applications. Nanoscale 2018;10:16365–97.
[81] Tung VC, Allen MJ, Yang Y, Kaner RB. High-throughput solution processing of large-scale graphene. Nat Nanotechnol 2009;4:25.
[82] Tung VC, Chen L-M, Allen MJ, et al. Low-temperature solution processing of graphene-carbon nanotube hybrid materials for high-performance transparent conductors. Nano Lett 2009;9:1949–55.
[83] Zheng J, Zhang H, Dong S, et al. High yield exfoliation of two-dimensional chalcogenides using sodium naphthalenide. Nat Commun 2014;5:2995.
[84] Ang PK, Wang S, Bao Q, Thong JT, Loh KP. High-throughput synthesis of graphene by intercalation-exfoliation of graphite oxide and study of ionic screening in graphene transistor. ACS Nano 2009;3:3587–94.
[85] Guo B. 2D noncarbon materials-based nonlinear optical devices for ultrafast photonics. Chin Opt Lett 2018;16:020004.
[86] Yang X, Li Q, Hu G, et al. Controlled synthesis of high-quality crystals of monolayer MoS_2 for nanoelectronic device application. Sci China Mater 2016;59:182–90.
[87] Kong J, Cassell AM, Dai H. Chemical vapor deposition of methane for single-walled carbon nanotubes. Chem Phys Lett 1998;292:567–74.
[88] Reina A, Jia X, Ho J, et al. Large area, few-layer graphene films on arbitrary substrates by chemical vapor deposition. Nano Lett 2008;9:30–5.
[89] Lee YH, Zhang XQ, Zhang W, et al. Synthesis of large-area MoS2 atomic layers with chemical vapor deposition. Adv Mater 2012;24:2320–5.
[90] Zhang Y, Zhang L, Zhou C. Review of chemical vapor deposition of graphene and related applications. Acc Chem Res 2013;46:2329–39.
[91] Wang J, Jiang Z, Chen H, et al. Magnetron-sputtering deposited WTe_2 for an ultrafast thulium-doped fiber laser. Opt Lett 2017;42:5010–3.
[92] Powers PE, Haus JW. Fundamentals of nonlinear optics. CRC press, 2017.
[93] Leuthold J, Koos C, Freude W. Nonlinear silicon photonics. Nature Photon 2010;4:535.
[94] Yamashita S. Nonlinear optics in carbon nanotube, graphene, and related 2D materials. APL Photon 2019;4:034301.
[95] Autere A, Jussila H, Dai Y, Wang Y, Lipsanen H, Sun Z. Nonlinear optics with 2D layered materials. Adv Mater 2018;30:1705963.
[96] Yamashita S. A tutorial on nonlinear photonic applications of carbon nanotube and graphene. J Lightwave Technol 2011;30:427–47.

[97] Keller U, Weingarten KJ, Kartner FX, et al. Semiconductor saturable absorber mirrors (SESAM's) for femtosecond to nanosecond pulse generation in solid-state lasers. IEEE J Sel Top Quantum Electron 1996;2:435–53.
[98] Tutt LW, Boggess TF. A review of optical limiting mechanisms and devices using organics, fullerenes, semiconductors and other materials. Prog Quantum Electron 1993;17:299–338.
[99] Wang K, Feng Y, Chang C, et al. Broadband ultrafast nonlinear absorption and nonlinear refraction of layered molybdenum dichalcogenide semiconductors. Nanoscale 2014;6:10530–5.
[100] Chen S, Zhao C, Li Y, et al. Broadband optical and microwave nonlinear response in topological insulator. Opt Mater Express 2014;4:587–96.
[101] Lu S, Zhao C, Zou Y, et al. Third order nonlinear optical property of Bi_2Se_3. Opt Express 2013;21:2072–82.
[102] Ouyang Q, Yu H, Zhang K, Chen Y. Saturable absorption and the changeover from saturable absorption to reverse saturable absorption of MoS_2 nanoflake array films. J Mater Chem C 2014;2:6319–25.
[103] Steinleitner P, Merkl P, Nagler P, et al. Direct observation of ultrafast exciton formation in a monolayer of WSe_2. Nano Lett 2017;17:1455–60.
[104] Li S, Yin Y, Ouyang Q, et al. Nanosecond passively Q-switched fibre laser using a NiS_2 based saturable absorber. Opt Express 2019;27:19843–51.
[105] Wang K, Szydłowska BM, Wang G, et al. Ultrafast nonlinear excitation dynamics of black phosphorus nanosheets from visible to mid-infrared. ACS Nano 2016;10:6923–32.
[106] Jiang X, Liu S, Liang W, et al. Broadband nonlinear photonics in few-layer MXene $Ti_3C_2T_x$ (T=F, O, or OH). Laser Photon Rev 2018;12:1700229–39.
[107] Liu Z, Wang Y, Zhang X, Xu Y, Chen Y, Tian J. Nonlinear optical properties of graphene oxide in nanosecond and picosecond regimes. Appl Phys Lett 2009;94:021902.
[108] Hendry E, Hale PJ, Moger J, Savchenko A, Mikhailov SA. Coherent nonlinear optical response of graphene. Phys Rev Lett 2010;105:097401.
[109] Ishikawa KL. Nonlinear optical response of graphene in time domain. Phys Rev B 2010;82:201402.
[110] Shi B, Miao L, Wang Q, et al. Broadband ultrafast spatial self-phase modulation for topological insulator Bi_2Te_3 dispersions. Appl Phys Lett 2015;107:151101.
[111] Zhang H, He X, Lin W, et al. Ultrafast saturable absorption in topological insulator Bi_2SeTe_2 nanosheets. Opt Express 2015;23:13376–83.
[112] Wang Y, Mu H, Li X, et al. Observation of large nonlinear responses in a graphene-Bi_2Te_3 heterostructure at a telecommunication wavelength. Appl Phys Lett 2016;108:221901.
[113] Miao L, Yi J, Wang Q, et al. Broadband third order nonlinear optical responses of bismuth telluride nanosheets. Opt Mater Express 2016;6:2244–51.
[114] Xu M, Liang T, Shi M, Chen H. Graphene-like two-dimensional materials. Chem Rev 2013;113:3766–98.
[115] Wang K, Wang J, Fan J, et al. Ultrafast saturable absorption of two-dimensional MoS_2 nanosheets. ACS Nano 2013;7:9260–7.
[116] Zhou KG, Zhao M, Chang MJ, et al. Size-dependent nonlinear optical properties of atomically thin transition metal dichalcogenide nanosheets. Small 2015;11:694–701.
[117] Jiang Y, Miao L, Jiang G, et al. Broadband and enhanced nonlinear optical response of MoS_2/graphene nanocomposites for ultrafast photonics applications. Sci Rep 2015;5:16372.
[118] Sun J, Gu Y-J, Lei DY, et al. Mechanistic understanding of excitation-correlated nonlinear optical properties in MoS_2 nanosheets and nanodots: the role of exciton resonance. ACS Photon 2016;3:2434–44.
[119] Dong N, Li Y, Zhang S, et al. Dispersion of nonlinear refractive index in layered WS_2 and WSe_2 semiconductor films induced by two-photon absorption. Opt Lett 2016;41:3936–9.
[120] Bikorimana S, Lama P, Walser A, et al. Nonlinear optical responses in two-dimensional transition metal dichalcogenide multilayer: WS_2, WSe_2, MoS_2 and $Mo_{0.5}W_{0.5}S_2$. Opt Express 2016;24:20685–95.
[121] Niu K, Sun R, Chen Q, Man B, Zhang H. Passively mode-locked Er-doped fiber laser based on SnS_2 nanosheets as a saturable absorber. Photon Res 2018;6:72–6.
[122] Niu K, Chen Q, Sun R, Man B, Zhang H. Passively Q-switched erbium-doped fiber laser based on SnS_2 saturable absorber. Opt Mater Express 2017;7:3934–43.
[123] Liu JS, Li XH, Guo YX, et al. $SnSe_2$ nanosheets for subpicosecond harmonic mode-locked pulse generation. Small 2019;15:1902811.
[124] Mao D, Cui X, Gan X, Li M, Zhang W, Lu H, Zhao J. Passively Q-switched and mode-locked fiber laser based on an ReS_2 saturable absorber. IEEE J Sel Top Quantum Electron 2017;24:1–6.
[125] Xu X, Jiang M, Li D, Wang R, Ren Z, Bai J. Passive Q-switching based on ReS_2 saturable absorber in Er-doped fiber laser at 1532 nm. Opt Quantum Electron 2018;50:39.
[126] Koo J, Jhon YI, Park J, Lee J, Jhon YM, Lee JH. Near-infrared saturable absorption of defective bulk-structured WTe_2 for femtosecond laser mode-locking. Adv Funct Mater 2016;26:7454–61.
[127] Gao W, Huang L, Xu J, et al. Broadband photocarrier dynamics and nonlinear absorption of PLD-grown WTe_2 semimetal films. Appl Phys Lett 2018;112:171112.
[128] Ge Y, Zhu Z, Xu Y, et al. Broadband nonlinear photoresponse of 2D TiS_2 for ultrashort pulse generation and all-optical thresholding devices. Adv Opt Mater 2018;6:1701166.
[129] Zhu X, Chen S, Zhang M, et al. TiS_2-based saturable absorber for ultrafast fiber lasers. Photon Res 2018;6:C44–8.
[130] Wang X, Lan S. Optical properties of black phosphorus. Adv Opt Photon 2016;8:618–55.
[131] Batmunkh M, Bat-Erdene M, Shapter JG. Phosphorene and phosphorene-based materials-prospects for future applications. Adv Mater 2016;28:8586–617.
[132] Zhang M, Wu Q, Zhang F, et al. 2D black phosphorus saturable absorbers for ultrafast photonics. Adv Opt Mater 2019;7:1800224.
[133] Lu S, Miao L, Guo Z, et al. Broadband nonlinear optical response in multi-layer black phosphorus: an emerging infrared and mid-infrared optical material. Opt Express 2015;23:11183–94.
[134] Wang Y, Huang G, Mu H, et al. Ultrafast recovery time and broadband saturable absorption properties of black phosphorus suspension. Appl Phys Lett 2015;107:091905.
[135] Zheng X, Chen R, Shi G, Zhang J, Xu Z, Jiang T. Characterization of nonlinear properties of black phosphorus nanoplatelets with femtosecond pulsed Z-scan measurements. Opt Lett 2015;40:3480–3.
[136] Chen R, Tang Y, Zheng X, Jiang T. Giant nonlinear absorption and excited carrier dynamics of black phosphorus few-layer nanosheets in broadband spectra. Appl Opt 2016;55:10307–12.

[137] Su Y, Kshirsagar CU, Robbins MC, Haratipour N, Koester SJ. Symmetric complementary logic inverter using integrated black phosphorus and MoS_2 transistors. 2D Mater 2016;3:011006.
[138] Yang T, Abdelwahab I, Lin H, et al. Anisotropic third-order nonlinearity in pristine and lithium hydride intercalated black phosphorus. ACS Photon 2018;5:4969–77.
[139] Li R, Zhang L, Shi L, Wang P. MXene Ti_3C_2: an effective 2D light-to-heat conversion material. ACS Nano 2017;11:3752–9.
[140] Peng Y-Y, Akuzum B, Kurra N, et al. All-MXene (2D titanium carbide) solid-state microsupercapacitors for on-chip energy storage. Energy Environ Sci 2016;9:2847–54.
[141] Youngblood N, Peng R, Nemilentsau A, Low T, Li M. Layer-tunable third-harmonic generation in multilayer black phosphorus. ACS Photon 2016;4:8–14.
[142] Cox JD, Garcia De Abajo FJ. Plasmon-enhanced nonlinear wave mixing in nanostructured graphene. ACS Photon 2015;2:306–12.
[143] Kislyakov IM, Nunzi J-M, Zhang X, Xie Y, Bocharov VN, Wang J. Stimulated Brillouin scattering in dispersed graphene. Opt Express 2018;26:34346–65.
[144] Zu Y, Zhang C, Guo X, et al. A solid-state passively Q-switched Tm,Gd:CaF_2 laser with a $Ti_3C_2T_x$ MXene absorber near 2 μm. Laser Phys Lett 2019;16:015803.
[145] Li C, Liu J, Guo Z, et al. Black phosphorus saturable absorber for a diode-pumped passively Q-switched Er:CaF_2 mid-infrared laser. Opt Commun 2018;406:158–62.
[146] Liu J, Liu J, Guo Z, et al. Dual-wavelength Q-switched Er:SrF_2 laser with a black phosphorus absorber in the mid-infrared region. Opt Express 2016;24:30289–95.
[147] Wu K, Chen B, Zhang X, et al. High-performance mode-locked and Q-switched fiber lasers based on novel 2D materials of topological insulators, transition metal dichalcogenides and black phosphorus: review and perspective. Opt Commun 2018;406:214–29.
[148] Tian Z, Wu K, Kong L, et al. Mode-locked thulium fiber laser with MoS_2. Laser Phys Lett 2015;12:065104.
[149] Wei C, Luo H, Zhang H, et al. Passively Q-switched mid-infrared fluoride fiber laser around 3 μm using a tungsten disulfide (WS_2) saturable absorber. Laser Phys Lett 2016;13:105108.
[150] Hou J, Zhao G, Wu Y, He J, Hao X. Femtosecond solid-state laser based on tungsten disulfide saturable absorber. Opt Express 2015;23:27292–8.
[151] Wu K, Zhang X, Wang J, Li X, Chen J. WS_2 as a saturable absorber for ultrafast photonic applications of mode-locked and Q-switched lasers. Opt Express 2015;23:11453–61.
[152] Guoyu H, Song Y, Li K, Dou Z, Tian J, Zhang X. Mode-locked ytterbium-doped fiber laser based on tungsten disulphide. Laser Phys Lett 2015;12:125102.
[153] Guo C, Chen B, Wang H, et al. Investigation on the stability of WSe_2-PVA saturable absorber in an all PM Q-switched fiber laser. IEEE Photon J 2016;8:1–12.
[154] Wu K, Zhang X, Wang J, Chen J. 463-MHz fundamental mode-locked fiber laser based on few-layer MoS_2 saturable absorber. Opt Lett 2015;40:1374–7.
[155] Wang Q, Chen Y, Miao L, et al. Wide spectral and wavelength-tunable dissipative soliton fiber laser with topological insulator nano-sheets self-assembly films sandwiched by PMMA polymer. Opt Express 2015;23:7681–93.
[156] Li S, Yu Y, Qiuyun O, et al. Dissipative soliton generation in Er-doped fibre laser using SnS_2 as saturable absorber. Appl Phys Express 2019;12:102008.
[157] Li S, Yin Y, Ran G, et al. Dual-wavelength mode-locked erbium-doped fiber laser based on tin disulfide thin film as saturable absorber. J Appl Phys 2019;125:243104.
[158] Li S, Yin Y, Lewis E, et al. Multiwavelength Q-switched pulse operation with gold nanoparticles as saturable absorber. Opt Eng 2019;58:066104.
[159] Maiman TH. Stimulated optical radiation in ruby. Nature 1960;187:493–4.
[160] Shi R, Bai Y, Qi M, et al. A passively mode-locked intracavity frequency doubled Nd: YVO_4 femtosecond green laser based on graphene. Laser Phys Lett 2013;11:025001.
[161] Cihan C, Kocabas C, Demirbas U, Sennaroglu A. Graphene mode-locked femtosecond Alexandrite laser. Opt Lett 2018;43:3969–72.
[162] Baek IH, Lee HW, Bae S, et al. Efficient mode-locking of sub-70-fs Ti: sapphire laser by graphene saturable absorber. Appl Phys Express 2012;5:032701.
[163] Xu J-L, Li X-L, He J-L, et al. Performance of large-area few-layer graphene saturable absorber in femtosecond bulk laser. Appl Phys Lett 2011;99:261107.
[164] Tan W, Su C, Knize R, Xie G, Li L, Tang D. Mode locking of ceramic Nd: yttrium aluminum garnet with graphene as a saturable absorber. Appl Phys Lett 2010;96:031106.
[165] Xu J-L, Li X-L, Wu Y-Z, Hao X-P, He J-L, Yang K-J. Graphene saturable absorber mirror for ultra-fast-pulse solid-state laser. Opt Lett 2011;36:1948–50.
[166] Li L, Ren Z, Chen X, et al. Passively mode-locked radially polarized Nd-doped yttrium aluminum garnet laser based on graphene-based saturable absorber. Appl Phys Express 2013;6:082701.
[167] Ma J, Huang H, Ning K, et al. Generation of 30 fs pulses from a diode-pumped graphene mode-locked Yb: $CaYAlO_4$ laser. Opt Lett 2016;41:890–3.
[168] Xu S, Man B, Jiang S, et al. Direct growth of graphene on quartz substrate as saturable absorber for femtosecond solid-state laser. Laser Phys Lett 2014;11:085801.
[169] Husaini S, Bedford R. Graphene saturable absorber for high power semiconductor disk laser mode-locking. Appl Phys Lett 2014;104:161107.
[170] Cho WB, Kim JW, Lee HW, et al. High-quality, large-area monolayer graphene for efficient bulk laser mode-locking near 1.25 μm. Opt Lett 2011;36:4089–91.
[171] Cafiso SDDD, Ugolotti E, Schmidt A, et al. Sub-100-fs Cr: YAG laser mode-locked by monolayer graphene saturable absorber. Opt Lett 2013;38:1745–7.
[172] Ma J, Xie G, Lv P, et al. Graphene mode-locked femtosecond laser at 2 μm wavelength. Opt Lett 2012;37:2085–7.
[173] Liu J, Wang Y, Qu Z, Zheng L, Su L, Xu J. Graphene oxide absorber for 2 μm passive mode-locking Tm: $YAlO_3$ laser. Laser Phys Lett 2011;9:15.
[174] Lagatsky A, Sun Z, Kulmala T, et al. 2 μm solid-state laser mode-locked by single-layer graphene. Appl Phys Lett 2013;102:013113.
[175] Cho WB, Choi SY, Zhu C, et al. Graphene mode-locked femtosecond $Cr2^+$: ZnS laser with ~300 nm tuning range. Opt Express 2016;24:20774–80.

[176] Tolstik N, Pospischil A, Sorokin E, Sorokina IT. Graphene mode-locked Cr: ZnS chirped-pulse oscillator. Opt Express 2014;22:7284–9.
[177] Tolstik N, Sorokin E, Sorokina IT. Graphene mode-locked Cr: ZnS laser with 41 fs pulse duration. Opt Express 2014;22:5564–71.
[178] Zhao W-F, Yu H, Liao M-Z, et al. Large area growth of monolayer MoS_2 film on quartz and its use as a saturable absorber in laser mode-locking. Semicond Sci Technol 2017;32:025013.
[179] Zou X, Leng Y, Li Y, et al. Passively Q-switched mode-locked Tm: LLF laser with a MoS_2 saturable absorber. Chin Opt Lett 2015;13:081405.
[180] Su X, Wang Y, Zhang B, et al. Femtosecond solid-state laser based on a few-layered black phosphorus saturable absorber. Opt Lett 2016;41:1945–8.
[181] Zhang B, Lou F, Zhao R, et al. Exfoliated layers of black phosphorus as saturable absorber for ultrafast solid-state laser. Opt Lett 2015;40:3691–4.
[182] Sun X, Zhang B, Yan B, et al. Few-layer $Ti_3C_2T_x$ (T=O, OH, or F) saturable absorber for a femtosecond bulk laser. Opt Lett 2018;43:3862–5.
[183] Lou F, Cui L, Li Y-B, et al. High-efficiency femtosecond Yb: $Gd_3Al_{0.5}Ga_{4.5}O_{12}$ mode-locked laser based on reduced graphene oxide. Opt Lett 2013;38:4189–92.
[184] Wang Y, Chen W, Mero M, et al. Sub-100 fs Tm: $MgWO_4$ laser at 2017 nm mode locked by a graphene saturable absorber. Opt Lett 2017;42:3076–9.
[185] Yu H, Chen X, Zhang H, et al. Large energy pulse generation modulated by graphene epitaxially grown on silicon carbide. ACS Nano 2010;4:7582–6.
[186] Xu B, Cheng Y, Wang Y, et al. Passively Q-switched Nd: $YAlO_3$ nanosecond laser using MoS_2 as saturable absorber. Opt Express 2014;22:28934–40.
[187] Serres JM, Jambunathan V, Mateos X, et al. Graphene Q-switched compact Yb:YAG laser. IEEE Photon J 2015;7:1–7.
[188] Chu H, Zhao S, Li T, et al. Dual-wavelength passively Q-switched Nd, Mg: $LiTaO_3$ Laser with a monolayer graphene as saturable absorber. IEEE J Sel Top Quantum Electron 2014;21:343–7.
[189] Men S, Liu Z, Zhang X, et al. A graphene passively Q-switched Nd: YAG ceramic laser at 1123 nm. Laser Phys Lett 2013;10:035803.
[190] Xu J-L, Li X-L, He J-L, et al. Efficient graphene Q switching and mode locking of 1.34 μm neodymium lasers. Opt Lett 2012;37:2652–4.
[191] Gao C, Wang R, Zhu L, et al. Resonantly pumped 1.645 μm high repetition rate Er: YAG laser Q-switched by a graphene as a saturable absorber. Opt Lett 2012;37:632–4.
[192] Zhao T, Wang Y, Chen H, Shen D. Graphene passively Q-switched Ho: YAG ceramic laser. Appl Phys B 2014;116:947–50.
[193] Serres JM, Loiko P, Mateos X, et al. Tm: $KLu(WO_4)_2$ microchip laser Q-switched by a graphene-based saturable absorber. Opt Express 2015;23:14108–13.
[194] Wang Q, Teng H, Zou Y, et al. Graphene on SiC as a Q-switcher for a 2 μm laser. Opt Lett 2012;37:395–7.
[195] Wang Z-W, Chen X-F, He J-L, et al. Graphene Q-switched Cr: ZnSe laser. IEEE J Quantum Electron 2015;51:1–5.
[196] Li X-L, Xu J-L, Wu Y-Z, He J-L, Hao X-P. Large energy laser pulses with high repetition rate by graphene Q-switched solid-state laser. Opt Express 2011;19:9950–5.
[197] Li L, Zheng X, Jin C, et al. High repetition rate Q-switched radially polarized laser with a graphene-based output coupler. Appl Phys Lett 2014;105:221103.
[198] Wen Q, Zhang X, Wang Y, Wang Y, Niu H. Passively Q-switched Nd: YAG laser with graphene oxide in heavy water. IEEE Photon J 2014;6:1–6.
[199] Jia F, Chen H, Liu P, Huang Y, Luo Z. Nanosecond-pulsed, dual-wavelength passively Q-switched c-Cut Nd: YVO_4 laser using a few-layer Bi_2Se_3 saturable absorber. IEEE J Sel Top Quantum Electron 2014;21:369–74.
[200] Xu B, Wang Y, Peng J, et al. Topological insulator Bi_2Se_3 based Q-switched Nd: $LiYF_4$ nanosecond laser at 1313 nm. Opt Express 2015;23:7674–80.
[201] Liu X, Yang K, Zhao S, et al. High-power passively Q-switched 2 μm all-solid-state laser based on a Bi_2Te_3 saturable absorber. Photon Res 2017;5:461.
[202] Yang J, Tian K, Li Y, et al. Few-layer Bi_2Te_3: an effective 2D saturable absorber for passive Q-switching of compact solid-state lasers in the 1-μm region. Opt Express 2018;26:21379–89.
[203] Qiao J, Zhao S, Yang K, et al. High-quality 2-μm Q-switched pulsed solid-state lasers using spin-coating-coreduction approach synthesized Bi_2Te_3 topological insulators. Photon Res 2018;6:314–20.
[204] Dou X, Yang J, Zhu M, et al. Watt-level passively Q-switched Yb: $LuPO_4$ miniature crystal laser with few-layer MoS_2 saturable absorber. Opt Express 2018;26:14232–40.
[205] Ge P, Liu J, Jiang S, Xu Y, Man B. Compact Q-switched 2 μm Tm: GdVO 4 laser with MoS_2 absorber. Photon Res 2015;3:256–9.
[206] Kong L, Xie G, Yuan P, et al. Passive Q-switching and Q-switched mode-locking operations of 2 μm Tm: CLNGG laser with MoS_2 saturable absorber mirror. Photon Res 2015;3:A47–50.
[207] Fan M, Li T, Zhao S, et al. Watt-level passively Q-switched Er: Lu 2 O 3 laser at 2.84 μm using MoS_2. Opt Lett 2016;41:540–3.
[208] Tang W, Wang Y, Yang K, et al. 1.36 W passively Q-switched YVO 4/Nd: YVO 4 laser with a WS_2 saturable absorber. IEEE Photon Technol Lett 2017;29:470–3.
[209] Tang CY, Cheng PK, Tao L, et al. Passively Q-switched Nd: YVO 4 laser using WS_2 saturable absorber fabricated by radio frequency magnetron sputtering deposition. J Lightwave Technol 2017;35:4120–4.
[210] Qiao J, Zhao S, Yang K, et al. Sub-nanosecond KTP-OPO pumped by a hybrid Q-switched laser with WS_2 saturable absorber and AOM. Opt Mater Express 2017;7:3998–4009.
[211] Guan X, Wang J, Zhang Y, et al. Self-Q-switched and wavelength-tunable tungsten disulfide-based passively Q-switched Er: Y_2O_3 ceramic lasers. Photon Res 2018;6:830–6.
[212] Ma J, Lu S, Guo Z, et al. Few-layer black phosphorus based saturable absorber mirror for pulsed solid-state lasers. Opt Express 2015;23:22643–8.
[213] Liu Q, Zhang B, Qi S, et al. Integration of helicity-control and pulse-modulation for vortex laser based on a black phosphorus plate. Opt Express 2016;24:30031–7.
[214] Liu H, Sun Z, Wang X, Wang Y, Cheng G. Several nanosecond Nd: YVO_4 lasers Q-switched by two dimensional materials: tungsten disulfide, molybdenum disulfide, and black phosphorous. Opt Express 2017;25:6244–52.
[215] Chu Z, Liu J, Guo Z, Zhang H. 2 μm passively Q-switched laser based on black phosphorus. Opt Mater Express 2016;6:2374–9.
[216] Nie H, Zhang P, Zhang B, et al. Watt-level continuous-wave and black phosphorus passive Q-switching operation of Ho^{3+},

Pr^{3+}: $LiLuF_4$ bulk laser at 2.95 μm. IEEE J Sel Top Quantum Electron 2017;24:1–5.
[217] Liu X, Zhang S, Yan Z, et al. WSe_2 as a saturable absorber for a passively Q-switched Ho, Pr: LLF laser at 2.95 μm. Opt Mater Express 2018;8:1213–20.
[218] Su X, Zhang B, Wang Y, et al. Broadband rhenium disulfide optical modulator for solid-state lasers. Photon Res 2018;6:498–505.
[219] Wang M, Wang Z, Xu X, Duan S, Du C. Tin diselenide-based saturable absorbers for eye-safe pulse lasers. Nanotechnology 2019;30:265703.
[220] Zhang Y, Wang J, Guan X, et al. $MoTe_2$-based broadband wavelength tunable eye-safe pulsed laser source at 1.9 μm. IEEE Photon Technol Lett 2018;30:1890–3.
[221] Yan B, Zhang B, Nie H, et al. Bilayer platinum diselenide saturable absorber for 2.0 μm passively Q-switched bulk lasers. Opt Express 2018;26:31657–63.
[222] Yao Y, Cui N, Wang Q, et al. Highly efficient continuous-wave and $ReSe_2$ Q-switched ~3 μm dual-wavelength Er: YAP crystal lasers. Opt Lett 2019;44:2839–42.
[223] Belforte DA. A great year for the industrial laser business in the USA. Laser Tech J 2018;15:30–1.
[224] Guo B, Wang S-H, Wu Z-X, et al. Sub-200 fs soliton mode-locked fiber laser based on bismuthene saturable absorber. Opt Express 2018;26:22750–60.
[225] Jiang X, Zhang L, Liu S, et al. Ultrathin metal-organic framework: an emerging broadband nonlinear optical material for ultrafast photonics. Adv Opt Mater 2018;6:1800561.
[226] Zhang M, Wu Q, Zhang F, et al. 2D Black phosphorus saturable absorbers for ultrafast photonics. Adv Opt Mater 2018;7:1800224.
[227] Song Y, Liang Z, Jiang X, et al. Few-layer antimonene decorated microfiber: ultra-short pulse generation and all-optical thresholding with enhanced long term stability. 2D Mater 2017;4:045010.
[228] Sun Z, Hasan T, Torrisi F, et al. Graphene mode-locked ultrafast laser. ACS Nano 2010;4:803–10.
[229] Song Y-W, Jang S-Y, Han W-S, Bae M-K. Graphene mode-lockers for fiber lasers functioned with evanescent field interaction. Appl Phys Lett 2010;96:051122.
[230] Popa D, Sun Z, Torrisi F, Hasan T, Wang F, Ferrari AC. Sub 200 fs pulse generation from a graphene mode-locked fiber laser. Appl Phys Lett 2010;97:203106.
[231] Chang YM, Kim H, Lee JH, Song Y-W. Multilayered graphene efficiently formed by mechanical exfoliation for nonlinear saturable absorbers in fiber mode-locked lasers. Appl Phys Lett 2010;97:211102.
[232] Sun Z, Popa D, Hasan T, et al. A stable, wideband tunable, near transform-limited, graphene-mode-locked, ultrafast laser. Nano Res 2010;3:653–60.
[233] Martinez A, Fuse K, Xu B, Yamashita S. Optical deposition of graphene and carbon nanotubes in a fiber ferrule for passive mode-locked lasing. Opt Express 2010;18:23054–61.
[234] Kim H, Cho J, Jang S-Y, Song Y-W. Deformation-immunized optical deposition of graphene for ultrafast pulsed lasers. Appl Phys Lett 2011;98:021104.
[235] Cunning B, Brown C, Kielpinski D. Low-loss flake-graphene saturable absorber mirror for laser mode-locking at sub-200-fs pulse duration. Appl Phys Lett 2011;99:261109.
[236] Liu Z-B, He X, Wang D. Passively mode-locked fiber laser based on a hollow-core photonic crystal fiber filled with few-layered graphene oxide solution. Opt Lett 2011;36:3024–6.
[237] Bao Q, Zhang H, Ni Z, et al. Monolayer graphene as a saturable absorber in a mode-locked laser. Nano Res 2011;4:297–307.
[238] Sobon G, Sotor J, Abramski KM. Passive harmonic mode-locking in Er-doped fiber laser based on graphene saturable absorber with repetition rates scalable to 2.22 GHz. Appl Phys Lett 2012;100:161109.
[239] Martinez A, Yamashita S. 10 GHz fundamental mode fiber laser using a graphene saturable absorber. Appl Phys Lett 2012;101:041118.
[240] Sotor J, Sobon G, Abramski KM. Scalar soliton generation in all-polarization-maintaining, graphene mode-locked fiber laser. Opt Lett 2012;37:2166–8.
[241] He X, Liu Z-B, Wang D. Wavelength-tunable, passively mode-locked fiber laser based on graphene and chirped fiber Bragg grating. Opt Lett 2012;37:2394–6.
[242] Huang PL, Lin S-C, Yeh C-Y, et al. Stable mode-locked fiber laser based on CVD fabricated graphene saturable absorber. Opt Express 2012;20:2460–5.
[243] Choi SY, Cho DK, Song Y-W, et al. Graphene-filled hollow optical fiber saturable absorber for efficient soliton fiber laser mode-locking. Opt Express 2012;20:5652–7.
[244] Sobon G, Sotor J, Jagiello J, et al. Graphene oxide vs. reduced graphene oxide as saturable absorbers for Er-doped passively mode-locked fiber laser. Opt Express 2012;20:19463–73.
[245] Xu J, Liu J, Wu S, Yang Q-H, Wang P. Graphene oxide mode-locked femtosecond erbium-doped fiber lasers. Opt Express 2012;20:15474–80.
[246] Cao Y, Gao L, Li Y, Zhang J, Li F, Zhu T. Graphene-based all-optical multi-parameter regulations for an ultrafast fiber laser. Opt Lett 2018;43:4378–81.
[247] Chen Y, Li C, Chen J-H, et al. Demonstration of a microelectromechanical tunable Fabry–Pérot cavity based on graphene-bonded fiber devices. Opt Lett 2019;44:1876–9.
[248] Liu M, Tang R, Luo A, Xu W, Luo Z. Graphene-decorated microfiber knot as a broadband resonator for ultrahigh-repetition-rate pulse fiber lasers. Photon Res 2018;6:C1–7.
[249] Chen T, Liao C, Wang D, Wang Y. Passively mode-locked fiber laser by using monolayer chemical vapor deposition of graphene on D-shaped fiber. Appl Opt 2014;53:2828–32.
[250] Rosa HG, Castañeda JA, Cruz CHB, et al. Controlled stacking of graphene monolayer saturable absorbers for ultrashort pulse generation in erbium-doped fiber lasers. Opt Mater Express 2017;7:2528–37.
[251] Chen T-H, Lin Y-H, Cheng C-H, Tsai C-T, Chi Y-C, Lin G-R. Unintentional polarization dependent pulsewidth of graphene mode-locked Er-doped fiber lasers. IEEE J Sel Top Quantum Electron 2016;23:50–9.
[252] Chen T-H, Cheng C-H, Lin Y-H, et al. Optimizing the self-amplitude modulation of different 2-D saturable absorbers for ultrafast mode-locked fiber lasers. IEEE J Sel Top Quantum Electron 2019;25:1–10.
[253] Popa D, Jiang Z, Bonacchini G, et al. A stable, power scaling, graphene-mode-locked all-fiber oscillator. Appl Phys Lett 2017;110:243102.
[254] Mouchel P, Semaan G, Niang A, Salhi M, Le Flohic M, Sanchez F. High power passively mode-locked fiber laser

based on graphene nanocoated optical taper. Appl Phys Lett 2017;111:031106.
[255] Baylam I, Zharar S, Kakenov N, Kocabaş C, Sennaroğlu A. Femtosecond pulse generation with voltage-controlled graphene saturable absorbers. Opt Lett 2014;39:5180–3.
[256] Yang Y, Loeblein M, Tsang S, Chow K, Teo E. Three-dimensional graphene based passively mode-locked fiber laser. Opt Express 2014;22:31458–65.
[257] Xin W, Liu Z-B, Sheng Q-W, et al. Flexible graphene saturable absorber on two-layer structure for tunable mode-locked soliton fiber laser. Opt Express 2014;22:10239–47.
[258] Meng Y, Niang A, Guesmi K, Salhi M, Sanchez F. 1.61 μm high-order passive harmonic mode locking in a fiber laser based on graphene saturable absorber. Opt Express 2014;22:29921–6.
[259] Xu J, Wu S, Liu J, et al. All-polarization-maintaining femtosecond fiber lasers using graphene oxide saturable absorber. IEEE Photon Technol Lett 2013;26:346–8.
[260] Lee EJ, Choi SY, Jeong H, et al. Active control of all-fibre graphene devices with electrical gating. Nat Commun 2015;6:6851.
[261] Purdie D, Popa D, Wittwer V, et al. Few-cycle pulses from a graphene mode-locked all-fiber laser. Appl Phys Lett 2015;106:253101.
[262] Mou C, Arif R, Lobach AS, et al. Poor fluorinated graphene sheets carboxymethylcellulose polymer composite mode locker for erbium doped fiber laser. Appl Phys Lett 2015;106:061106.
[263] Park J, Park K, Spoor D, Hall B, Song Y-W. Hand-manageable graphene sticker for ultrafast mode-locked fiber lasers. Opt Express 2015;23:7940–5.
[264] Wang J, Luo Z, Zhou M, et al. Evanescent-light deposition of graphene onto tapered fibers for passive Q-switch and mode-locker. IEEE Photon J 2012;4:1295–305.
[265] Fu B, Hua Y, Xiao X, Zhu H, Sun Z, Yang C. Broadband graphene saturable absorber for pulsed fiber lasers at 1, 1.5, and 2 μm. IEEE J Sel Top Quantum Electron 2014;20:411–5.
[266] Zhao L, Tang D, Zhang H, Wu X, Bao Q, Loh KP. Dissipative soliton operation of an ytterbium-doped fiber laser mode locked with atomic multilayer graphene. Opt Lett 2010;35:3622–4.
[267] Luo Z, Huang Y, Wang J, Cheng H, Cai Z, Ye C. Multiwavelength dissipative-soliton generation in Yb-fiber laser using graphene-deposited fiber-taper. IEEE Photon Technol Lett 2012;24:1539–42.
[268] Zhou J, Luo A, Luo Z, Wang X, Feng X, Guan B-O. Dual-wavelength single-longitudinal-mode fiber laser with switchable wavelength spacing based on a graphene saturable absorber. Photon Res 2015;3:A21–4.
[269] Li X, Tang Y, Yan Z, et al. Broadband saturable absorption of graphene oxide thin film and its application in pulsed fiber lasers. IEEE J Sel Top Quantum Electron 2014;20:441–7.
[270] Cheng Z, Li H, Shi H, Ren J, Yang Q-H, Wang P. Dissipative soliton resonance and reverse saturable absorption in graphene oxide mode-locked all-normal-dispersion Yb-doped fiber laser. Opt Express 2015;23:7000–6.
[271] Li X, Wang Y, Wang Y, et al. All-normal-dispersion passively mode-locked Yb-doped fiber ring laser based on a graphene oxide saturable absorber. Laser Phys Lett 2013;10:075108.
[272] Huang S, Wang Y, Yan P, Zhao J, Li H, Lin R. Tunable and switchable multi-wavelength dissipative soliton generation in a graphene oxide mode-locked Yb-doped fiber laser. Opt Express 2014;22:11417–26.
[273] Lin J-H, Huang G-H, Ou C-H, et al. Q-Switched pulse and mode-locked pulse generation from a Yb^{3+}-Doped fiber laser based on Bi_2Se_3. IEEE Photon J 2018;10:1–10.
[274] Yan P, Lin R, Chen H, et al. Topological insulator solution filled in photonic crystal fiber for passive mode-locked fiber laser. IEEE Photon Technol Lett 2014;27:264–7.
[275] Kowalczyk M, Bogusławski J, Zybała R, et al. Sb_2Te_3-deposited D-shaped fiber as a saturable absorber for mode-locked Yb-doped fiber lasers. Opt Mater Express 2016;6:2273–82.
[276] Zhang H, Lu S, Zheng J, et al. Molybdenum disulfide (MoS_2) as a broadband saturable absorber for ultra-fast photonics. Opt Express 2014;22:7249–60.
[277] Lv R, Chen Z, Liu S, et al. Optical properties and applications of molybdenum disulfide/SiO_2 saturable absorber fabricated by sol-gel technique. Opt Express 2019;27:6348–56.
[278] Du J, Wang Q, Jiang G, et al. Ytterbium-doped fiber laser passively mode locked by few-layer molybdenum disulfide (MoS_2) saturable absorber functioned with evanescent field interaction. Sci Rep 2014;4:6346.
[279] Yang H, Liu X. Nonlinear optical response and applications of tin disulfide in the near-and mid-infrared. Appl Phys Lett 2017;110:171106.
[280] Wang T, Wang J, Wu J, et al. Near-infrared optical modulation for ultrashort pulse generation employing indium monosulfide (InS) two-dimensional semiconductor nanocrystals. Nanomaterials 2019;9:865.
[281] Long H, Tang CY, Cheng PK, Wang XY, Qarony W, Tsang YH. Ultrafast laser pulses generation by using 2D layered PtS_2 as a saturable absorber. J Lightwave Technol 2018;37:1174–9.
[282] Li L, Jiang S, Wang Y, et al. WS_2/fluorine mica (FM) saturable absorbers for all-normal-dispersion mode-locked fiber laser. Opt Express 2015;23:28698–706.
[283] Mao D, Zhang S, Wang Y, et al. WS_2 saturable absorber for dissipative soliton mode locking at 1.06 and 1.55 μm. Opt Express 2015;23:27509–19.
[284] Hisyam MB, Rusdi MFM, Latiff AA, Harun SW. Generation of mode-locked ytterbium doped fiber ring laser using few-layer black phosphorus as a saturable absorber. IEEE J Sel Top Quantum Electron 2016;23:39–43.
[285] Li Y, He Y, Cai Y, et al. Black phosphorus: broadband nonlinear optical absorption and application. Laser Phys Lett 2018;15:025301.
[286] Tuo M, Xu C, Mu H, et al. Ultrathin 2D transition metal carbides for ultrafast pulsed fiber lasers. ACS Photon 2018;5:1808–16.
[287] Bao Q, Zhang H, Yang JX, et al. Graphene–polymer nanofiber membrane for ultrafast photonics. Adv Funct Mater 2010;20:782–91.
[288] Zhang M, Howe RC, Woodward RI, et al. Solution processed MoS_2-PVA composite for sub-bandgap mode-locking of a wideband tunable ultrafast Er: fiber laser. Nano Res 2015;8:1522–34.
[289] Zhang H, Tang D, Zhao L, et al. Compact graphene mode-locked wavelength-tunable erbium-doped fiber lasers: from all anomalous dispersion to all normal dispersion. Laser Phys Lett 2010;7:591.

[290] Sobon G, Sotor J, Pasternak I, et al. Chirped pulse amplification of a femtosecond Er-doped fiber laser mode-locked by a graphene saturable absorber. Laser Phys Lett 2013;10:035104.
[291] Meng Y, Zhang S, Li X, Li H, Du J, Hao Y. Passive harmonically mode-locked fiber laser with low pumping power based on a graphene saturable absorber. Laser Phys Lett 2012;9:537.
[292] Sobon G, Sotor J, Pasternak I, et al. Er-doped fiber laser mode-locked by CVD-graphene saturable absorber. J Lightwave Technol 2012;30:2770–5.
[293] Castellani C, Kelleher E, Luo Z, et al. Harmonic and single pulse operation of a Raman laser using graphene. Laser Phys Lett 2012;9:223.
[294] Sobon G, Sotor J, Abramski K. All-polarization maintaining femtosecond Er-doped fiber laser mode-locked by graphene saturable absorber. Laser Phys Lett 2012;9:581.
[295] Song YF, Li L, Tang DY. Quasi-periodicity of vector solitons in a graphene mode-locked fiber laser. Laser Phys Lett 2013;10:125103.
[296] Cai Y, Zhu J, Liu QH. Tunable enhanced optical absorption of graphene using plasmonic perfect absorbers. Appl Phys Lett 2015;106:043105.
[297] Lee H, Kwon WS, Kim JH, Kang D, Kim S. Polarization insensitive graphene saturable absorbers using etched fiber for highly stable ultrafast fiber lasers. Opt Express 2015;23:22116–22.
[298] Xu H, Wan X, Ruan Q, et al. Effects of nanomaterial saturable absorption on passively mode-locked fiber lasers in an anomalous dispersion regime: simulations and experiments. IEEE J Sel Top Quantum Electron 2017;24:1–9.
[299] Lau K, Bakar MA, Muhammad F, et al. Dual-wavelength, mode-locked erbium-doped fiber laser employing a graphene/polymethyl-methacrylate saturable absorber. Opt Express 2018;26:12790–800.
[300] Zhu P-F, Lin Z-B, Ning Q-Y, et al. Passive harmonic mode-locking in a fiber laser by using a microfiber-based graphene saturable absorber. Laser Phys Lett 2013;10:105107.
[301] Sheng Q-W, Feng M, Xin W, et al. Tunable graphene saturable absorber with cross absorption modulation for mode-locking in fiber laser. Appl Phys Lett 2014;105:041901.
[302] He X, Wang D, Liu Z-B. Pulse-width tuning in a passively mode-locked fiber laser with graphene saturable absorber. IEEE Photon Technol Lett 2013;26:360–3.
[303] Qi Y-L, Liu H, Cui H, et al. Graphene-deposited microfiber photonic device for ultrahigh-repetition rate pulse generation in a fiber laser. Opt Express 2015;23:17720–6.
[304] Yu S, Meng C, Chen B, et al. Graphene decorated microfiber for ultrafast optical modulation. Opt Express 2015;23:10764–70.
[305] Liu X, Yang H, Cui Y, et al. Graphene-clad microfibre saturable absorber for ultrafast fibre lasers. Sci Rep 2016;6:26024.
[306] Luo Z, Wang J, Zhou M, Xu H, Cai Z, Ye C. Multiwavelength mode-locked erbium-doped fiber laser based on the interaction of graphene and fiber-taper evanescent field. Laser Phys Lett 2012;9:229.
[307] Lee J, Koo J, Debnath P, Song Y, Lee J. A Q-switched, mode-locked fiber laser using a graphene oxide-based polarization sensitive saturable absorber. Laser Phys Lett 2013;10:035103.
[308] Park NH, Jeong H, Choi SY, Kim MH, Rotermund F, Yeom D-I. Monolayer graphene saturable absorbers with strongly enhanced evanescent-field interaction for ultrafast fiber laser mode-locking. Opt Express 2015;23:19806–12.
[309] Zapata J, Steinberg D, Saito LA, De Oliveira R, Cárdenas A, De Souza ET. Efficient graphene saturable absorbers on D-shaped optical fiber for ultrashort pulse generation. Sci Rep 2016;6:1–8.
[310] Choi SY, Jeong H, Hong BH, Rotermund F, Yeom D-I. All-fiber dissipative soliton laser with 10.2 nJ pulse energy using an evanescent field interaction with graphene saturable absorber. Laser Phys Lett 2013;11:015101.
[311] Lin Y-H, Yang C-Y, Liou J-H, Yu C-P, Lin G-R. Using graphene nano-particle embedded in photonic crystal fiber for evanescent wave mode-locking of fiber laser. Opt Express 2013;21:16763–76.
[312] Boguslawski J, Sotor J, Sobon G, et al. Graphene oxide paper as a saturable absorber for Er-and Tm-doped fiber lasers. Photon Res 2015;3:119–24.
[313] Wu K, Li X, Wang Y, Wang QJ, Shum PP, Chen J. Towards low timing phase noise operation in fiber lasers mode locked by graphene oxide and carbon nanotubes at 1.5 μm. Opt Express 2015;23:501–11.
[314] Li X, Wu K, Sun Z, et al. Single-wall carbon nanotubes and graphene oxide-based saturable absorbers for low phase noise mode-locked fiber lasers. Sci Rep 2016;6:25266.
[315] Xu J, Wu S, Li H, et al. Dissipative soliton generation from a graphene oxide mode-locked Er-doped fiber laser. Opt Express 2012;20:23653–8.
[316] Wang Z, Wang Z, Liu Y, et al. Self-organized compound pattern and pulsation of dissipative solitons in a passively mode-locked fiber laser. Opt Lett 2018;43:478–81.
[317] Liu H, Zheng X-W, Liu M, et al. Femtosecond pulse generation from a topological insulator mode-locked fiber laser. Opt Express 2014;22:6868–73.
[318] Guo B, Yao Y. Tunable triple-wavelength mode-locked fiber laser with topological insulator Bi_2Se_3 solution. Opt Eng 2016;55:081315.
[319] Guo B, Yao Y, Yang Y-F, et al. Topological insulator: Bi_2Se_3/polyvinyl alcohol film-assisted multi-wavelength ultrafast erbium-doped fiber laser. J Appl Phys 2015;117:063108.
[320] Guo B, Yao Y, Yang Y-F, et al. Dual-wavelength rectangular pulse erbium-doped fiber laser based on topological insulator saturable absorber. Photon Res 2015;3:94–9.
[321] Jin L, Ma X, Zhang H, Zhang H, Chen H, Xu Y. 3 GHz passively harmonic mode-locked Er-doped fiber laser by evanescent field-based nano-sheets topological insulator. Opt Express 2018;26:31244–52.
[322] Lee J, Koo J, Jhon YM, Lee JH. A femtosecond pulse erbium fiber laser incorporating a saturable absorber based on bulk-structured Bi_2Te_3 topological insulator. Opt Express 2014;22:6165–73.
[323] Lee J, Koo J, Jhon YM, Lee JH. Femtosecond harmonic mode-locking of a fiber laser based on a bulk-structured Bi_2Te_3 topological insulator. Opt Express 2015;23:6359–69.
[324] Yan P, Lin R, Ruan S, Liu A, Chen H. A 2.95 GHz, femtosecond passive harmonic mode-locked fiber laser based on evanescent field interaction with topological insulator film. Opt Express 2015;23:154–64.
[325] Mao D, Jiang B, Gan X, et al. Soliton fiber laser mode locked with two types of film-based Bi_2Te_3 saturable absorbers. Photon Res 2015;3:A43–6.

[326] Sotor J, Sobon G, Macherzynski W, Paletko P, Grodecki K, Abramski KM. Mode-locking in Er-doped fiber laser based on mechanically exfoliated Sb_2Te_3 saturable absorber. Opt Mater Express 2014;4:1–6.
[327] Sotor J, Sobon G, Macherzynski W, Abramski K. Harmonically mode-locked Er-doped fiber laser based on a Sb_2Te_3 topological insulator saturable absorber. Laser Phys Lett 2014;11:055102.
[328] Bogusławski J, Soboń G, Zybała R, et al. Investigation on pulse shaping in fiber laser hybrid mode-locked by Sb_2Te_3 saturable absorber. Opt Express 2015;23:29014–23.
[329] Sotor J, Sobon G, Abramski KM. Sub-130 fs mode-locked Er-doped fiber laser based on topological insulator. Opt Express 2014;22:13244–9.
[330] Sotor J, Sobon G, Grodecki K, Abramski K. Mode-locked erbium-doped fiber laser based on evanescent field interaction with Sb_2Te_3 topological insulator. Appl Phys Lett 2014;104:251112.
[331] Xia H, Li H, Lan C, et al. Ultrafast erbium-doped fiber laser mode-locked by a CVD-grown molybdenum disulfide (MoS_2) saturable absorber. Opt Express 2014;22:17341–8.
[332] Liu H, Luo A-P, Wang F-Z, et al. Femtosecond pulse erbium-doped fiber laser by a few-layer MoS_2 saturable absorber. Opt Lett 2014;39:4591–4.
[333] Lü R, Wang Y, Wang J, et al. Soliton and bound-state soliton mode-locked fiber laser based on a MoS_2/fluorine mica Langmuir–Blodgett film saturable absorber. Photon Res 2019;7:431–6.
[334] Aiub EJ, Steinberg D, De Souza EAT, Saito LA. 200-fs mode-locked Erbium-doped fiber laser by using mechanically exfoliated MoS 2 saturable absorber onto D-shaped optical fiber. Opt Express 2017;25:10546–52.
[335] Khazaeizhad R, Kassani SH, Jeong H, Yeom D-I, Oh K. Mode-locking of Er-doped fiber laser using a multilayer MoS_2 thin film as a saturable absorber in both anomalous and normal dispersion regimes. Opt Express 2014;22:23732–42.
[336] Liu M, Zheng X-W, Qi Y-L, et al. Microfiber-based few-layer MoS_2 saturable absorber for 2.5 GHz passively harmonic mode-locked fiber laser. Opt Express 2014;22:22841–6.
[337] Cui Y, Lu F, Liu X. MoS_2-clad microfibre laser delivering conventional, dispersion-managed and dissipative solitons. Sci Rep 2016;6:30524.
[338] Khazaeinezhad R, Kassani SH, Jeong H, et al. Ultrafast pulsed all-fiber laser based on tapered fiber enclosed by few-layer WS_2 nanosheets. IEEE Photon Technol Lett 2015;27:1581–4.
[339] Yan P, Liu A, Chen Y, et al. Microfiber-based WS_2-film saturable absorber for ultra-fast photonics. Opt Mater Express 2015;5:479–89.
[340] Liu W, Pang L, Han H, et al. Tungsten disulfide saturable absorbers for 67 fs mode-locked erbium-doped fiber lasers. Opt Express 2017;25:2950–9.
[341] Guo B, Yao Y, Yan P-G, et al. Dual-wavelength soliton mode-locked fiber laser with a WS_2-based fiber taper. IEEE Photon Technol Lett 2015;28:323–6.
[342] Guo B, Li S, Fan Y-X, Wang P. Versatile soliton emission from a WS_2 mode-locked fiber laser. Opt Commun 2018;406:66–71.
[343] Yan P, Chen H, Yin J, et al. Large-area tungsten disulfide for ultrafast photonics. Nanoscale 2017;9:1871–7.
[344] Luo Z, Li Y, Zhong M, et al. Nonlinear optical absorption of few-layer molybdenum diselenide ($MoSe_2$) for passively mode-locked soliton fiber laser. Photon Res 2015;3:A79–86.
[345] Koo J, Park J, Lee J, Jhon YM, Lee JH. Femtosecond harmonic mode-locking of a fiber laser at 3.27 GHz using a bulk-like, $MoSe_2$-based saturable absorber. Opt Express 2016;24:10575–89.
[346] Mao D, Du B, Yang D, et al. Nonlinear saturable absorption of liquid-exfoliated molybdenum/tungsten ditelluride nanosheets. Small 2016;12:1489–97.
[347] Wang J, Jiang Z, Chen H, et al. High energy soliton pulse generation by a magnetron-sputtering-deposition-grown $MoTe_2$ saturable absorber. Photon Res 2018;6:535–41.
[348] Yin J, Li J, Chen H, et al. Large-area highly crystalline WSe_2 atomic layers for ultrafast pulsed lasers. Opt Express 2017;25:30020–31.
[349] Li S, Yin Y, Ouyang Q, et al. Dissipative soliton generation in Er-doped fibre laser using SnS_2 as a saturable absorber. Appl Phys Express 2019;12:102008.
[350] Xu X, He M, Quan C, et al. Saturable absorption properties of ReS_2 films and mode-locking application based on double-covered ReS_2 micro fiber. J Lightwave Technol 2018;36:5130–6.
[351] Fu S, Li J, Zhang S, Bai Z, Wu T, Man Z. Large-energy mode-locked Er-doped fiber laser based on indium selenide as a modulator. Opt Mater Express 2019;9:2662–71.
[352] Yan P, Jiang Z, Chen H, et al. α-In_2Se_3 wideband optical modulator for pulsed fiber lasers. Opt Lett 2018;43:4417–20.
[353] Huang B, Du L, Yi Q, et al. Bulk-structured $PtSe_2$ for femtosecond fiber laser mode-locking. Opt Express 2019;27:2604–11.
[354] Zhang K, Feng M, Ren Y, et al. Q-switched and mode-locked Er-doped fiber laser using $PtSe_2$ as a saturable absorber. Photon Res 2018;6:893–9.
[355] Sotor J, Sobon G, Macherzynski W, Paletko P, Abramski KM. Black phosphorus saturable absorber for ultrashort pulse generation. Appl Phys Lett 2015;107:051108.
[356] Xu Y, Jiang X-F, Ge Y, et al. Size-dependent nonlinear optical properties of black phosphorus nanosheets and their applications in ultrafast photonics. J Mater Chem C 2017;5:3007–13.
[357] Jin X, Hu G, Zhang M, et al. 102 fs pulse generation from a long-term stable, inkjet-printed black phosphorus-mode-locked fiber laser. Opt Express 2018;26:12506–13.
[358] Mao D, Li M, Cui X, et al. Stable high-power saturable absorber based on polymer-black-phosphorus films. Opt Commun 2018;406:254–9.
[359] Chen Y, Chen S, Liu J, Gao Y, Zhang W. Sub-300 femtosecond soliton tunable fiber laser with all-anomalous dispersion passively mode locked by black phosphorus. Opt Express 2016;24:13316–24.
[360] Zhao R, Li J, Zhang B, et al. Triwavelength synchronously mode-locked fiber laser based on few-layered black phosphorus. Appl Phys Express 2016;9:092701.
[361] Yun L. Black phosphorus saturable absorber for dual-wavelength polarization-locked vector soliton generation. Opt Express 2017;25:32380–5.
[362] Zhang M, Kelleher E, Torrisi F, et al. Tm-doped fiber laser mode-locked by graphene-polymer composite. Opt Express 2012;20:25077–84.
[363] Wang Q, Chen T, Zhang B, Li M, Lu Y, Chen KP. All-fiber passively mode-locked thulium-doped fiber ring laser using optically deposited graphene saturable absorbers. Appl Phys Lett 2013;102:131117.
[364] Sobon G, Sotor J, Pasternak I, Krajewska A, Strupinski W, Abramski KM. Thulium-doped all-fiber laser mode-locked

by CVD-graphene/PMMA saturable absorber. Opt Express 2013;21:12797–802.
[365] Fu B, Gui L, Li X, Xiao X, Zhu H, Yang C. Generation of 35-nJ nanosecond pulse from a passively mode-locked Tm, Ho-codoped fiber laser with graphene saturable absorber. IEEE Photon Technol Lett 2013;25:1447–9.
[366] Sotor J, Bogusławski J, Martynkien T, et al. All-polarization-maintaining, stretched-pulse Tm-doped fiber laser, mode-locked by a graphene saturable absorber. Opt Lett 2017;42:1592–5.
[367] Yin K, Zhang B, Li L, Jiang T, Zhou X, Hou J. Soliton mode-locked fiber laser based on topological insulator Bi_2Te_3 nanosheets at 2 μm. Photon Res 2015;3:72–6.
[368] Jeong H, Choi SY, Kim MH, et al. All-fiber Tm-doped soliton laser oscillator with 6 nJ pulse energy based on evanescent field interaction with monoloayer graphene saturable absorber. Opt Express 2016;24:14152–8.
[369] Yang G, Liu Y-G, Wang Z, Lou J, Wang Z, Liu Z. Broadband wavelength tunable mode-locked thulium-doped fiber laser operating in the 2 μm region by using a graphene saturable absorber on microfiber. Laser Phys Lett 2016;13:065105.
[370] Pawliszewska M, Martynkien T, Przewłoka A, Sotor J. Dispersion-managed Ho-doped fiber laser mode-locked with a graphene saturable absorber. Opt Lett 2018;43:38–41.
[371] Wang J, Lu W, Li J, et al. Ultrafast thulium-doped fiber laser mode locked by monolayer WSe_2. IEEE J Sel Top Quantum Electron 2017;24:1–6.
[372] Pawliszewska M, Ge Y, Li Z, Zhang H, Sotor J. Fundamental and harmonic mode-locking at 2.1 μm with black phosphorus saturable absorber. Opt Express 2017;25:16916–21.
[373] Sobon G, Sotor J, Pasternak I, Krajewska A, Strupinski W, Abramski KM. All-polarization maintaining, graphene-based femtosecond Tm-doped all-fiber laser. Opt Express 2015;23:9339–46.
[374] Zhu G, Zhu X, Wang F, et al. Graphene mode-locked fiber laser at 2.8 μm. IEEE Photon Technol Lett 2015;28:7–10.
[375] Qin Z, Xie G, Zhao C, Wen S, Yuan P, Qian L. Mid-infrared mode-locked pulse generation with multilayer black phosphorus as saturable absorber. Opt Lett 2016;41:56–9.
[376] Qin Z, Hai T, Xie G, et al. Black phosphorus Q-switched and mode-locked mid-infrared Er: ZBLAN fiber laser at 3.5 μm wavelength. Opt Express 2018;26:8224–31.
[377] Qin Z, Xie G, Ma J, Yuan P, Qian L. 2.8 μm all-fiber Q-switched and mode-locked lasers with black phosphorus. Photon Res 2018;6:1074–8.
[378] Yu S, Wu X, Wang Y, Guo X, Tong L. 2D materials for optical modulation: challenges and opportunities. Adv Mater 2017;29:1606128.
[379] Woodward R, Howe R, Runcorn T, et al. Wideband saturable absorption in few-layer molybdenum diselenide ($MoSe_2$) for Q-switching Yb-, Er-and Tm-doped fiber lasers. Opt Express 2015;23:20051–61.
[380] Ahmad H, Rashid F, Azzuhri SR, et al. The generation of passive dual wavelengths Q-switched YDFL by MoSe2 film. Laser Phys Lett 2016;13:115102.
[381] Han X, Zhang H, Jiang S, et al. Improved laser damage threshold of In_2Se_3 saturable absorber by PVD for high-power mode-locked Er-doped fiber laser. Nanomaterials 2019;9:1216.
[382] Ahmad H, Reduan SA, Ooi SI, Ismail MA. Mechanically exfoliated In_2Se_3 as a saturable absorber for mode-locking a thulium-doped fluoride fiber laser operating in S-band. Appl Opt 2018;57:6937–42.
[383] Li L, Yu Y, Ye GJ, et al. Black phosphorus field-effect transistors. Nat Nanotechnol 2014;9:372.
[384] Xia F, Wang H, Jia Y. Rediscovering black phosphorus as an anisotropic layered material for optoelectronics and electronics. Nat Commun 2014;5:4458.
[385] Abbas AN, Liu B, Chen L, et al. Black phosphorus gas sensors. ACS Nano 2015;9:5618–24.
[386] Castellanos-Gomez A. Black phosphorus: narrow gap, wide applications. J Phys Chem Lett 2015;6:4280–91.
[387] Li J, Luo H, Zhai B, et al. Black phosphorus: a two-dimension saturable absorption material for mid-infrared Q-switched and mode-locked fiber lasers. Sci Rep 2016;6:30361.
[388] Cui Y, Liu X. Graphene and nanotube mode-locked fiber laser emitting dissipative and conventional solitons. Opt Express 2013;21:18969–74.
[389] Gao B, Ma C, Huo J, Guo Y, Sun T, Wu G. Influence of gain fiber on dissipative soliton pairs in passively mode-locked fiber laser based on BP as a saturable absorber. Opt Commun 2018;410:191–6.
[390] Song H, Wang Q, Zhang Y, Li L. Mode-locked ytterbium-doped all-fiber lasers based on few-layer black phosphorus saturable absorbers. Opt Commun 2017;394:157–60.
[391] Shao Z, Qiao X, Rong Q, Su D. Observation of the evolution of mode-locked solitons in different dispersion regimes of fiber lasers. Opt Commun 2015;345:105–10.
[392] Zhang H. Ultrathin two-dimensional nanomaterials. ACS Nano 2015;9:9451–69.
[393] Luo Z, Zhou M, Weng J, et al. Graphene-based passively Q-switched dual-wavelength erbium-doped fiber laser. Opt Lett 2010;35:3709–11.
[394] Liu J, Wu S, Yang Q-H, Wang P. Stable nanosecond pulse generation from a graphene-based passively Q-switched Yb-doped fiber laser. Opt Lett 2011;36:4008–10.
[395] Luo Z, Huang Y, Zhong M, et al. 1-, 1.5-, and 2-μm fiber lasers Q-switched by a broadband few-layer MoS_2 saturable absorber. J Lightwave Technol 2014;32:4077–84.
[396] Tao M, Ye X, Wang Z, et al. Modeling of Tm–Ho codoped fiber saturable absorber based passive Q-switching of an Er-doped fiber laser. Laser Phys 2014;24:085110.
[397] Ahmad H, Samion M, Muhamad A, et al. Tunable 2.0 μm Q-switched fiber laser using a silver nanoparticle based saturable absorber. Laser Phys 2017;27:065110.
[398] Rashid F, Azzuhri SR, Salim M, et al. Using a black phosphorus saturable absorber to generate dual wavelengths in a Q-switched ytterbium-doped fiber laser. Laser Phys Lett 2016;13:085102.
[399] Yi J, Du L, Li J, et al. Unleashing the potential of Ti_2CT_x MXene as a pulse modulator for mid-infrared fiber lasers. 2D Mater 2019;6:045038.
[400] Luo Z, Zhou M, Wu D, et al. Graphene-induced nonlinear four-wave-mixing and its application to multiwavelength Q-switched rare-earth-doped fiber lasers. J Lightwave Technol 2011;29:2732–9.
[401] Wu D, Luo Z, Xiong F, et al. Passive synchronization of 1.06- and 1.53 μm fiber lasers Q-switched by a common graphene SA. IEEE Photon Technol Lett 2014;26:1474–7.
[402] Ren A, Feng M, Song F, et al. Actively Q-switched ytterbium-doped fiber laser by an all-optical Q-switcher

based on graphene saturable absorber. Opt Express 2015;23:21490–6.
[403] Luo Z, Huang Y, Weng J, et al. 1.06 μm Q-switched ytterbium-doped fiber laser using few-layer topological insulator Bi_2Se_3 as a saturable absorber. Opt Express 2013;21:29516–22.
[404] Woodward R, Kelleher E, Howe R, et al. Tunable Q-switched fiber laser based on saturable edge-state absorption in few-layer molybdenum disulfide (MoS_2). Opt Express 2014;22:31113–22.
[405] Zhang M, Hu G, Hu G, et al. Yb-and Er-doped fiber laser Q-switched with an optically uniform, broadband WS_2 saturable absorber. Sci Rep 2015;5:17482.
[406] Huang K-X, Lu B-L, Li D, et al. Black phosphorus flakes covered microfiber for Q-switched ytterbium-doped fiber laser. Appl Opt 2017;56:6427–31.
[407] Popa D, Sun Z, Hasan T, Torrisi F, Wang F, Ferrari AC. Graphene Q-switched, tunable fiber laser. Appl Phys Lett 2011;98:073106.
[408] Cao W, Wang H, Luo A, Luo Z, Xu W. Graphene-based, 50 nm wide-band tunable passively Q-switched fiber laser. Laser Phys Lett 2011;9:54.
[409] Sobon G, Sotor J, Jagiello J, et al. Linearly polarized, Q-switched Er-doped fiber laser based on reduced graphene oxide saturable absorber. Appl Phys Lett 2012;101:241106.
[410] Wang Z, Chen Y, Zhao C, Zhang H, Wen S. Switchable dual-wavelength synchronously Q-switched erbium-doped fiber laser based on graphene saturable absorber. IEEE Photon J 2012;4:869–76.
[411] Ahmad H, Muhammad F, Zulkifli M, Harun S. Graphene-oxide-based saturable absorber for all-fiber Q-switching with a simple optical deposition technique. IEEE Photon J 2012;4:2205–13.
[412] Chen Y, Zhao C, Huang H, et al. Self-assembled topological insulator: Bi_2Se_3 membrane as a passive Q-switcher in an Erbium-doped fiber laser. J Lightwave Technol 2013;31:2857–63.
[413] Sun L, Lin Z, Peng J, Weng J, Huang Y, Luo Z. Preparation of few-layer bismuth selenide by liquid-phase-exfoliation and its optical absorption properties. Sci Rep 2014;4:4794.
[414] Yu Z, Song Y, Tian J, et al. High-repetition-rate Q-switched fiber laser with high quality topological insulator Bi_2Se_3 film. Opt Express 2014;22:11508–15.
[415] Li W, Zou J, Huang Y, et al. 212-kHz-linewidth, transform-limited pulses from a single-frequency Q-switched fiber laser based on a few-layer Bi_2Se_3 saturable absorber. Photon Res 2018;6:C29–35.
[416] Yan K, Lin J, Zhou Y, et al. Bi_2Te_3 based passively Q-switched fiber laser with cylindrical vector beam emission. Appl Opt 2016;55:3026–9.
[417] Koo J, Lee J, Lee JH. Integrated fiber-optic device based on a combination of a piezoelectric transducer and a bulk-structured Bi_2Te_3 topological insulator for Q-Switched mode-locking of a fiber laser. J Lightwave Technol 2017;35:2175–82.
[418] Koo J, Lee J, Chi C, Lee JH. Passively Q-switched 1.56 μm all-fiberized laser based on evanescent field interaction with bulk-structured bismuth telluride topological insulator. JOSA B 2014;31:2157–62.
[419] Huang Y, Luo Z, Li Y, et al. Widely-tunable, passively Q-switched erbium-doped fiber laser with few-layer MoS_2 saturable absorber. Opt Express 2014;22:25258–66.
[420] Chen J-H, Deng G-Q, Yan S-C, et al. Microfiber-coupler-assisted control of wavelength tuning for Q-switched fiber laser with few-layer molybdenum disulfide nanoplates. Opt Lett 2015;40:3576–9.
[421] Li H, Xia H, Lan C, et al. PassivelyQ-switched erbium-doped fiber laser based on few-layer MoS_2 saturable absorber. IEEE Photon Technol Lett 2014;27:69–72.
[422] Xia H, Li H, Lan C, et al. Few-layer MoS_2 grown by chemical vapor deposition as a passive Q-switcher for tunable erbium-doped fiber lasers. Photon Res 2015;3:A92–6.
[423] Wei R, Zhang H, Hu Z, et al. Ultra-broadband nonlinear saturable absorption of high-yield MoS_2 nanosheets. Nanotechnology 2016;27:305203.
[424] Khazaeinezhad R, Kassani SH, Nazari T, et al. Saturable optical absorption in MoS_2 nano-sheet optically deposited on the optical fiber facet. Opt Commun 2015;335:224–30.
[425] Ren J, Wang S, Cheng Z, et al. Passively Q-switched nanosecond erbium-doped fiber laser with MoS_2 saturable absorber. Opt Express 2015;23:5607–13.
[426] Lin J, Hu Y, Chen C, Gu C, Xu L. Wavelength-tunable Yb-doped passively Q-switching fiber laser based on WS_2 saturable absorber. Opt Express 2015;23:29059–64.
[427] Lin J, Yan K, Zhou Y, Xu L, Gu C, Zhan Q. Tungsten disulphide based all fiber Q-switching cylindrical-vector beam generation. Appl Phys Lett 2015;107:191108.
[428] Li L, Wang Y, Wang ZF, Wang X, Yang G. High energy Er-doped Q-switched fiber laser with WS_2 saturable absorber. Opt Commun 2018;406:80–4.
[429] Chen H, Chen Y, Yin J, Zhang X, Guo T, Yan P. High-damage-resistant tungsten disulfide saturable absorber mirror for passively Q-switched fiber laser. Opt Express 2016;24:16287–96.
[430] Kassani SH, Khazaeinezhad R, Jeong H, Nazari T, Yeom D-I, Oh K. All-fiber Er-doped Q-switched laser based on tungsten disulfide saturable absorber. Opt Mater Express 2015;5:373–9.
[431] Liu W, Liu M, Han H, et al. Nonlinear optical properties of WSe_2 and $MoSe_2$ films and their applications in passively Q-switched erbium doped fiber lasers. Photon Res 2018;6:C15–21.
[432] Yin J, Chen H, Lu W, et al. Large-area and highly crystalline $MoSe_2$ for optical modulator. Nanotechnology 2017;28:484001.
[433] Chen B, Zhang X, Guo C, Wu K, Chen J, Wang J. Tungsten diselenide Q-switched erbium-doped fiber laser. Opt Eng 2016;55:081306.
[434] Du L, Jiang G, Miao L, et al. Few-layer rhenium diselenide: an ambient-stable nonlinear optical modulator. Opt Mater Express 2018;8:926–35.
[435] Wang X, Cheng PK, Tang CY, et al. Laser Q-switching with PtS_2 microflakes saturable absorber. Opt Express 2018;26:13055–60.
[436] Jiang M, Ma H, Ren Z, et al. A graphene Q-switched nanosecond Tm-doped fiber laser at 2 μm. Laser Phys Lett 2013;10:055103.
[437] Zhao J, Zheng Z, Ouyang D, et al. 70-W graphene-oxide passively Q-switched thulium-doped double-clad fiber laser. IEEE J Sel Top Quantum Electron 2016;23:13–9.
[438] Liu C, Ye C, Luo Z, et al. High-energy passively Q-switched 2 μm Tm^{3+}-doped double-clad fiber laser using graphene-oxide-deposited fiber taper. Opt Express 2013;21:204–9.

[439] Wei C, Zhu X, Wang F, et al. Graphene Q-switched 2.78 μm Er^{3+}-doped fluoride fiber laser. Opt Lett 2013;38:3233–6.
[440] Liu S, Zhu X, Zhu G, et al. Graphene Q-switched Ho^{3+}-doped ZBLAN fiber laser at 1190 nm. Opt Lett 2015;40:147–50.
[441] Li J, Luo H, Wang L, et al. 3-μm mid-infrared pulse generation using topological insulator as the saturable absorber. Opt Lett 2015;40:3659–62.
[442] Li W, Peng J, Zhong Y, et al. Orange-light passively Q-switched Pr^{3+}-doped all-fiber lasers with transition-metal dichalcogenide saturable absorbers. Opt Mater Express 2016;6:2031–9.
[443] Luo Z, Wu D, Xu B, et al. Two-dimensional material-based saturable absorbers: towards compact visible-wavelength all-fiber pulsed lasers. Nanoscale 2016;8:1066–72.
[444] Wu D, Cai Z, Zhong Y, et al. Compact passive Q-switching Pr^{3+}-doped ZBLAN fiber laser with black phosphorus-based saturable absorber. IEEE J Sel Top Quantum Electron 2016;23:7–12.
[445] Woodward R, Majewski M, Macadam N, et al. Q-switched Dy: ZBLAN fiber lasers beyond 3 μm: comparison of pulse generation using acousto-optic modulation and inkjet-printed black phosphorus. Opt Express 2019;27:15032–45.
[446] Liu J, Li X, Zhang S, et al. Polarization domain wall pulses in a microfiber-based topological insulator fiber laser. Sci Rep 2016;6:29128.
[447] Liu M, Tang R, Luo A-P, Xu W-C, Luo Z-C. Graphene-decorated microfiber knot as a broadband resonator for ultrahigh-repetition-rate pulse fiber lasers. Photon Res 2018;6:C1–7.
[448] Li S, Yi Y, Yin Y, et al. A microfiber knot incorporating a tungsten disulfide saturable absorber based multi-wavelength mode-locked erbium-doped fiber laser. J Lightwave Technol 2018;36:5633–9.
[449] Li S, Yin Y, Lewis E, Garrell G, Wang P. A twelve-wavelength thulium-doped fibre laser based on a microfibre coil resonator incorporating black phosphorus. Opt Commun 2019;437:342–5.
[450] Gan X, Zhao C, Wang Y, et al. Graphene-assisted all-fiber phase shifter and switching. Optica 2015;2:468–71.
[451] Yu S, Wu X, Chen K, et al. All-optical graphene modulator based on optical Kerr phase shift. Optica 2016;3:541–4.
[452] Ni G, Wang L, Goldflam M, et al. Ultrafast optical switching of infrared plasmon polaritons in high-mobility graphene. Nat Photon 2016;10:244.
[453] Joonákim B, Kyungájeon E, Hoácho J. Optical switching of the Dirac point in graphene multilayer field-effect transistors functionalized with spiropyran. Chem Commun 2012;48:10978–80.
[454] Xu B, Martinez A, Yamashita S. Mechanically exfoliated graphene for four-wave-mixing-based wavelength conversion. IEEE Photon Technol Lett 2012;24:1792–4.
[455] Hu X, Long Y, Ji M, et al. Graphene-silicon microring resonator enhanced all-optical up and down wavelength conversion of QPSK signal. Opt Express 2016;24:7168–77.
[456] Wang J, Hu X. Recent advances in graphene-assisted nonlinear optical signal processing. J Nanotechnol 2016;2016. Article ID: 7031913, 18 pages.
[457] Bao Q, Zhang H, Wang B, et al. Broadband graphene polarizer. Nat Photon 2011;5:411.
[458] He X, Liu J. Flexible and broadband graphene polarizer based on surface silicon-core microfiber. Opt Mater Express 2017;7:1398–405.
[459] Guan C, Li S, Shen Y, Yuan T, Yang J, Yuan L. Graphene-coated surface core fiber polarizer. J Lightwave Technol 2015;33:349–53.
[460] Ghosh S, Mandal D, Chandra A, Bhaktha SN. Effect of laser irradiation on graphene oxide integrated TE-pass waveguide polarizer. J Lightwave Technol 2019;37:2380–5.
[461] Chang Z, Chiang K S. Ultra-broadband mode filters based on graphene-embedded waveguides. Opt Lett 2017;42:3868–71.
[462] Ma J, Xi X, Yu Z, Sun X. Hybrid graphene/silicon integrated optical isolators with photonic spin–orbit interaction. Appl Phys Lett 2016;108:151103.
[463] Solnyshkov D, Bleu O, Malpuech G. Topological optical isolator based on polariton graphene. Appl Phys Lett 2018;112:031106.
[464] Debnath PC, Uddin S, Song Y-W. Ultrafast all-optical switching incorporating in situ graphene grown along an optical fiber by the evanescent field of a laser. ACS Photon 2017;5:445–55.
[465] Lu L, Wang W, Wu L, et al. All-optical switching of two continuous waves in few layer bismuthene based on spatial cross-phase modulation. ACS Photon 2017;4:2852–61.
[466] Manjappa M, Solanki A, Kumar A, Sum TC, Singh R. Solution-processed lead iodide for ultrafast all-optical switching of terahertz photonic devices. Adv Mater 2019;31:1901455.
[467] Wu Y, Yao B, Cheng Y, et al. Four-wave mixing in a microfiber attached onto a graphene film. IEEE Photon Technol Lett 2013;26:249–52.
[468] Zhang D, Guan H, Zhu W, et al. All light-control-light properties of molybdenum diselenide ($MoSe_2$)-coated-microfiber. Opt Express 2017;25:28536–46.
[469] Chen S, Miao L, Chen X, et al. Few-layer topological insulator for all-optical signal processing using the nonlinear Kerr effect. Adv Opt Mater 2015;3:1769–78.
[470] Zheng J, Yang Z, Si C, et al. Black phosphorus based all-optical-signal-processing: toward high performances and enhanced stability. ACS Photon 2017;4:1466–76.
[471] Cai Z-R, Liu M, Hu S, et al. Graphene-decorated microfiber photonic device for generation of rogue waves in a fiber laser. IEEE J Sel Top Quantum Electron 2016;23:20–5.